



CYTOPROTECTIVE EFFECT OF *PHYLLANTHUS EMBLICA* FRUIT EXTRACT AGAINST
UVB-INDUCED KERATINOCYTE DAMAGE



KHWANDOW KUNCHANA

Graduate School Srinakharinwirot University

2020

ฤทธิ์การปกป้องเซลล์ของผลมะขามป้อมสกัดต่อรังสีอัลตราไวโอเล็ตบีที่เหนี่ยวนำให้เซลล์คอราติ
โนไซต์เกิดการบาดเจ็บ



ขวัญดาว คุณชนะ

ปริญญาานิพนธ์นี้เป็นส่วนหนึ่งของการศึกษาตามหลักสูตร
ปรัชญาดุษฎีบัณฑิต สาขาวิชาอณูชีววิทยา
คณะแพทยศาสตร์ มหาวิทยาลัยศรีนครินทรวิโรฒ
ปีการศึกษา 2563
ลิขสิทธิ์ของมหาวิทยาลัยศรีนครินทรวิโรฒ

CYTOPROTECTIVE EFFECT OF *PHYLLANTHUS EMBLICA* FRUIT EXTRACT AGAINST
UVB-INDUCED KERATINOCYTE DAMAGE



KHWANDOW KUNCHANA

A Dissertation Submitted in Partial Fulfillment of the Requirements
for the Degree of DOCTOR OF PHILOSOPHY
(Molecular Biology)

Faculty of Medicine, Srinakharinwirot University

2020

Copyright of Srinakharinwirot University

THE DISSERTATION TITLED
CYTOPROTECTIVE EFFECT OF *PHYLLANTHUS EMBLICA* FRUIT EXTRACT AGAINST
UVB-INDUCED KERATINOCYTE DAMAGE

BY
KHWANDOW KUNCHANA

HAS BEEN APPROVED BY THE GRADUATE SCHOOL IN PARTIAL FULFILLMENT
OF THE REQUIREMENTS FOR THE DOCTOR OF PHILOSOPHY
IN MOLECULAR BIOLOGY AT SRINAKHARINWIROT UNIVERSITY

(Assoc. Prof. Dr. Chatchai Ekpanyaskul, MD.)
Dean of Graduate School

ORAL DEFENSE COMMITTEE

..... Major-advisor Chair
(Assoc. Prof.Suvara Wattanapitayakul)	(Assoc. Prof.Nuntiya Somparn)
..... Co-advisor Committee
(Assoc. Prof.Linda Chularojmontri)	(Assoc. Prof.Punnee Nusuetrong)
 Committee
	(Assoc. Prof.Teeraporn Bureerug)

Title	CYTOPROTECTIVE EFFECT OF <i>PHYLLANTHUS EMBLICA</i> FRUIT EXTRACT AGAINST UVB-INDUCED KERATINOCYTE DAMAGE
Author	KHWANDOW KUNCHANA
Degree	DOCTOR OF PHILOSOPHY
Academic Year	2020
Thesis Advisor	Associate Professor Suvara Wattanapitayakul
Co Advisor	Associate Professor Linda Chularojmontri

The overexposure to UVB rays on the skin can induce inflammation and skin cell damage via the induction of DNA damage and ROS production. Long-term exposure to UVB leads to skin cancer promotion. For this reason, the protective effect of *Phyllanthus Emblica* (PE), was examined. PE is an aqueous extract and a high antioxidant medical plant, and on UVB-irradiated HaCaT cells induced skin cell damage. The phytochemical constituents of PE were identified by HPLC. The antioxidant and scavenging activities of PE were determined using ORAC, FRAP, and ROS and free-radicals scavenging assays. An MTT assay was used to investigate cell viability. Intracellular ROS levels and enzymatic antioxidant activities were evaluated by flow cytometry and ELISA, respectively. Hoechst staining was probed and detected apoptotic cells under a fluorescence microscope. PGE₂ secretion was detected by ELISA and cell-signaling protein expression in each pathway was determined by western blot analysis. PE showed high antioxidant potential, as it is composed of antioxidant compounds, such as ascorbic acid, gallic acid, ellagic acid, chlorogenic acid, and quercetin. PE protection of HaCaT cells death were also observed. PE also decreased the intracellular ROS levels leading to the reduction of cellular inflammation by decreasing PGE₂ release, the expression of NF- κ B, COX-2, and c-Jun phosphorylation expression. Moreover, PE improved the survival of HaCaT cells by inhibiting death signaling pathways. Therefore, these results clearly suggest that PE may protect HaCaT cells from UVB irradiation via the reduction of intracellular ROS, an attenuating protein cascade in the inflammatory pathway, and the improvement of the survival of HaCaT cells.

Keyword : ROS, UVB, Oxidative stress, Antioxidant, Inflammation

ACKNOWLEDGEMENTS

I wish to show my appreciation to my advisor, Assoc. Prof. Suvara Wattanapitayakul and my co-advisor, Assoc. Prof. Linda Chularojanamontri offered an opportunity to study in the Ph.D. program. I would like to thank the Royal Golden Jubilee Ph.D. program (Grant No. PHD/0048/2558) to support the scholarship, research funding, and study abroad experiences. Finally, I would also like to thank Wattanased Jarisarapurin, my best friend, and our families.

KHWANDOW KUNCHANA



TABLE OF CONTENTS

	Page
ABSTRACT	D
ACKNOWLEDGEMENTS.....	E
TABLE OF CONTENTS.....	F
TABLE OF TABLES.....	J
TABLE OF FIGURES.....	K
LIST OF ABBREVIATIONS.....	N
CHAPTER 1 INTRODUCTION.....	1
1.1 Background.....	1
1.2 Objectives of the study	4
1.3 Hypothesis	4
1.4 Conceptual framework.....	5
CHAPTER 2 LITERATURE REVIEW.....	6
2.1 UV radiation.....	6
2.2 Skin.....	6
2.2.1 Skin structures.....	6
2.2.2 Skin functions	8
2.2.2 HaCaT keratinocyte model.....	9
2.3 Skin cancer	10
2.3.1 Non-melanoma skin cancer	10
2.3.2 Melanoma.....	10
2.4 Effects of ultraviolet radiation B on the skin.....	11

2.4.1 Direct DNA damage	11
2.4.2 Oxidative stress	12
2.4.3 Photoaging	17
2.4.4 Program cell death	18
2.4.5 Inflammation	20
2.5 The defense mechanisms in the skin	21
2.5.1 Antioxidant enzymes mechanism	21
2.5.2 Nrf2 signaling pathway.....	22
2.5.3 NER repair mechanism	23
2.5.4 Cell survival signaling pathway.....	23
2.6 <i>Phyllanthus emblica</i>	28
CHAPTER 3 RESEARCH METHODOLOGY	35
3.1 Materials and Chemicals	35
3.2 Methods	39
3.2.1 HPLC analysis	39
3.2.2 <i>Phyllanthus emblica</i> (PE) fresh fruit juice extraction	41
3.2.3 Ferric reducing antioxidant power (FRAP) assay	41
3.2.4 Oxygen radical absorbance capacity (ORAC) assay	42
3.2.5 Determination of hydroxyl radical scavenging activity	43
3.2.6 Determination of superoxide scavenging activity.....	44
3.2.7 Determination of hydrogen peroxide scavenging activity	45
3.2.8 Cell culture.....	46
3.2.9 PE treatment for keratinocytes	47

3.2.10 UVB treatment	47
3.3.11 Optimal dose of UVB by MTT assay	48
3.2.12 Cytotoxicity and photoprotective of PE by MTT assay	48
3.2.13 Determination of intracellular ROS generation	49
3.2.14 Detection of Hydrogen Peroxide Release assay	50
3.2.15 Detection of superoxide release assay.....	51
3.2.16 Catalase activity assay.....	51
3.2.17 Superoxide dismutase activity assay.....	53
3.2.18 Glutathione peroxidase activity assay	54
3.2.19 Apoptotic analysis by Hoechst 33342	55
3.2.20 Prostaglandin E ₂ detection	55
3.2.21 Preparation of cell lysates	56
3.2.22 Western blot analysis	58
3.2.23 Statistical analysis	59
CHAPTER 4 RESULT	60
4.1 Identification of phytochemical constituents in PE	60
4.2 Antioxidant capacity of PE	68
4.2.1 Ferric-reducing antioxidant power (FRAP)	68
4.2.2 Oxygen radical absorbance capacity (ORAC).....	70
4.3 Antioxidant scavenging activity	72
4.3.1 Hydroxyl radical scavenging activity	72
4.3.2 Superoxide anion scavenging activity	74
4.3.3 Hydrogen peroxide scavenging activity	75

4.4 Effect of UVB on keratinocyte cell viability	76
4.5 Effect of PE on UVB-induced keratinocyte cell viability	77
4.6 Effect of PE on UVB-induced intracellular ROS production	78
4.7 Effect of PE on UVB-induced intracellular superoxide production	81
4.8 Effect of PE on UVB-induced hydrogen peroxide production	82
4.9 Effect of PE on UVB-induced CAT enzyme antioxidant activity	83
4.10 Effect of PE on UVB-induced SOD enzyme antioxidant activity	85
4.11 Effect of PE on UVB-induced GPx enzyme antioxidant activity	87
4.12 Effect of PE on UVB-induced apoptosis in HaCaT cells	87
4.13 Effect of PE on UVB-induced PGE ₂ production	89
4.14 Effect of PE on UVB-induced COX-2 protein expression	90
4.15 Effect of PE on UVB-induced NF- κ B protein expression	92
4.16 Effect of PE on UVB-induced Akt protein expression	94
4.17 Effect of PE on UVB-induced p38 protein expression	96
4.18 Effect of PE on UVB-induced cytochrome c protein expression	98
4.19 Effect of PE on UVB-induced c-Jun protein expression	100
CHAPTER 5 SUMMARY DISCUSSION AND SUGGESTION	102
REFERENCES	107
VITA	122

TABLE OF TABLES

Page	
Table 1	Summary of chemical constituents and activity of <i>Phyllanthus emblica</i> 30
Table 2	Summary of previous studies pharmacological activity of <i>Phyllanthus emblica</i> 32
Table 3	The summary content of compound analytes in PE 61
Table 4	The antioxidant capacities of PE..... 68



TABLE OF FIGURES

Page	
Figure 1 The structure of UVB-induced damage to DNA	12
Figure 2 Schematic representation of the generation of reactive oxygen species (ROS) and antioxidant enzyme mechanism.	14
Figure 3 ROS stimulates the peroxidation of polyunsaturated fatty acids (PUFA) and carbonylation of proteins.	16
Figure 4 Extrinsic and intrinsic apoptotic signaling pathways.	19
Figure 5 Classical and alternative of the NF- KB signaling pathway.	21
Figure 6 The mitogen-activated protein kinases (MAPKs) signaling pathways response to UV radiation.	26
Figure 7 The transcription factors response to UV radiation.	27
Figure 8 A representative of HPLC analysis of ascorbic acid detected at 243 nm.	62
Figure 9 A representative of HPLC analysis of gallic acid detected at 270 nm.	63
Figure 10 A representative of HPLC analysis of ellagic acid detected at 253 nm.	64
Figure 11 A representative of HPLC analysis of chlorogenic acid detected at 325 nm.	65
Figure 12 A representative of HPLC analysis of quercetin was detected at 255 nm.	66
Figure 13 A representative of HPLC analysis of phyllanthin was detected at 280 nm.	67
Figure 14 FRAP antioxidant capacities of ASC reference standard and the PE fruit extract are expressed in FeSO ₄ equivalent.	69
Figure 15 Determination of ORAC assay of Trolox	71
Figure 16 Determination of ORAC assay of PE extract	72
Figure 17 Hydroxyl radical scavenging activities of the Trolox reference and PE extract.	73

Figure 18 Superoxide anion scavenging activities of the Trolox standard and PE extract.	74
Figure 19 Hydrogen peroxide scavenging activities of the Trolox standard and PE extract.....	75
Figure 20 Relative cell viability of HaCaT cells after exposure to various doses of UVB.	76
Figure 21 Cytotoxicity of PE on HaCaT cells viability.	77
Figure 22 Protective effect of PE on HaCaT cells viability stimulated with 40 mJ/cm ² UVB irradiation.....	78
Figure 23 The dot-plot and histogram plots of intracellular ROS via flow cytometer.....	80
Figure 24 The fluorescent mean intensity of intracellular ROS is detected by a flow cytometer.....	81
Figure 25 Relative superoxide production in HaCaT cells after treatment with or without UVB irradiation.....	82
Figure 26 The intracellular H ₂ O ₂ production in HaCaT cells.....	83
Figure 27 The CAT activity in HaCaT cells after induced with UVB radiation.....	84
Figure 28 The SOD activity in HaCaT cells.....	86
Figure 29 The GPx activity in HaCaT cells induced with UVB radiation.	87
Figure 30 Cell apoptosis in HaCaT cells by Hoechst staining.	88
Figure 31 Representative of PGE ₂ releasing in HaCaT cells.....	89
Figure 32 Western blot analysis of COX-2 expression in HaCaT cells induced by UVB.	91
Figure 33 Western blot analysis of NF- K B expression in HaCaT cells induced by UVB.	93
Figure 34 Western blot analysis of Akt expression in HaCaT cells induced by UVB ray.	95
Figure 35 Western blot analysis of p38 expression in HaCaT cells induced by UVB ray.	97

Figure 36 Western blot analysis of cytochrome c expression in HaCaT cells induced by UVB radiation.....	99
Figure 37 western blot analysis of p-c-Jun expression in HaCaT cells induced by UVB.	101
Figure 38 The preventive effect of PE on UVB-induced oxidative stress in keratinocytes.	106



LIST OF ABBREVIATIONS

AAPH	2,2'-azobis(2-amidino-propane) dihydrochloride
AIF	Apoptosis inducing factor
Akt	Protein kinase B
ANOVA	One-way analysis of variance
AP-1	Activator protein 1
ARE	Antioxidant response element
AUC	Area under the curve
ASR	Age-standardized rate
Apaf-1	Apoptotic protease activating factor-1
BCC	Basal cell carcinomas
BER	Base excision repair
b.w.	Body weight
BH ₄	Tetrahydrobiopterin
BH ₂	Dihydrobiopterin
BAD	Bcl-2-associated death promoter
BSA	Bovine serum albumin
CFCs	Chlorofluorocarbons
CPD	Cyclobutane pyrimidine dimer
CAT	Catalase enzyme
cGMP	Cyclic guanosine monophosphate
CoQ	Coenzyme Q
COX	Cyclooxygenase
Cyt c	Cytochrome C
CYP	Cytochrome p450
DCFH-DA	2',7'-Dichlorofluorescein diacetate
DMEM	Dulbecco's modified Eagle medium
DMSO	Dimethyl sulfoxide

dsDNA	Double stand DNA
DTNB	5,5'-dithiobis(2-nitrobenzoic acid)
ECM	Extracellular matrix
EDTA	Ethylenediaminetetraacetic acid
EGF	Epidermal growth factor
ERK	Extracellular signal-regulated protein kinase
8-OHdG	8-hydroxy-20-deoxyguanosine
FeSOD	Iron SOD
FAK	Focal adhesion kinase
FBS	Fetal bovine serum
Fe	Ferrous
FeCl ₃	Ferrous (III) chlorite
FeSO ₄	Ferrous (II) sulfate
FOXO	Forkhead box O
FRAP	Ferric reducing antioxidant power
GDP	Guanosine diphosphate
GPX	Glutathione peroxidase
GR	Glutathione reductase
GSH	Glutathione reduced form
GSSG	Glutathione oxidized form
GTP	Guanosine triphosphate
GG-NER	Global genome NER
HCl	Hydrochloric acid
HOCl	Hypochlorous acid
H ₂ O ₂	Hydrogen peroxide
HRP	Horseradish peroxidase
H ₂ SO ₄	Sulfuric acid
HVA	Homovanillic acid
IKK	IκB kinase complex

JNK	C-Jun N-terminal kinase
Keap1	Kelch ECH associating protein 1
KH_2PO_4	Potassium phosphate buffer
KIO_4	Potassium periodate
KOH	Potassium hydroxide
LDL	low-density lipoprotein
LOO^\bullet	Lipid peroxy radical
MAPK	Mitogen-activated protein kinase
MAPKK	Mitogen-activated protein kinase kinase
MAPKKK	Mitogen-activated protein kinase kinase kinase
MDA	Malondialdehyde
MPK	MAP kinase phosphatase
mTOR	Mammalian target of rapamycin (mTOR)
MTT	3-(4,5-dimethylthiazol-2-yl)-2,5-diphenyl-2h-tetrazolium bromide
MEFs	Mouse embryo fibroblasts
MnSOD	Manganese SOD
MMR	DNA mismatch repair
NaBH_4	Sodium borohydride
NaCl	Sodium chlorite
NaF	Sodium fluoride
NaHCO_3	Sodium bicarbonate
Na_2HPO_4	Sodium phosphate dibasic
NaOCl	Sodium hypochlorite
NAC	N-acetylcysteine
NADPH	Nicotinamide adenine dinucleotide phosphate
NIK	NF-kappa-B-inducing kinase
NBT	Nitro blue tetrazolium
NF- κ B	Nuclear factor kappa light chain enhancer of activated B cells
Nrf2	Nuclear factor erythroid 2-related factor 2

NMSC	Non-melanoma skin cancers
NER	Nucleotide excision repair
NPs	Nanoparticles
O ₂	Oxygen
O ₂ ^{•-}	Superoxide anion
OH [•]	Hydroxyl radical
OONO ⁻	Peroxynitrite
ORAC	Oxygen radical absorbance capacity
ODCs	Ozone depleting chemicals
6-4PPs	Pyrimidine-pyrimidone (6-4) photodimers
PE	<i>Phyllanthus emblica</i>
PGE ₂	Prostaglandin E ₂
PI	Propidium iodide
PI3K	Phosphoinositide-3-kinase
PIP2	Phosphatidylinositol 4,5-di phosphate
PIP3	Phosphatidylinositol 3,4,5-di phosphate
PKC	Protein kinase C
PKC- α	Protein kinase C alpha
PUFA	Polyunsaturated fatty acid
PTEN	Phosphatase and tensin homolog
RFU	Reactive fluorescence unit
ROO [•]	Peroxyl radical
ROS	Reactive oxygen species
SD	Standard deviation
SDS-PAGE	SDS-poly acrylamide gel electrophoresis
SEM	Standard error of the mean
SOD	Superoxide dismutase
SCC	Squamous cell carcinoma
TC-NER	Transcription-coupled repair

TBA	2-Thiobarbituric acid
TBST	Tris buffer saline containing 0.1% Tween
TCA	Trichloroacetic acid
TEMED	Tetramethyl ethylenediamine
TLRs	Toll-like receptors
TNF- α	Tumor necrosis factor-alpha
TNFR	Tumor necrosis factor receptor
TPTZ	2,4,6-Tri(2-pyridyl)-s-triazine
TRAIL-R	TNF-related apoptosis-inducing ligand
Trolox	6-Hydroxy-2,5,7,8-tetramethylchroman-2-carboxylic acid
WST-1	(2-(4-Iodophenyl) -3-(4-nitrophenyl) -5-(2,4-disulfophenyl) -2H-tetrazolium, monosodium salt
XO	Xanthine oxidase

CHAPTER 1

INTRODUCTION

1.1 Background

Ozone depletion has been defined as one of the most prominent environmental issues over the past decades (1). By 2011, the Antarctic polar ozone hole had become the world's biggest ozone hole and ozone depletion was much more serious in 2020, following reported from World Meteorological Organization (WMO) and National Aeronautics and Space Administration (NASA). This revealed the global consequences of human action on the environment. Ozone-depleting chemicals such as chlorofluorocarbons, bromine, and halogenated hydrocarbons are widely used as refrigeration systems and propellants in aerosol sprays. UV rays destroy ozone-depleting chemicals into halogen atoms, which then break down ozone to generate oxygen. It is one of the factors contributing to ozone disruption. However, manufacturers are now using ozone-friendly refrigerants, hydrofluorocarbons. But this alternative chemical is a potent heat-trapping greenhouse gas that promotes to global warming and climate change. Finally, these circumstances would indirectly raise ozone-depleting chemicals and further eliminate the ozone layer, which could be the next problem. The ozone layers generally filter and absorb dangerous UV radiation before it reaches the earth's surface (2). The reduction of the ozone layer will increase the harmful UV-radiation in the biosphere.

Long-term exposure to ultraviolet radiation and especially ultraviolet B radiation can destroy the skin function and structure, which is the main cause of skin cancer and other diseases in humans. The incidence of skin cancer increases worldwide, especially in the Caucasian population. Each year in the United States about 3.5 million new cases of skin cancer patients have been diagnosed and it also found about 6,023 cases in southeast Asia according to World Health Organization (WHO). An hour, more than two people die from skin cancer. Although the Asian population has a lower prevalence of skin cancer, the incidence of skin cancer in the Asian population has risen year by year.

According to the National Cancer Institute of Thailand, the prevalence of skin cancer in Thailand is very high. The analysis of cancer cases from the world age-standardized incidence rate (ASR) found that 4.0 per 100,000 in the male population and 3.9 per 100,000 in the female population (3). Despite having a lower prevalence of skin cancer than America due to their high melanin content, dark skin population groups have a significantly high death rate. The lack of consideration about skin health in this population has resulted in the late detection of skin cancer (4). These circumstances show the major public health problems of the world population are affected by UV radiation.

The negative effects of prolonged UVB exposure have been linked to photoaging of the skin. UVB ray activates AP-1 and NF- κ B transcription factors leading to increased matrix metalloproteinases (MMPs) production, which degrade collagen, the main composition of extracellular matrix (ECM) (5). Furthermore, AP-1 also inhibits the expression of type 1 collagen, resulting in reduced collagen synthesis in photoaged skin (6). As a result, MMPs increased loss of ECM and reduced expression of structural collagen fibers, ECM and tissue instability (7), leading to an increased skin pigment, dryness of skin, fragility of the skin, inflexibility, delayed wound healing, dimness, and premature skin aging (8).

UVB exposure alters the biochemical and physiological functions of skin cells. UVB radiation can cause direct damage to the DNA double-strand causing the formation of cyclobutane pyrimidine dimer (CPDs), pyrimidine-pyrimidone (6-4) photo dimers (6-4PPs), and 8-hydroxy-2'-deoxyguanosine (8-OHdG) (9). These lesions on the polynucleotide strand will disrupt gene expression by changing the conformation of DNA structure. Therefore, changes in the structure of DNA can affect the coding genes and proteins that finally lead to mutation and cancer.

UVB radiation may also trigger oxidative stress by producing reactive oxygen species (ROS) including hydrogen peroxide (H_2O_2), superoxide anion ($O_2^{\cdot-}$), and hydroxyl radical (OH^{\cdot}) which can attack DNA, protein, and other biomolecules resulting in activating different signal transduction pathways. Therefore, free radicals and their

products are involved in the pathophysiology of many diseases, especially photoaging and skin cancer. Normally, skin cells appear to have an antioxidant defense system including enzymatic antioxidants and non-enzymatic antioxidants that can counteract ROS within cells. However, skin cells are affected by UVB leading to the excessive production of ROS. An imbalance between overproduction free radical and antioxidant defenses can lead to a pathological condition called oxidative stress.

Over the last decade, many sunscreen products have been developed to absorb, reflect, or scatter the UV radiation on the skin. The organic sunscreen used as active ingredients absorbs UV rays. Some active ingredients, such as octyl methoxycinnamate, benzophenone-3, 3-benzylidene camphor, and octocrylene, have been identified to easily penetrate the body through the skin, accumulate in blood circulation and various tissues, and cause skin sensitization (10). Moreover, inorganic sunscreen ingredients including titanium dioxide and zinc oxide can reflect or scatter UV radiation. More advantages of inorganic sunscreen than organic sunscreen are the lack of skin sensitization and limited skin absorption. Products are reduced in size to nanoparticles (NPs), which become simpler to apply and skin-transparent. However, the size of nanoparticles allows them to enter the bloodstream as well as other organs, resulting in more harmful effects on the body. (11). In an alternative way, the natural compounds for dermatological application in humans are also not toxic to the skin and environment. There seems to be a continually expanding cosmetic industry for photoprotective products focused on natural compounds.

Thus, traditional herbal medicines are interested in an important area of research to prevent oxidative stress and skin cancer. Therefore, plant extracts and herbs have been used in cosmetics and sunscreen due to their antioxidant activity from complex composition, which can protect the skin from UV radiation. Antioxidants such as vitamin C, vitamin E, flavonoids, and phenolic acids play a key role in counteracting with ROS, which is the main cause of various skin diseases (12). The medical plant, *Phyllanthus emblica* (PE) distributes throughout tropical and subtropical countries like Thailand, India, and China. The highest amount of vitamin C is found in PE fruit juice (13). Vitamin

C has several effects to the skin, including improved production of collagen and photoprotection. Moreover, PE has several pharmacological properties such as anti-radical activity, anti-inflammatory, anti-hypertensive, anti-diabetic, and cardioprotective effects. Interestingly, PE has not been investigated for its protective effect against UV-induced skin cell damage.

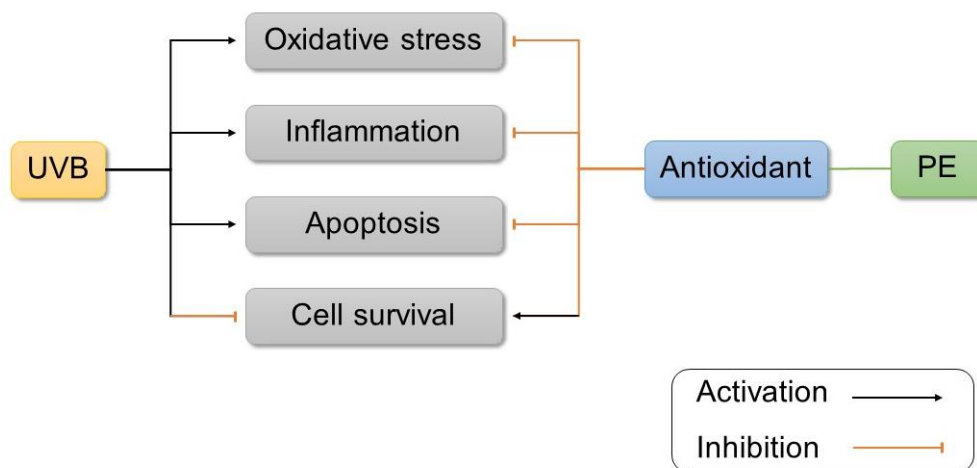
1.2 Objectives of the study

1. To determine the scavenging activities and antioxidant capacities of *Phyllanthus emblica* extract.
2. To investigate the cytoprotective effect of *Phyllanthus emblica* extract on UVB-induced keratinocyte inflammation.
3. To investigate the cytoprotective effect of *Phyllanthus emblica* extract on UVB-induced keratinocyte cell death.
4. To assess the antioxidant defense mechanisms against UVB-induced cellular damage.

1.3 Hypothesis

Phyllanthus emblica increases the antioxidant activities and inhibits UVB-induced cell damage in keratinocytes.

1.4 Conceptual framework



CHAPTER 2

LITERATURE REVIEW

2.1 UV radiation

The sun is the primary source of ultraviolet radiation that enters the earth's atmosphere. On the other hand, UV radiation may also be generated by a human-made source, such as a tanning bed. The UV radiation can be separated into three types including UVA, UVB, and UVC, depending on the spectrum of energy and wavelength. UV radiation wavelength falls between visible light and gamma rays. The wavelengths of UV radiation can be divided into UVC (wavelengths 100 - 280 nm), UVB (wavelengths 280 - 320 nm) and UVA (wavelengths 320 - 400 nm). UVC has more energy than the others but it is blocked by the atmospheric ozone layer of the earth, thus ambient sunlight is importantly 90–95 percent of UVA and 5 – 10 percent of UVB (14). UVA radiation has the weakest energy and the longest wavelengths but can cause indirect damage to the skin cells by penetrating deeply into the dermis and causing wrinkles and pucker, which finally develop into some skin cancer. On the other hand, UVB is nearly totally captured by the epidermis, with just a small amount reaching the dermis. UVB radiation can destroy skin cells by directly destroy DNA and indirectly trigger reactive oxygen species, which are the main cause of various diseases, including skin cancer.

2.2 Skin

2.2.1 Skin structures

The two primary layers of the skin are the epidermis and dermis. Squamous cells make up the epidermis, which is the skin's outer layer. Most of the cells in the epidermis are keratinocytes (approximately 95%), which grow from basal cells in the epidermis' deepest layer and migrate up to the surface of the skin, making up most of the epidermis cells. The epidermis also contains melanocytes, which produce skin color from the melanin pigment. When skin is exposed to UV radiation, melanin can filter and absorb UV radiation that reduces the penetration of UV rays through the skin. The layers

of the epidermis include stratum corneum, stratum lucidum, stratum granulosum, stratum spinosum, and stratum basale.

Corneocytes are non-nucleus keratinocyte cells that make up the stratum corneum, which is the outermost layer of the epidermis. These cells contain a complex mixture of lipid and keratin, a protein that maintains the skin hydrated by resisting evaporation of water, and the high-water content of cells. Corneocytes are distributed in 15 to 20 layers (the thickness 10 - 40 μm) in the stratum corneum. The volume and amount of uptake of a substance through the skin are controlled by the stratum corneum. One of the most key factors influencing the absorption of the skin layers is skin humidity and external humidity. Thus, in healthy skin with normal hydration levels, the drug or cream will easily pass through the keratin layer between cells and enter the stratum corneum layer. When the top layer of the skin is weakened due to dermatitis or radiation. The rate of absorption through the dry skin has reduced. When applying a moisturizer or cream to the skin, they are penetrated through tissues and skin structure via the skin layers. Furthermore, it is distributed to the circulatory system.

Between the stratum granulosum and stratum corneum is the stratum lucidum, a transparent layer, which can be observed under a microscope. It mainly consists of 3 - 5 layers of stretched and dead keratinocytes. These cells are tightly filled with a lipid-rich clear protein called eleidin, obtained from keratohyalin. The protein eleidin made up a stratum lucidum layer translucent and prevents penetration of water from the environment.

Stratum granulosum consisting of keratinocytes are stacked 3 - 5 layers, the distinguishing feature of these cells are the intracellular lamellar granules, which are keratin and keratohyalin granules responsible for keratin formation.

The stratum spinosum is built up of 8 - 10 layers of keratinocytes, which are developed by cellular division in the basal layers. Keratinocytes in the stratum spinosum produced the keratin and water-repellent glycolipids to prevent water loss from the body and render the skin waterproof. It is found in some types of dendritic cells among keratinocytes, Langerhans cells have functioned as a macrophage by protecting the

immune system, consuming bacteria, foreign substances invasion, and cellular debris that grow in this layer (14). The cell layer consists of irregular polygonal cells that stretch upward, as well as protruding cell processes that link the cells through a desmosome structure.

The stratum basale is the lowest layer of the epidermis, which lies on the collagen fibers known as the basement membrane. A single basal cell is largely made up of basal cells, cube-shaped stem cells that grow into keratinocyte progenitors. These cells undergo mitosis to produce new keratinocytes. This single layer of cells, which is actively moving through mitosis cell division to create new cells, produces all of the keratinocytes. When new keratinocytes are produced, old cells are moved to the stratum spinosum layers of the skin. Moreover, the stratum basale also contains two other cell groups that are distributed among the basal cells. First, Merkel cells serve as sensors, activating the sensory nerves that the brain interprets as touch. These cells are particularly dominant on the superficial of the palms and feet. Another cell, the cells that make up the melanin pigment are known as melanocytes. Melanin is responsible for the appearance of the color of human hair and skin, as well as protecting human tissue from sun exposure.

The dermis is the thick layer under the epidermis. This layer also contains hair follicles, blood vessels, lymph vessels, nerve endings, sebaceous glands, sweat glands, and connective tissue. Collagen is the main component of fibrous and elastic tissue, which provides the skin resilience and strength in the extracellular matrix. Besides, the nerve endings are sensitive to touch, pressure, pain, and temperature. The production of perspiration by sweat glands in the dermis, which helps to regulate body temperature. Moreover, the sebaceous glands secrete oils into hair follicles, acts as a skin moisturizer and barrier against foreign substances (14).

2.2.2 Skin functions

The main organ of the body is the skin. The functions of normal skin include protection of the body from infection by pathogenic bacterial and dangerous external substances, control and maintenance of relatively constant body temperature,

prevention of moisture loss and skin permeability, synthesis of vitamin D, and sensation. In addition, skin protects the body from the heat and injuries caused by ultraviolet (UV) rays from the solar system. (15).

2.2.2 HaCaT keratinocyte model

The HaCaT is a spontaneously immortal adherent human keratinocyte cell line from a long-term culture of more than 140 passages in low calcium (0.2 mM) medium and high-temperature condition (38.5 °C) of human adult skin keratinocytes, which was created by Boukamp et. al., in 1988. Thus, HaCaT is the first transformed keratinocyte cell line from adult human skin that without transfect with viruses or viral leading to competent immortal form tumorigenic cell lines. However, the HaCaT cell line has a transformed phenotype with the potential for unlimited growth but remains completely differentiated cellular capacity and maintains a non-tumorigenic keratinocyte cell line. The HaCaT cell can differentiate and form a structure of epidermal tissue when transplanted onto the nude mice, similar to normal keratinocytes (16). Since HaCaT cells have two-point mutants at p53 genes, which play a key role in apoptosis induction, the function of p53 in HaCaT cells which respond to UVB-induced apoptosis is still unclear. This study has shown that HaCaT cells were transfected with wild type p53 cDNA and western blotting was used to check for p53 expression. The mutated-p53 HaCaT cells increase expression of p53 after UVB irradiation and more extended protein p53 half-life than wild-type p53. The decrease in p53 protein levels of cell clones after UVB radiation when compared with normal HaCaT cells line. Therefore, the blocking of mutated p53 can partially inhibit apoptosis in HaCaT cells. Moreover, this data suggest that p53 signaling pathway is a key role for UVB-induced apoptosis but there are other pathways responses to UVB radiation in HaCaT cell (17). Thus, the HaCaT cell has been widely used in many studying mechanisms, which is involved in UVB-induced apoptosis as a model for normal human keratinocytes (18).

2.3 Skin cancer

2.3.1 Non-melanoma skin cancer

Non-melanoma skin cancers (NMSC) are the most common malignant tumor in the white population. There are two types of NMSC, including basal cell carcinomas (BCC) and squamous cell carcinoma (SCC) (19). Between the periods 1976 to 1984 and 2000 to 2010, the total incidence of BCC and SCC increased by 145 and 263 percent, respectively. NMSC incidence rates of both BCC and SCC are increasing in patients younger than 40 years, and occurring in women more than men from the cohort study report populations in Olmsted County, Minnesota, United States (20). BCC arises from the stratum basale, the deepest layer of the epidermis. SCC usually occurs in the squamous cells of the epidermis. Although both types of skin cancer rarely metastasize to lymph nodes and other organs of the body; however, the prevalence of NMSC is increasing annually worldwide, demonstrating major public health problems of the world population affected by UV radiation (21). The major risk factor of Non-melanoma skin cancers is exposure to UV radiation. The risk levels of skin cancer depend on the total amount of all life of sun exposure to the skin. Moreover, NMSC can occur in all parts of the body such as the head, neck, face, arms, and legs, which exposes to UV rays (22). Moreover, some countries in the equatorial regions have higher UV radiation levels, which damage to skin leading to mortality from NMSC (23). Moreover, there are other risk factors for skin cancer such as skin color and age of skin. Patients who died from skin cancer It is mostly caused by excessive UV exposure. Thus, decreased exposure to high levels of UV radiation, wearing protective clothes, sunglasses, using sunscreen, and avoiding sunbathing will indeed help to prevent skin cancer.

2.3.2 Melanoma

Melanoma can occur in both women and men, in any skin color, and it can appear anywhere else on the body's surface, even though it has not been exposed to sunlight. Although melanoma skin cancer reports for approximately 1% of all skin cancer cases, but it is the main cause of death from this type of cancer (24-26). Due to the fact that Melanoma arises from melanocyte cells and it rapidly grows and spreads to the other organ in the body. The melanoma symptoms include broad dark-brown blotches,

a mole that bleeds or changes color, scale, or texture, and a sore, itchy, or burning lesion (27). Since the mid-seventies, the prevalence of melanoma has been increasingly expanding. While this pattern reduces the incidence of the young people population, the mortality rate increased by around 2% each year from 2008 to 2017 (28).

2.4 Effects of ultraviolet radiation B on the skin

2.4.1 Direct DNA damage

DNA molecules are made up of two polynucleotides in the appearance double helix. The two sugar-phosphate backbones from 5 to 3 directions, which called antiparallel. Each polynucleotide contains nitrogenous bases pair hold together by hydrogen bonds. In base pairing, bases Adenine (A) pairs with Thymine (T) and Guanine (G) pairs with Cytosine (C). When the cell reproduces, the polynucleotide strands transfer genetic information to the other cells. Thus, the structural changes in DNA can affect to gene and protein encoded, leading to cancer (29). Most ultraviolet radiation is UVB, which directly damages the DNA. UVB-excited photon was absorbed by DNA, especially pyrimidine base pair. As a result, the pyrimidine base bound with the next pyrimidine base with covalent bonds in the same polynucleotide strand (30). The reaction called Cyclobutane pyrimidine dimer (CPDs) and pyrimidine-pyrimidone (6-4) photoproduct (6-4PPs), which change the conformation of DNA structure and interrupt transcription factors that bind to the initial site leading to inhibition of enzyme production (Figure 1) (31). Activation of p53 and its downstream targets can occur in response to DNA damage and cellular stresses. Under normal conditions, p53 levels are maintained at an inactive state. But DNA damage can activate p53 rapidly. The increased levels of p53 bind to DNA and mediate transcriptional activation. This then leads to inhibition of tumorigenesis by initiating cell cycle arrest and activation of programmed cell death or DNA repair (32). Moreover, the p53 responses to the nucleotide excision repair (NER). Therefore, the mutation in the p53 protein leads to a lack of tumor suppression activity and deficiency in NER. Recent studies have demonstrated that after being exposed to UV radiation, mouse embryo fibroblasts (MEFs) deficiency the p53 protein or its downstream effector of the p53-associated DNA

repair pathway, gadd45 (Gadd45a) or p21 (Cdkn1a), display a partial deficit in NER (33). A recent study indicates that p53-dependent apoptosis plays an active role in balancing cellular growth. The p53R172P embryonic fibroblasts undergo cellular senescence if lacking the p53 protein (34). Besides, the loss of function and mutation in p53 is particularly common in melanoma and NMSC (35). Thus, the p53 gene plays an important role in the DNA repair process of basal keratinocytes.

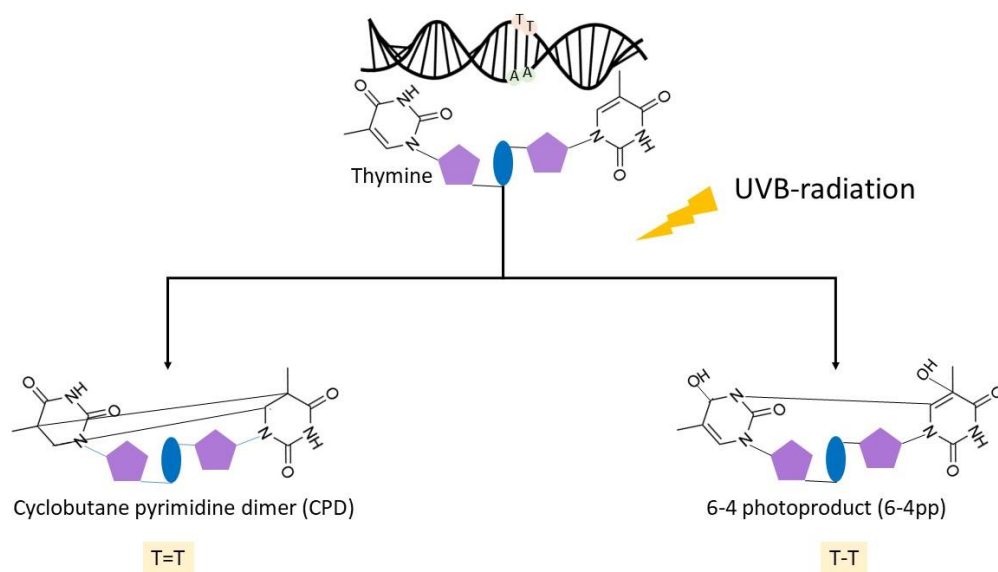


Figure 1 The structure of UVB-induced damage to DNA

Source: Knips A and Zacharias M. (2017). Both DNA global deformation and repair enzyme contacts mediate flipping of thymine dimer damage: Scientific reports. p. 5.

2.4.2 Oxidative stress

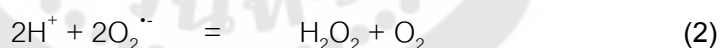
Reactive oxygen species (ROS) are common byproducts of cellular synthesis and inflammation. However, exogenous factors such as drugs, smoking, and UVB ray may cause excessive ROS generation (36). The hydroxyl radical (OH^\bullet),

superoxide anion ($O_2^{\cdot-}$), and hydrogen peroxide (H_2O_2) are the most common ROS. These free radicals and non-free radicals are formed by the reduction of an oxygen molecule (O_2) (Figure 2). UVB induces cell damage by directly attacking DNA strands and also induces the generation of reactive oxygen species (ROS) which affected cellular homeostasis causing oxidative damage and cell death.

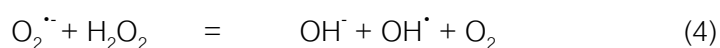
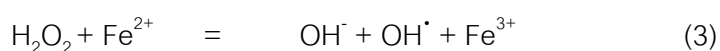
Superoxide anion ($O_2^{\cdot-}$) was produced by activation of O_2 molecule by NADPH oxidase, which produces superoxide from gaining of electrons leading to the formation of singlet state (equation 1). Occurring of the unpaired electrons in the molecules, which are unstable molecules and easily reacting with other biological molecules within the cells (37).



Hydrogen peroxide (H_2O_2) is produced from the dismutation of superoxide anion (equation 2). H_2O_2 is formed in cells under both normal and stressful conditions. The major sources of H_2O_2 include mitochondria, endoplasmic reticulum, and lipid peroxidation.



From a ROS, Hydroxyl radical (OH^{\cdot}) is the most harmful and reactive molecule which interacts with all biological molecules and causes DNA damage, protein damage, and lipid peroxidation, which finally leads to cellular damages. Hydroxyl radical is also generated from hydrogen peroxide and superoxide anion by Fenton reactions (equation 3) and Haber–Weiss reactions (equation 4) (36).



A disparity between the production and scavenging activity of reactive oxygen species (ROS) within a biological system is defined as oxidative stress. The biomolecular products of the cell, including DNA, proteins, and lipids can be harmed by an excessive amount of ROS (38).

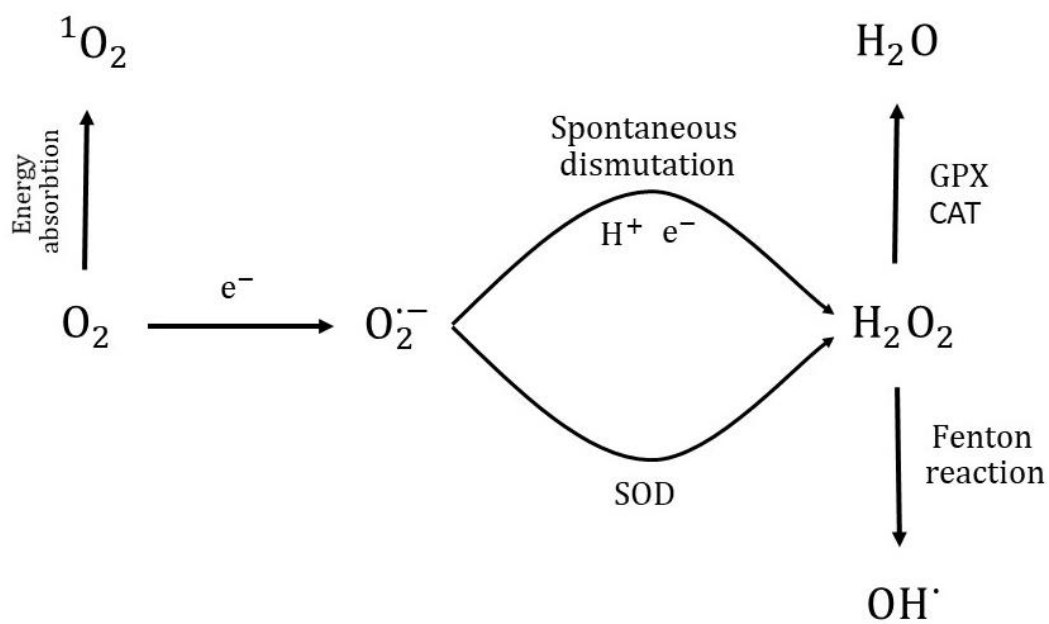
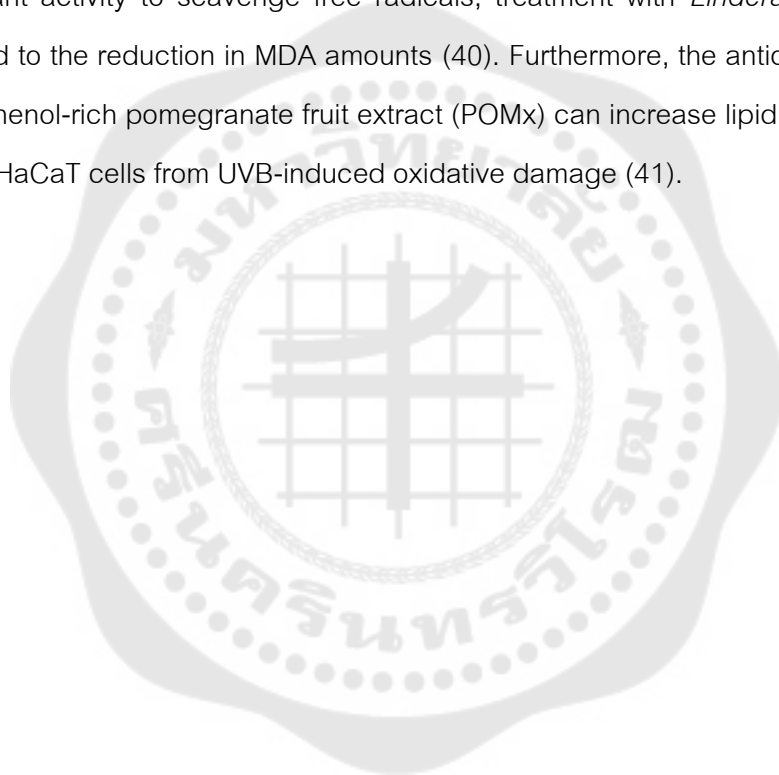


Figure 2 Schematic representation of the generation of reactive oxygen species (ROS) and antioxidant enzyme mechanism.

Source: Sharma P, Jha AB, Dubey RS, Pessarakli M. (2012). Reactive oxygen species, oxidative damage, and antioxidative defense mechanism in plants under stressful conditions: Journal of Botany. p. 3.

By attacking polyunsaturated fatty acids (PUFAs), phospholipid molecules with two carbon atoms, and the ester binding site between fatty acids and glycerol molecules, ROS increases lipid peroxidation. Peroxidation of unsaturated fatty acids generates lipoperoxyl radical (LOO^{\bullet}) and hydroperoxide ($LOOH$), which are unstable

and mostly decomposed to secondary products. Those reactive products found in cell membrane damage from ROS, including malonaldehyde (MDA), acrolein, 4-hydroxynonenal (HNE), or hexanal (Figure 3) (39). As a result, MDA has been commonly used as a marker of ROS-mediated cell membrane disruption in the presence of oxidative stress (39). A recent report has been shown that MDA levels in UVB-irradiated HaCaT cells increased, indicating a lack of membrane integrity, inhibition of membrane proteins, and increased skin cell membrane permeability. However, owing to its antioxidant activity to scavenge free radicals, treatment with *Lindera coreana* leaves (LCE) led to the reduction in MDA amounts (40). Furthermore, the antioxidant properties of polyphenol-rich pomegranate fruit extract (POMx) can increase lipid peroxidation and prevent HaCaT cells from UVB-induced oxidative damage (41).



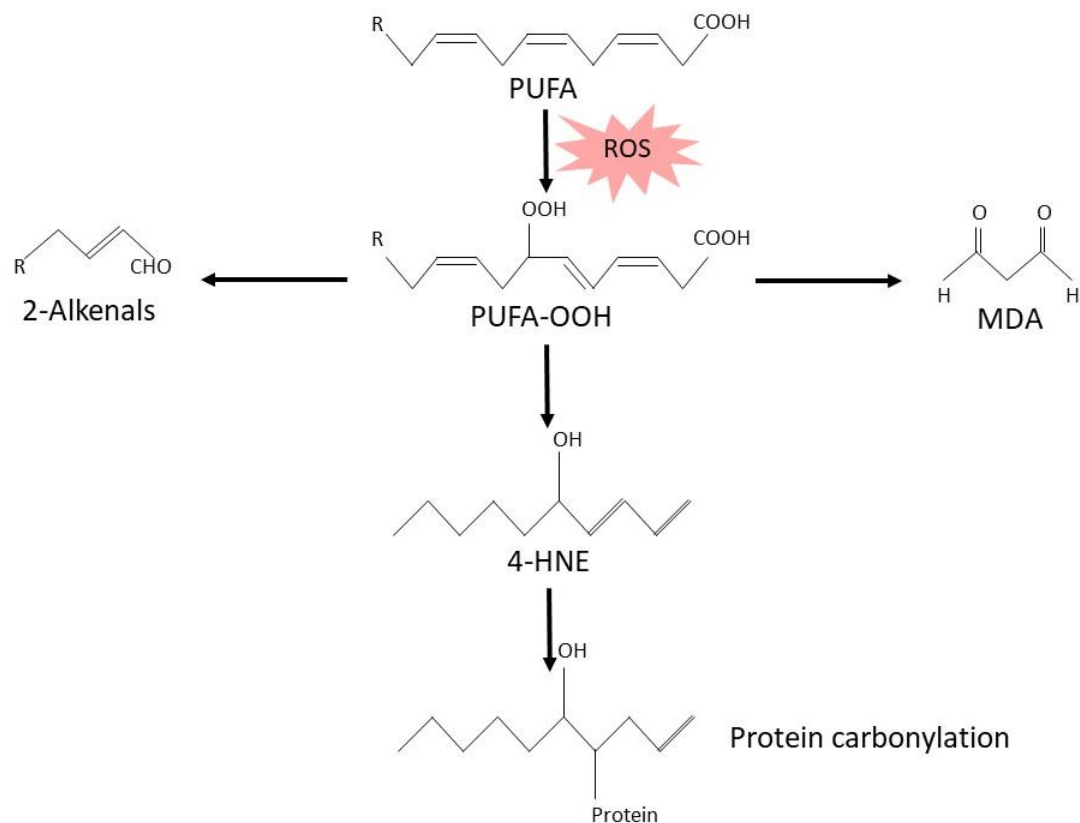


Figure 3 ROS stimulates the peroxidation of polyunsaturated fatty acids (PUFA) and carbonylation of proteins.

Source: Grimsrud PA, Xie H, Griffin TJ, Bernlohr DA. (2008). Oxidative stress and covalent modification of protein with bioactive aldehydes: *The Journal of biological chemistry*. p. 21838.

The UV radiation-induced ROS can damage proteins by direct and indirect modifications, resulting in the loss of protein or enzymatic activity, fragmentation, misfolding, protein aggregation, and degradation. The direct modification of proteins includes nitrosylation, carbonylation, disulfide bond formation, and glutathionylation. Additionally, oxidation of protein with metals and hydrogen peroxide can cause the formation of protein carbonyls, mostly occurring with lysine, arginine, threonine, and

proline residues (42). Alternatively, proteins can be modified by an indirect mechanism through hydroxyl radical-mediated fatty acid peroxidation (43).

The hydroxyl radical (OH^\cdot) also react with deoxyribose sugar-phosphate backbone, purine, and pyrimidine bases (44); especially, the guanine base is frequently attacked by free radical and generates lethal lesions on the DNA strand. The saturated products, hydroxymethyl urea, deoxyguanosine, urea, thymine, and thymine glycol are products of oxidative damage of DNA (38). ROS can affect intrastrand cross-links, purine 5',8-cyclonucleosides, 8-hydroxy-2'-deoxyguanosine (8-OHdG), DNA-protein adducts, and interstrand cross-links (45). Moreover, ROS continuously attacks DNA, resulting in modifications in gene structure and function, alteration of protein-encoding, malfunctions of the encoded proteins, leading to mutation, cancer, and many other diseases.

2.4.3 Photoaging

The UVB part of sunlight is thought to be the most harmful to the skin. Because UVB is able to penetrate the epidermis to enter the top layer of the dermis, it induced accumulating DNA damage and inducing over generating of oxidative stress in the skin. The long-term effects of UVB exposure have been linked to photoaging and carcinogenesis (46). Skin photoaging is induced by UVB irradiation, which is marked by changes in the extracellular matrix (ECM) such as excessive matrix metalloproteinases and collagen deterioration, leading to an increased skin pigment, dry skin, fragility of the skin, inflexibility, delayed wound healing, dimness, and premature aging. UVB caused oxidative stress in fibroblasts, resulting in the production of reactive oxygen species (ROS) and an increase in the expression of matrix metalloproteinase-1 (MMP-1). MMP-1 is an enzyme that destroys collagen type 1, a major component of the extracellular matrix (ECM) that maintains the skin in shape. As a result of collagen break down, the dermis deteriorates, and the development of skin photoaging (47). Molecular signaling pathway response to the photoaging induced by UVB ray including the activation of AP-1-dependent transcriptional through the ERK1/2 pathway, as well as the regurgitation of AP-1-independent mRNA via p38 MAPK. In which, these cascades regulate the

proteolytic pathway of fibroblasts in response to UVB, both AP-1 signaling pathways are essential in photodamage skin cells. The transcription factor AP-1 activates MMPs transcription to produce MMP-1, MMP-2/9, and MMP-3 are some of the MMPs that individually modify the ECM. UVB ray activates the transcription factor NF- κ B, which can lead to an increase in MMP-8 and MMP-9 expression. Likewise, AP-1 also inhibits the type I collagen gene from being expressed leading to the diminishing of collagen synthesis in photoaged skin. While the procollagen is significantly reduced after UVB irradiation, in which the downregulation of collagen synthesis is controlled by AP-1 and transforming growth factor (TGF). As a consequence, the increased depletion of ECM by MMPs, as well as the downregulating of structural collagen fibers, causes severe ECM and tissue stability (48).

2.4.4 Program cell death

Severely DNA damage induced by ultraviolet (UV) radiation can trigger signals that lead to program cell death. These signals involve the tumor suppressor p53 tumor suppressor protein, which controls many pathways responses to DNA damage in keratinocytes. The activation of p53 can release cytochrome c to promote caspase activation. Moreover, UV radiation can also activate cell membrane death receptors (extrinsic pathway) and promote the releasing of cytochrome c, leading to apoptosis (49). The four stages of apoptosis are cellular shrinkage and chromatin condensation, membrane blebbing, organelle separation, and nucleus fragmentation. Apoptotic cells are generally consumed by phagocytic cells before they become apoptotic bodies. This process does not release the cellular components to the extracellular fluid (50). The intrinsic and extrinsic pathways are the two main apoptosis pathways (Figure 4). The mitochondrial response to cellular stress, such as DNA injury, is the focus of the intrinsic pathway. The anti-apoptotic Bcl-2 family is involved in the oligomerization of Bax and Bak and translocation to the mitochondria. Then the caspase complex and cascade are activated when cytochrome c is released from the mitochondria into the cytosol. Then cytochrome c binds to apoptotic protease activating factor-1 (Apaf-1), causing an apoptosome to form and caspase-9 to be activated (49). The binding of death ligands to

death receptors on the cell surface initiates the extrinsic pathway, which consists of cell surface receptors. UV radiation causes the tumor necrosis factor (TNF) receptor family, such as CD95 (Fas/APO-1), to multimerize, resulting in the recruitment of the FADD adaptor protein and caspase-8/10 to transform on the caspase-activating DISC, following by caspase 3 activation. Procaspase3 can be activated to become active caspase3, which also induces apoptosis, in both pathways. Furthermore, the Bcl-2 protein family collaborates on two pathways, and Bid is cleaved by caspase-8 (50). The previous studies showed that UVB irradiation induces apoptosis via both mitochondrial (intrinsic) and caspase-8 stimulation (extrinsic) mechanisms in human keratinocyte HaCaT cells (51).

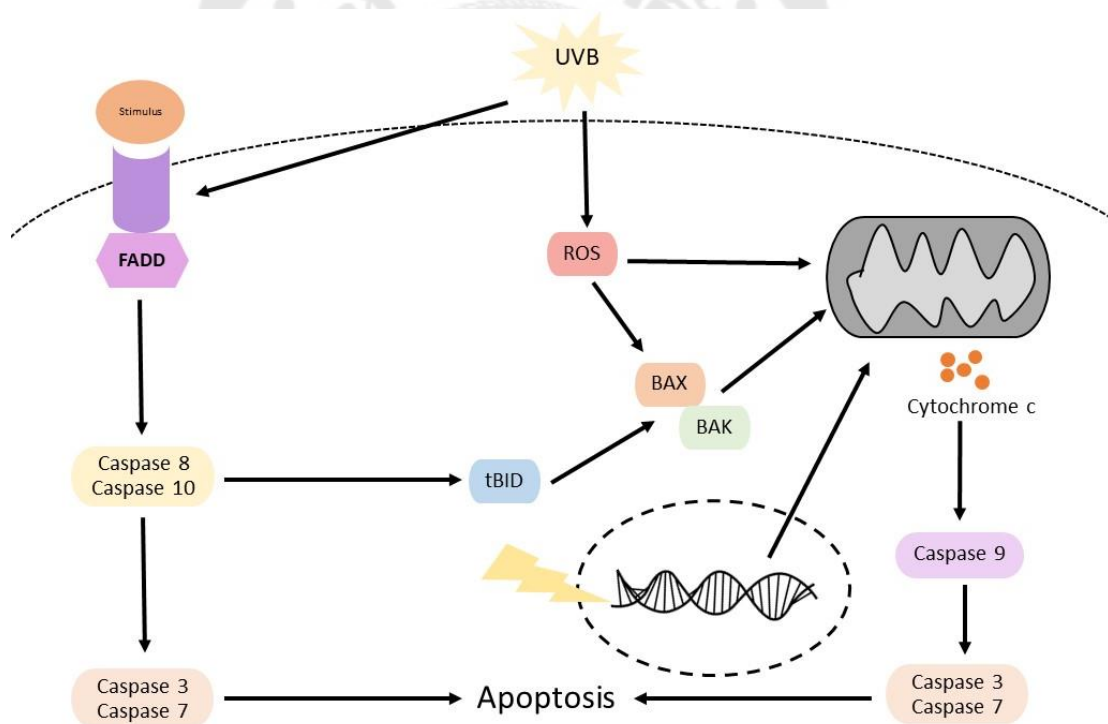


Figure 4 Extrinsic and intrinsic apoptotic signaling pathways.

Source: Ichim G and Tait SWG. (2016). A fate worse than death: apoptosis as an oncogenic process: *Nat Rev Cancer*. p. 540.

2.4.5 Inflammation

By the inducible expression of several genes, the nuclear factor kappa-light-chain-enhancer of activated B cells (NF- κ B) plays a key role in cytokine synthesis, innate and adaptive immune responses, cell proliferation, cell death, cell survival, B-cell growth, lymphoid organogenesis, and inflammation. Furthermore, NF- κ B is found in all cell types which are activated by cytokines, stress, free radicals, heavy metals, viral or bacterial infection, oxidized LDL, and UV radiation. Thus, interruption of the NF- κ B signaling pathway has been contributed to many diseases, including autoimmune diseases, septic shock, and cancer. The NF- κ B signaling pathway can be divided into two pathways base on their variant patterns inactivation and production of protein and enzymes (52). In the classical (canonical) pathway, NF- κ B(p50)/RelA proteins complex bound to independent I κ B molecule (I κ B α) in the cytoplasm. Then the tumor necrosis factor receptor (TNF-R) or Toll-like receptors are activated by proinflammatory cytokines, LPS, growth factors, and antigen receptors leading to induce an IKK complex (containing the IKK β , IKK α catalytic subunits and two molecules of the regulatory scaffold NEMO), which phosphorylates I κ B proteins. Phosphorylation of I κ B protein leads to proteasomal degradation of the I κ B α inhibitors, generation of free NF- κ B(p50)/RelA complex, entering to the nucleus, and also a transcription of target antioxidant genes such as CAT, MnSOD, HO-1, and Gpx-1 (52). The alternative (noncanonical) NF- κ B pathway differs from the classical pathway, p100/RelB complexes are activated during B-and T-cell organ development by certain ligands, including Lymphotoxin B (LTb), B-cell activating factor (BAFF), and CD40(53). The LT β R, CD40, and BR3 receptors are activated lead to send signaling to kinase NIK, which stimulates IKK α complexes. Moreover, phosphorylation of IKK α complexes at NF- κ B(p100)/RelB complexes contributes to activation of NF- κ B(p52)/RelB complexes that translocate to the nucleus and induce target pro-oxidant gene expressions such as iNOS, nNOS, and cyclooxygenase 2 (COX-2) (Figure 5) (54).

UVB-induced ROS causes the transcription factor NF-B to produce pro-inflammatory cytokines like interleukin-1 (IL-1), interleukin-6 (IL-6), and tumor necrosis

factor-alpha (TNF), which leads to immune cell recruitment and activation and is related to transformation, proliferation, and anti-apoptosis (55). Moreover, the arachidonic acid is transformed into Prostaglandin E₂ (PGE₂) via COX-2 enzymes within cells. Thus, PGE₂ is a key mediator in inflammation, angiogenesis, apoptosis tolerance, tumor invasion, and host immune suppression (56).

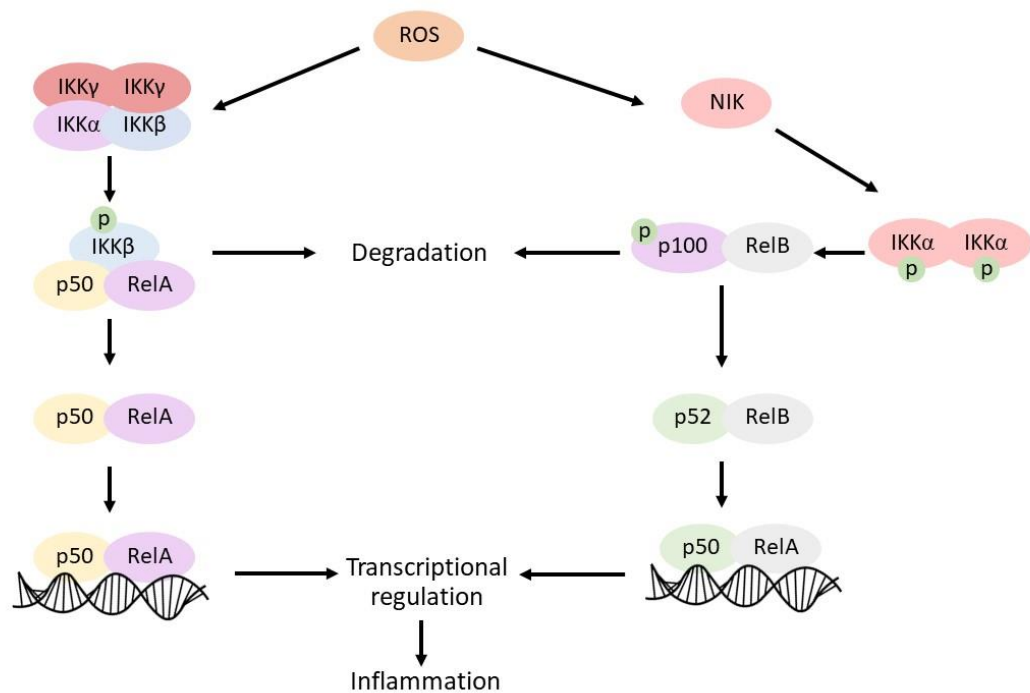


Figure 5 Classical and alternative of the NF- κ B signaling pathway.

Source: Morgan MJ and Liu ZG. (2011). Crosstalk of reactive oxygen species and NF-kappaB signaling: Cell research. p. 106.

2.5 The defense mechanisms in the skin

2.5.1 Antioxidant enzymes mechanism

The higher amounts of ROS are involved in many diseases, including cancer, ischemia, and failures in immunity. But our body has a defense system against excessive ROS. The antioxidant enzymes such as superoxide dismutase, glutathione

peroxidase, and catalase, that enzymes working together and help balance the reactive oxygen species in human cells (36).

Superoxide dismutases (SODs) are metal-containing enzymes, which catalyze the dismutation of the superoxide anion into O_2 and H_2O_2 . SODs have many isoforms, depending on metal ion cofactors such as copper/zinc SOD (Cu/ZnSOD), manganese SOD (MnSOD), and iron SOD (FeSOD), which are found in the cytosol, mitochondria, and extracellular matrix of all aerobic cells(57). Additionally, The Cu/ZnSOD is prominent in the normal human epidermis and its activity is increased in response to UVB damage to the skin (58).

Catalase (CAT) is a heme-containing enzyme that catalyzes the conversion of hydrogen peroxide (H_2O_2) to oxygen and water. CAT is largely present in peroxisomes, but the endoplasmic reticulum and mitochondria contain a little of CAT. A previous study has been reported that UV-induced overexpression of CAT and CuZn-SOD after treated normal human keratinocytes at low temperature, decreased apoptosis by 40% with a reduction of caspase-9 activation (59).

Glutathione peroxidase (GPx) is one of the most essential antioxidant enzymes involved in eliminating fatty acid and H_2O_2 to alcohols and water by coupling with GSH co-substrate. Together with other enzymatic antioxidants, including SOD, CAT, GPx, and glutathione reductase (GR), the GPx activity is decreased dramatically after mouse epidermis and dermis exposed to UV radiation (60).

2.5.2 Nrf2 signaling pathway

Nuclear factor erythroid 2-related factor 2 (Nrf2) is a powerful protein transcription factor. Nrf2 signaling pathway regulates the production of antioxidant enzymes or survival genes that protect cells from UV radiation-induced oxidative damage (61). In normal conditions, Nrf2 is attached by Kelch ECH associating protein 1 (Keap1) and promotes degradation by the ubiquitin-proteasome pathway. The genes are inactive due to repressive factors (Bach1) and small Maf dimers bound to the antioxidant response elements (AREs). Under oxidative stress conditions, the Nrf2-Keap1 complex is degraded and Nrf2 migrates into the nucleus, followed by the

formation of Nrf2-small Maf dimers bound to the ARE. As a result, the antioxidant gene is expressed to maintain cellular homeostasis (62). Furthermore, the alkylation of the Keap1 by 4-HNE, lead to the aggregation of the Keap1-Nrf2 complex. Thus Nrf2 translocate into the nucleus and activates the expression of ARE-containing genes, which increasing antioxidant defenses (42). The study revealed that the Nrf2 signaling pathway can directly activate by PKC, MAPK, ERK, and other protein kinases, thereby upregulating the expression of antioxidant enzymes (63). On the other hand, the Nrf2 signaling pathway and downstream target genes HO-1, NQO1, P-glycoprotein (P-gp), MRP2 are activated by *Phyllanthus emblica* L. extract in HepG2 cells (64)

2.5.3 NER repair mechanism

Generally, an organism has a mechanism to prevent or repair the damage. There are three pathways of DNA repair, including Nucleotide excision repair (NER), base excision repair (BER), and DNA mismatch repair (MMR) (65). The NER is the main mechanism, which can remove DNA lesions and prevent mutagenesis in UVB-induced cells (66). In the global genome NER (GG-NER), the detection site of DNA damage is recognized by the XPC-RAD23B protein, while the lesions are defined by RNA Pol II in transcription-coupled repair (TC-NER). The damaged double strands DNA is unwound, followed by endonucleases (XPF/ ERCC1 heterodimer to XPG protein) excise the damaged DNA fragment. After, DNA polymerase synthesizes the corrected DNA strand. Finally, DNA ligase joins the nick between the newly synthesized and older DNA strand (67). NER is hampered in the absence of a functioning p53 protein, which may lead to non-melanoma skin cancers (68). The study previously found that UV irradiation promotes by inhibition of gap-filling DNA synthesis in the NER process in keratinocytes (69).

2.5.4 Cell survival signaling pathway

The cell survival-associated signaling phosphoinositide 3-kinase (PI3K) and serine/threonine kinase Akt pathway plays a crucial role in the prevention of apoptosis, growth, transcription, protein synthesis, and proliferation in UVB-induced skin cell (70). Growth factors and cytokines activate the PI3K/Akt signaling cascade, which raises the amount of intracellular Reactive Oxygen Species (ROS) and UV-induced DNA damage.

The dimerization and activation of membrane receptors tyrosine kinases (RTKs) promote signaling cascades. Thus, The PI3K phosphorylates phosphatidylinositol (3,4,5) trisphosphates (PIP3). Then PIP3 activates PDK1, which partially phosphorylates Akt at Thr308 residue. Accordingly, Akt is stimulated as full enzymatic activity by mTOR, which phosphorylates at Ser473 residue (Figure 6) (71). The Phosphorylated Akt can activate IKK α and regulates NF- κ B activation to transcript the pro-survival genes. Cell survival is also promoted by Akt phosphorylation of FoxOs proteins, which regulate the pro-apoptotic protein Bim, TRAIL, and FasL (72). Moreover, the tumor suppressor phosphatase and tensin homolog deleted from chromosome ten (PTEN) can dephosphorylate PIP3 to PIP2 which turns down the PI3K/Akt signaling pathway. In many cancers, PTEN is mutated leading to dysregulation of the PI3K/Akt pathway (73). As a result, the Akt signal transduction pathway promotes proliferation, migration, cell survival, tissue invasion, and angiogenesis in melanoma. This pathway is overactive in cell cycle transition and hyper-proliferation in skin cancer cells due to mutations of certain tumor suppressor genes, PTEN, encoding the abnormal inhibitor protein of the AKT signaling pathway (74). Results from previous studies have shown that myricetin treatment inhibited Akt signaling pathway, leading to inhibition of its protein kinase activity and a decrease in phosphorylation of a pro-apoptotic protein BAD in UVB-irradiated HaCaT cells (75).

The mitogen-activated protein kinases (MAPKs) are serine and threonine protein kinases which are also known to play fundamental roles in cell survival, death, differentiation, proliferation, and apoptosis (76). The three different MAPKs family subgroups consist of the c-Jun NH2-terminal kinase (JNK) pathway, extracellular signal-regulated kinase (ERK), and p38 (Figure 6). Each MAPK signaling cascade includes a certain three components, MAPK kinase kinase (MAP3K), MAPK kinase (MAP2K), and MAPK. The activated MAP3K phosphorylate MAP2K, which phosphorylate and activate MAPK respectively. The activation of MAPK pathways has generated the interaction between the kinase components with specific scaffold proteins such as MEK partner 1 (MP1) and kinase suppressor of Ras-1 (KSR) for ERK cascade, JNK-interacting proteins

(JIPs) for the JNK pathway, whereas β -Arrestin 2 acts as a scaffold protein for both the ERK and JNK cascades (75). Besides, the MAPKs cascades are activated by various extracellular stimuli such as mitogens, growth factors and cytokines, and a variety of intracellular stressors including UV light, oxidative stress, endoplasmic reticulum stress, lipopolysaccharide (LPS), Ca^{2+} influx, and inflammation. Especially, UV radiation can induce cellular responses in three different MAPK signaling pathways. A previous report suggested that the UVB exposure of normal human keratinocytes (NHKs) triggers oxidative stress and activates p38 and JNKs signaling pathway, followed by the activation of proapoptotic proteins Noxa and Bim (77). Furthermore, The JNK and ERK mitogen-activated protein kinase (MAPK) is activated by ROS from UVB irradiation in human primary epidermal keratinocytes. In turn, the keratinocytes treated with MAPK, and JNK inhibitors, showed a significant decrease in cell survival and an increase in apoptosis (78).

The activation of the ERK signaling pathway through RTKs such as the epidermal growth factor receptor (EGFR) is initiated by various stimuli, which intern activate MAP4K and Ras GTPase. The Ras GTPase activates MAP3K or Raf, which phosphorylate MEKs. As a result, ERK is activated by MEKs leading to the translocate of MEKs into the nucleus and transactivation of several protein transcription factors, which are involved in cell survival and proliferation (79). It has been suggested that stimulation of EGFR by H_2O_2 generation from UV rays may lead to activation and autophosphorylation of intracellular signaling pathways through PI3K and ERKs, but not JNKs or p38 kinase signaling cascades (80). Importantly, UV irradiation rapidly activates translocation and accumulation of EGFR from the cell surface membrane to the nucleus in HaCaT and primary human keratinocytes, which regulate gene transcription and cell proliferation (81). The four members of the p38 MAP-Kinases pathway consist of p38 α , p38 β , p38 γ , and p38 δ . The activation of membrane receptor phosphorylates MAP3K and stimulate MKK3/6. Moreover, The MKK3/4 can also activate p38 MAPK kinases, which stimulate several transcription factors including ATF2, Elk-1, and Stat1 (82). The JNK signaling pathway is induced by proinflammatory cytokines such as TNF- α and IL-

1β , which activate MAP3K such as ASK1 and MEKK1. The MAP3K activates JUNKK and JNKs. Therefore, the activated JNK translocates into the nucleus and phosphorylate transcription factors such as Elk-1, c-Jun, ATF2, and AP-1, triggering cellular responses (83). The phosphorylate c-Jun can regulate cell proliferation, survival, death, DNA repair, and metabolism in skin cells.

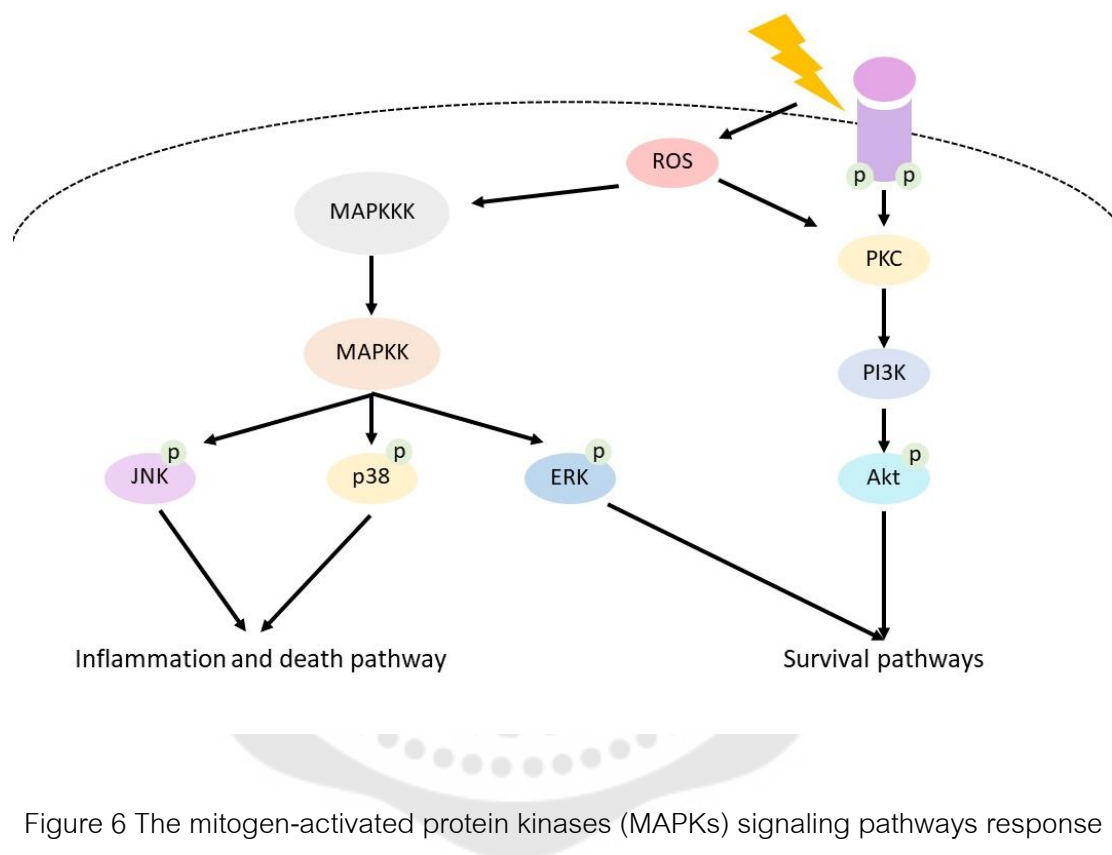


Figure 6 The mitogen-activated protein kinases (MAPKs) signaling pathways response to UV radiation.

Source: López-Camarillo C, Ocampo EA, Casamichana ML, Pérez-Plasencia C, Álvarez-Sánchez E and Marchat LA. (2012). Protein kinases and transcription factors activation in response to UV-radiation of skin: implications for carcinogenesis: International journal of molecular sciences. p. 145.

ROS-related UVB production induces skin photo aging through both NF- κ B and AP-1 pathways, along with an activation of Nrf2 antioxidant pathway. The induction

of MAPK pathways including p38 and JNK act as key factor roles, in which phosphorylation of p38 induces NF- κ B translocation into the nucleus producing inflammation mediator protein, COX-2 leading to skin inflammation. While activation of JNK drives AP-1 pathway promoting MMPs production and releases to destroy collagens resulting in skin aging. Although the rise of ROS induces oxidative stress and damage cell, antioxidant mechanisms also activated to eliminate and balance excessive ROS via Nrf2 signaling promoting cell homeostasis (Figure 7).

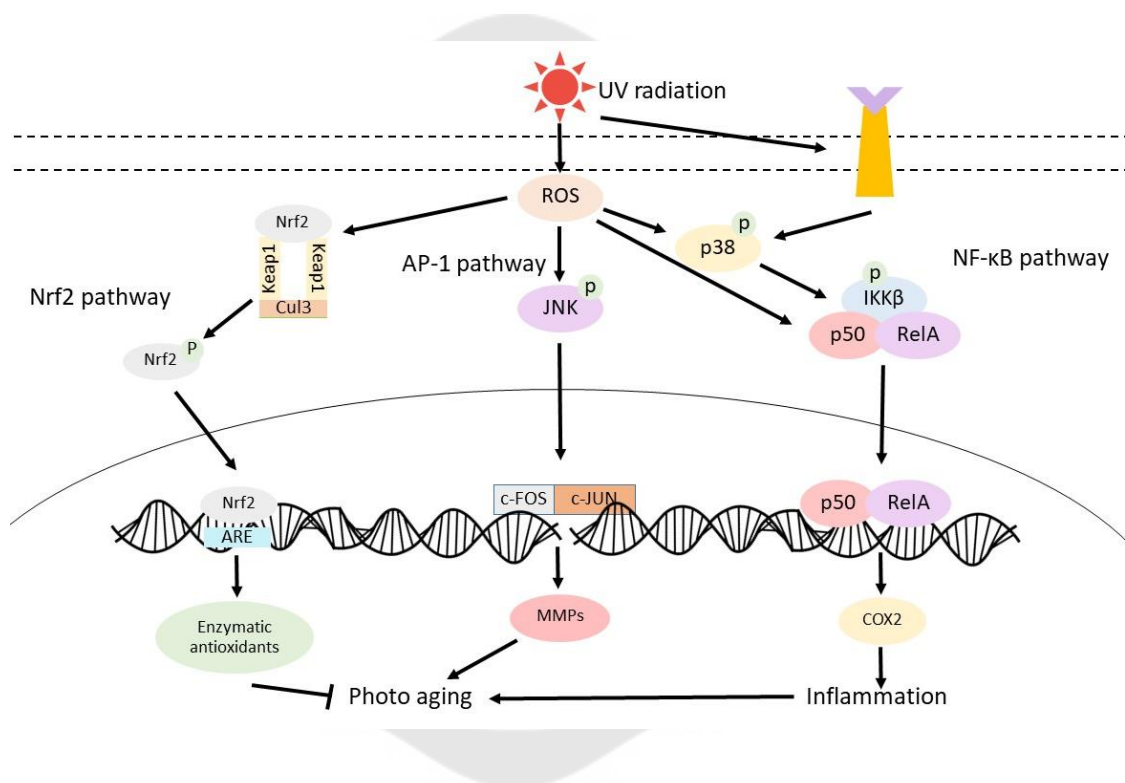


Figure 7 The transcription factors response to UV radiation.

Source: López-Camarillo C, Ocampo EA, Casamichana ML, Pérez-Plasencia C, Álvarez-Sánchez E and Marchat LA. (2012). Protein kinases and transcription factors activation in response to UV-radiation of skin: implications for carcinogenesis: International journal of molecular sciences. p. 152.

2.6 *Phyllanthus emblica*

Natural products are chemical compounds which are generated by living organisms in the environment, such as bacteria, fungi, plants, and animals. Natural compounds for dermatological application in humans are often used as oral nutritional supplements and also as topical skincare. As natural substances have been produced by nature, these natural products are also not toxic to our skin and ecosystem. Additionally, the risk of skin irritation is minimized by natural resources found in natural health and skincare products, particularly people who are highly allergic to synthetic chemicals. There seems to be a continually expanding cosmetic industry for photoprotective products focused on natural compounds. The goal of natural product skincare study is not only to enhance the overall appearance of the skin but also to prevent and cure skin disorders (84, 85). Nonetheless, in skincare products, extracts from plants and other natural ingredients have widely been used, but the effectiveness of many of these compounds is still yet to be tested.

The next generation of sunscreen produces from phytochemical to long-life endogenous skin healthy protection. Many phytochemicals have been informed to be effective in protecting UVB-induced oxidative damage in vitro and in vivo (86). One of them, *Phyllanthus emblica* (PE) Linn. (syn. *Embllica officinalis*), family Euphorbiaceae, is commonly known as Indian gooseberry or amla and called Makham Pom in Thailand. PE is a significant medicinal herb which has long been used in Asian traditional medicine to defend against a variety of diseases (41). The PE distribute throughout tropical and subtropical countries such as Thailand, India, and China (87). The PE is a moderate-sized tree, and its fruits are spherical in shape, light greenish yellow with six vertical stripes having a sour, astringent, and acidic taste. The various parts of PE also are used in Ayurveda medicine, including the fruit, seed, leaves, root, bark, and flowers (88). The extracts from various parts of PE contain active constituents including tannins, mucic acid, alkaloids, flavonoids, and alkaloids (Table 1). Many studies have been reported that ellagic acid and its derivative ellagic acid-4-O-glucoside, ellagic acid-4-O-xyloside, and ellagic acid-4-O-rhamnoside (89), gallic acid (90) and its derivative methyl gallate,

1-O-galloyl-glucoside, mucic acid 3-O-gallate (91), corilagin, mucic acid-1,4-lactone-3-O-gallate (92), 1,6-di-O-galloylglucoside was found in PE. Especially, the highest amount of vitamin C found in fruit juice extract of PE compared to other fruits. (93). For several decades, the PE fruit extract had been confirmed to have a high antioxidant potential and its antioxidant properties can protect normal human dermal fibroblasts from UVB-induced ROS and UVB-induced photo-aging lead to collagen damage (94). Moreover, PE has a potential for pharmacological application such as an anti-diabetic (95), cardio-protective (96), anti-inflammation (97) (Table 2). Fruit juice extract of PE has been found anti-radical activity (98). Interestingly, PE has not been investigated protective effect against UV-induced skin cell damage yet.

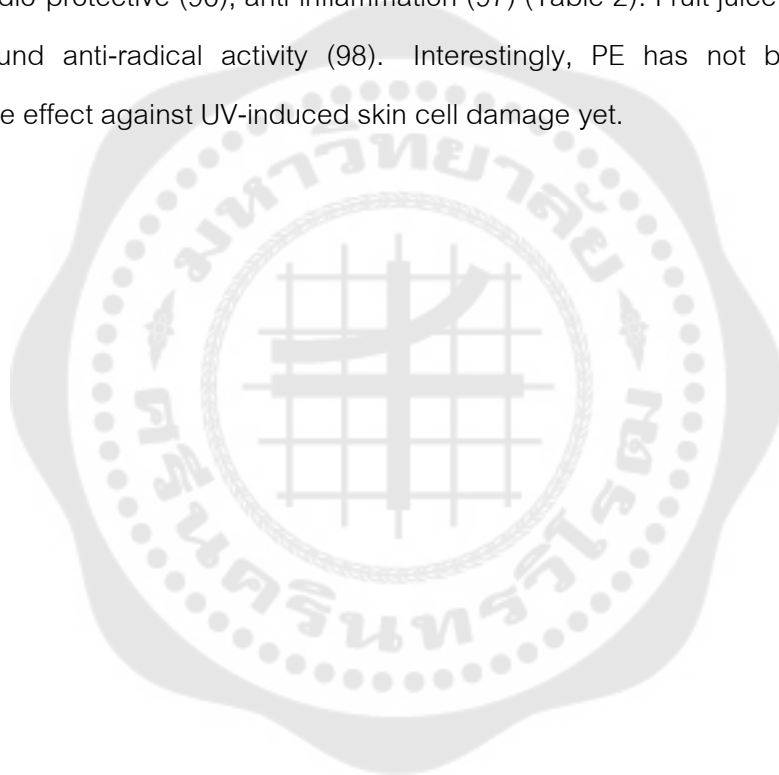


Table 1 Summary of chemical constituents and activity of *Phyllanthus emblica*

Part used	Extraction method	Main composition	Methods	<i>In vitro</i> activity	References
Fruit	Aqueous acetone extract	Galloyl mucic acid, phyllanemblinins A–F, and chebulagic acid	DPPH scavenging assay	Antioxidant and scavenging activities	Zhang et al., 2001 (99)
Fruit	Aqueous extract	Vitamin C (Ascorbic acid)	Different antioxidant tests	Antioxidant and scavenging activities	Scartezzini et al., 2006 (63)
Fruit	Methanolic extract	Geraniin, quercetin 3- β -d-glucopyranoside, kaempferol 3- β -d-glucopyranoside, isocorilagin, quercetin, and kaempferol	Lipid peroxidation and DPPH systems.	Antioxidant and scavenging activities	Liu et al., 2008 (64)
Fruit	Ethanollic extract	Gallic acid, ellagic acid, mucic acid 1,4-lactone 3-O-gallate, isocorilagin, chebulanin, chebulagic acid and mallotusin	Superoxide anion, DPPH and ABTS scavenging, lipid peroxidation	Antioxidant and scavenging activities	Luo et al., 2011 (3)
Fruit	Aqueous extract	Carbohydrate polymers	DPPH scavenging assay and FRAP assay	Antioxidant and scavenging activities	Chatterjee et al., 2011 (59)
Fruit	Ethanollic extract	Mucic acid 1,4-lactone 3-o-gallate, isocorilagin, chebulanin, chebulagic acid and isomallotusin	DPPH and ABTS radical scavenging assay	Antioxidant and scavenging activities	Luo et al., 2012 (69)

Table 1 (Continued)

Part used	Extraction method	Main composition	Methods	<i>In vitro</i> activity	References
Fruit	Aqueous ethanolic extract	3,4,8,9,10-pentahydroxy-dibenzo[b,d]pyran-6-one, gallic acid, ethyl gallate, and methyl gallate	DPPH scavenging assay	Antioxidant and scavenging activities	Zhang et al., 2017 (100)
Fruit	Aqueous ethanolic extract	Ethyl gallate	MTT assay, DCFH-DA and flow cytometry	Cyto-protective effects and anti-oxidative stress	Zhang et al., 2017 (100)
Roots	Aqueous ethanolic extract	Glochicoccinoside D	Anti-virus assay	Anti-viral	Lv et al., 2015 (101)
Roots	Aqueous ethanolic extract	Phyllaemblicin H1	MTT assay	Cytotoxicity against human cancer cell	Lv et al., 2015 (101)
Branches and leaves	Ethanolic extract	Trihydroxysitosterol	MTT assay	Cytotoxicity	Qi et al., 2013 (102)

Table 2 Summary of previous studies pharmacological activity of *Phyllanthus emblica*

Part used	Extraction method	Dose	Model of study	Pharmacological activity	References
Fruits	Methanolic extract	10 - 1000 $\mu\text{g/mL}$	Male Wister albino rats	Dermato-protective activity	Kumar et al., 2008 (103)
Fruits	Ethanollic extract	0 - 40 g/mL	Human skin fibroblast	Dermato-protective activity	Fujii et al., 2008 (104)
Fruits	Ethanollic extract	0.1 mg/mL	Primary mouse fibroblast cells	Dermato-protective activity	Chanvorachote et al., 2009 (105)
Fruits	Aqueous extract	500 mg/kg b.w.	Adult male Swiss albino mice	Hepatoprotective activity	Sharma et al., 2009 (106)
Fruits	Ethanollic extract	50 - 100 $\mu\text{g/mL}$	Human cancer cell lines, A549 (lung), hepg2 (liver), hela (cervical), MDA-MB-231 (breast), SK-OV3 (ovarian) and SW620 (colorectal)	Anti-tumour activity	Ngamkitidec hakul et al., 2010 (107)
Fruits	Ethanollic extract	10 - 40 g/mL	Human skin fibroblasts	Dermato-protective activity	Adil et al., 2010 (108)
Fruits	Aqueous extract	0.5 mg/mL	Normal human dermal fibroblasts.	Dermato-protective activity	Majeed et al., 2011 (94)
Fruits	Ethanollic extract	1 g	C57BL/6 mice	Hair growth-promoting activities	Kumar et al., 2012 (109)

Table 2 (Continued)

Part used	Extraction method	Dose	Model of study	Pharmacological activity	References
Fruits	Hydro-alcoholic extract	100, 250 and 500 mg/kg b.w.	Wistar male albino rats	Cardio-protective activity	Ojha et al., 2012 (110)
Fruits	Hydro-alcoholic extracts	2.5, 5,10,25,50 and 100 µg/mL	Rinm5f cell line	Anti-diabetic activity	Kalekar et al., 2013 (111)
Fruits	Hydro-alcoholic extracts	200 µg/mL	The 3T3 L1 fibroblast cells	Anti-diabetic activity	Kalekar et al., 2013 (112)
Fruits	Ethanollic extract	500 mg/kg b.w.	Balb/c male mice	Antioxidant activity	Singh et al., 2013 (113)
Fruits	Ethanollic Extract	1.25 g/kg b.w.	Rats	Anti-diabetic activity	Sultana et al., 2014 (114)
Fruits	Aqueous extract	100 mg/kg b.w.	Rats	Cardio-protective activity	Thirunavukkarasu et al., 2015 (115)
Fruits	Aqueous extract	100 mg three times/day for 6 months	Patients with vitiligo	Dermato-protective activity	Colucci et al., 2015 (116)
Fruits	Commercially available crude extract	200 and 400 mg/kg b.w.	Rats	Anti-diabetic activity	Pathak et al., 2016 (117)
Fruits	Methanollic extracts	25, 50, and 75 mg/kg b.w.	Rats	Anti-diabetic activity	Srinivasan et al., 2017 (118)

Table 2 (Continued)

Part used	Extraction method	Dose	Model of study	Pharmacological activity	References
Fruits	Methanolic extract	250 or 500 mg/kg b.w.	Rats	Anti-diabetic activity	Fatima et al., 2017 (119)
Fruits	Aqueous extract	250 - 750 mg/kg, b.w.	Male Wistar rats	Cardio-protective activity	Kumar et al., 2017 (120)
Leaves	Hydro-methanolic extract	100, 200, 300 and 400 mg/kg b.w.	Rats	Anti-diabetic activity	Nain et al., 2012 (121)
Leaves	Ethanollic Extract	10 µg/g b.w. /day	Male Swiss albino mice	Protecting against arsenic-mediated toxicity	Sayed et al., 2015 (122)
Seeds	Aqueous extract	300 mg/kg body weight	Rats	Anti-diabetic activity	Mehta et al., 2009 (123)

CHAPTER 3

RESEARCH METHODOLOGY

3.1 Materials and Chemicals

Elix [®] type 2 pure water systems	Merck Millipore, USA
Milli-Q [®] type 1 ultrapure water systems	Merck Millipore, USA
Biological safety cabinet, class II (NU440 400E model)	NuAire, USA
AutoFlow water jacket CO ₂ incubator (NU-4750 model)	NuAire, USA
High-speed centrifuge (Z 32 HK model)	HERMLE, Germany
Centrifuge (5430R model)	Eppendorf, Germany
Inverted microscope (CKX41 model)	Olympus, Japan
Microscope camera (DP20 model)	Olympus, Japan
Analytical balances (A200S model)	Sartorius, Germany
Microplate reader SpectraMax [®] M2e	Molecular Devices, USA
Microplate reader Synergy [™] HT	BioTek, USA
Liquid nitrogen tank (LS750 model)	Taylor-Wharton, USA
Vortex mixer Genie 2 (G560E model)	Scientific industries, USA
Hotplate magnetic stirrer (C-MAG HS 7 model)	IKA, Germany
Hotplate magnetic stirrer (MSH-20A)	WiseStir, Germany
Mini rocker shaker (MR-1 model)	Biosan, Latvia
Plate shaker (LD40 model)	Labinco, Netherlands
Ultrasonic cleaning unit (Elmasonic S 450 H)	ElmaSchmidbauer, Germany
UV-VIS spectrophotometer (UV-1800)	Shimadzu, Japan
Fume Hood	FLEXLAB, Thailand
Chemical storage cabinet	FLEXLAB, Thailand
Flammable storage cabinet	FLEXLAB, Thailand
Autoclave (ACV-3167 model)	IWAKI, Japan
Autoclave (SX-500E model)	TOMY, Japan

Oven (UF260 model)	Memmert, Germany
Circulating water bath	Heto Therm, USA
Dry bath (HB-48 one block model)	Witeg, Germany
Benchtop pH Meter (Lab 855 model)	Analytics, Germany
Benchtop pH meter (pH 700 model)	Eutech Instruments, UK
IDS Electrode BlueLine 14 pH	SI Analytics, Germany
Vibra-Cell™ Ultrasonic Liquid Processors	Sonics & Materials, USA
Analytical Weighing Balances (BSA3202S-CW model)	Sartorius, Germany
Analytical Weighing Balances (BSA2245S-CW model)	Sartorius, Germany
Analytical Weighing Balances (A 200 S model)	Sartorius, Germany
Filtration assembly, 300 mL	Auxilab, Spain
Freezing Container	Thermo Fisher, USA
Cryogenic vial	Thermo Fisher, USA
Counting Chamber (0.100 mm)	HBG, Germany
Single channel pipette 0.1-2 μ L	Rainin, USA
Single channel pipette 0.5-10 μ L	Rainin, USA
Single channel pipette 10-100 μ L	Rainin, USA
Single channel pipette 20-250 μ L	Rainin, USA
Single channel pipette 100-1,000 μ L	Rainin, USA
Single channel pipette 500-5,000 μ L	Rainin, USA
Single channel pipette 1-1,000 mL	Rainin, USA
Multichannel pipette 5-50 μ L	Rainin, USA
Multichannel pipette 20-200 μ L	Rainin, USA
Pipette controller	Rainin, USA
Non-sterile 96-well plate, Flat bottom	PL Life Sciences, Korea
96-well black immunoplate	SPL Life Sciences, Korea
6-well cell culture plate	Corning, USA
96-well cell culture plate	Corning, USA
Sterile centrifuge tube 15 mL	Corning, USA

Sterile centrifuge tube 50 mL	Corning, USA
Sterile 25 cm ² cell culture flask	Nunc, Denmark
Sterile 75 cm ² cell culture flask	Corning, USA
Sterile 35 mm cell culture dish	Nunc, Denmark
Sterile 60 mm cell culture dish	Nunc, Denmark
Sterile 100 mm cell culture dish	Nunc, Denmark
DeckWorks pipet tips 200 µL	Corning, USA
Pipet Tips 250 µL	Rainin, USA
Pipet Tips 1,000 µL	Sarstedt, Germany
Laboratory glass bottle 50 mL	Duran, Germany
Laboratory glass bottle 100 mL	Duran, Germany
Laboratory glass bottle 200 mL	Duran, Germany
Laboratory glass bottle 500 mL	Duran, Germany
Laboratory glass bottle 1000 mL	Duran, Germany
Examination gloves	Sri Trang, Thailand
Safe seal microcentrifuge tube 1.7 mL	Sorenson Bioscience, USA
LC pump (LC-20AD)	Shimadzu, Japan
Autosampler (SIL-20AC HT)	Shimadzu, Japan
HPLC column oven (CTO-20A)	Shimadzu, Japan
Photodiode array detector (SPD-M20A)	Shimadzu, Japan
System controller (CBM-20A)	Shimadzu, Japan
Inertsil [®] ODS-3 analytical Reversed-phase C18 columns	GL Sciences, Japan
0.45 µm nylon syringe filter	Johnson test papers, UK
2 mL, Screw neck ND9 vial, clear/amber	CeiExpert, Thailand
9 mm, PP screw thread cap with PTFE/silicone septa	CeiExpert, Thailand
Syringe 10 mL	Terumo, Japan
Nylon filter membrane, 0.45 µm pore size	Merck Millipore, USA
Nalgene [™] Reusable Filter Holders with Receiver	Nalge company, USA
UV incubator BIO SUN Ultra violets	Vilber Lourmat, Germany

Mr. Frosty™ Freezing container	Thermo Scientific
Cryotube	Thermo Scientific
Sodium bicarbonate (NaHCO ₃)	Sigma-Aldrich, USA
HaCaT cell line	Cell line service, Germany
Sodium carbonate (Na ₂ CO ₃)	Merck Millipore, USA
Sodium hydroxide (NaOH)	Merck Millipore, USA
Dulbecco's modified Eagle medium (DMEM)	Life Technologies, USA
Fetal bovine serum (FBS)	Life Technologies, USA
Penicillin Streptomycin	Life Technologies, USA
2.5% Trypsin (10x)	Life Technologies, USA
200 mM L-Glutamine	Life Technologies, USA
Thiazolyl blue tetrazolium bromide (MTT)	Bio Basic, USA
Dimethyl sulfoxide (DMSO)	Sigma-Aldrich, USA
Trolox	Sigma-Aldrich, USA
Hydrogen peroxide (H ₂ O ₂)	Sigma-Aldrich, USA
2-Deoxy-D-ribose	Sigma-Aldrich, USA
Ethylenediaminetetraacetic acid (EDTA) trisodium salt	Sigma-Aldrich, USA
Iron (III) chloride (FeCl ₃)	Sigma-Aldrich, USA
Sodium L-ascorbate	Sigma-Aldrich, USA
Trichloroacetic acid (TCA)	Sigma-Aldrich, USA
Thiobarbituric acid (TBA)	Sigma-Aldrich, USA
Hydrogen peroxide (H ₂ O ₂)	Sigma-Aldrich, USA
NaOH	Sigma-Aldrich, USA
Sodium phosphate dibasic dihydrate (Na ₂ HPO ₄ ·2H ₂ O)	Merck Millipore, USA
Sodium dihydrogen phosphate monohydrate	Merck Millipore, USA
Sodium hypochlorite (NaOCl)	Sigma-Aldrich, USA
Sodium borohydride (NaBH ₄)	Sigma-Aldrich, USA
5,5'-dithiobis (2-nitrobenzoic acid) (DTNB)	Sigma-Aldrich, USA
Sulfuric acid (H ₂ SO ₄)	Merck Millipore, USA

Dipotassium phosphate, dibasic dihydrate	Merck Millipore, USA
Potassium phosphate, monobasic, monohydrate	Merck Millipore, USA
Acetonitrile HPLC grade	Merck Millipore, USA
Methanol HPLC grade	Merck Millipore, USA
Phosphoric acid	Merck Millipore, USA
Standard ascorbic acid	Merck Millipore, USA
Standard ellagic acid	Sigma-Aldrich, USA
Standard gallic acid	Sigma-Aldrich, USA
Standard chlorogenic acid	Sigma-Aldrich, USA
Standard quercetin	Sigma-Aldrich, USA
Standard phyllanthin	Sigma-Aldrich, USA
Purpald	Sigma-Aldrich, USA
Potassium periodate	Sigma-Aldrich, USA

3.2 Methods

3.2.1 HPLC analysis

HPLC analysis was run on Shimadzu chromatographic system (Shimadzu, Japan). Acetonitrile, methanol, HPLC grade water, and 20 mM Phosphate buffer (pH 2.5) were used as the mobile phase in HPLC. The 20 mM Phosphate buffer (pH 2.5) was prepared by combining 200 mL of 100 mM Sodium dihydrogen phosphate buffer with 200 mL of 100 mM phosphoric acid and added HPLC grade water to create the buffer solution of total volume 1 L. The phosphate buffer was adjusted pH value to 2.5 using a pH meter by adding phosphoric acid. All solutions and solvents were filtered through nylon membrane filters and degassed before use. Standard chemical ascorbic acid, ellagic acid, gallic acid, chlorogenic acid, quercetin, and phyllanthin were used for reference compounds and created standard curves in reverse phase HPLC analysis. All standards were prepared as a stock solution of 10 mg/mL. An ascorbic acid stock solution was dissolved and diluted to 6.25, 12.5, 25, 50, and 100 µg/mL in HPLC grade water. The Ellagic acid stock solution was dissolved in 0.1 M NaOH following manufacturer recommendation and then diluted to 6.25, 12.5, 25, 50, and 100 µg/mL in

50% methanol. Gallic acid stock solution was dissolved in 100% methanol and diluted to 12.5, 25, 50, 100, and 200 µg/mL in methanol with HPLC grade water (1:1). Moreover, Standard mixture combining with quercetin, chlorogenic acid, and phyllanthin, each stand stock solution was also diluted in 100% methanol and diluted to 6.25, 12.5, 25, 50, and 100 µg/mL in 100% methanol. The PE crude extract was dissolved in HPLC grade water and mixed for 10 min using a vortex mixer to prepare stock solution 50 mg/mL. Afterward, PE solution was sonicated using Vibra-Cell™ Ultrasonic Liquid Processors, 35% amplitude for 30 sec. PE solution was diluted to 5 and 10 mg/mL in 50% methanol for HPLC analysis. After preparation, all standard solutions and PE solutions were filtered through a 0.45 µm nylon membrane syringe filter to prevent column blockage. HPLC condition determination of ascorbic acid in PE was conducted using isocratic elution at a flow rate of 0.5 mL/min and wavelength detection at 243 nm. The samples and standard volume were injected at 20 µL. Liquid chromatography running time was stopped at 15 min. A graph peak of ascorbic acid appeared at the retention time of 9.806 min. One hundred percent of 20 mM Phosphate buffer (pH 2.5) was used as a mobile phase. The optimization of chromatographic condition for determination of ellagic acid in PE was modified from Sawant et al. The mobile phase contained 70% of 20 mM Phosphate buffer (pH 2.5) (eluent A) and 30% of acetonitrile (eluent B). The isocratic elution was used for detection following criteria; flow rate 1 mL/min, wavelength detection at 253 nm, injection volume of 20 µL, and liquid chromatography running time of 10 min. A spectra peak of ascorbic acid appeared at the retention time of 4.993 min. The optimization of chromatographic conditions for the determination of gallic acid in PE was performed under isocratic elution at a flow rate of 1.5 mL/min and wavelength detection at 270 nm. The samples and standards volume were injected at 20 µL. Liquid chromatography running time was stopped at 10 min. A graph peak of ascorbic acid appeared at the retention time of 4.949 min. The mobile phase contained 95% of 20 mM Phosphate buffer (pH 2.5) (eluent A) and 5% of acetonitrile (eluent B). The samples and standard solutions were analyzed using a gradient elution of 20 mM Phosphate buffer (pH 2.5) (eluent A) and acetonitrile (eluent B) at a flow rate 1.5 mL/min to determine

chlorogenic acid, quercetin, and phyllanthin in PE. The optimization of chromatographic parameters was modified from Sawant et al. The gradient elution was performed as the following condition: 0-3 min, 0-10% B; 3-15 min, 0-90% B; 15-21 min, 90% B; 21-22 min, 90-10% B; 22-30 min, 10% B. The UV detection wavelength of chlorogenic acid, quercetin, and phyllanthin was set at 325 nm, 255 nm, and 280 nm, respectively. The samples and standard volume were constantly injected at 20 μ L. Liquid chromatography running time was stopped at 30 min. A graph of chlorogenic acid, quercetin, and phyllanthin were shown at the retention time of 8.626 min, 12.677 min, and 17.187 min, respectively.

3.2.2 *Phyllanthus emblica* (PE) fresh fruit juice extraction

The PE fruits were obtained from Nakhon Ratchasima province, Northeast of Thailand. The extraction procedures were controlled under the semi-sterile condition to prevent contamination in further experiments. For removing dirt, PE was washed with sterile water. Then, PE fruits were peeled and removed the seed. The fruit juice extractor was used to extract PE juices. PE fresh fruit juices were stored on ice during the experiment to prevent the structure of active compounds from degrading. The juice was filtered through sterile Whatman paper no. 1 (pore size 11 μ m) three times using laboratory filtration equipment and transferred to 1000 mL sterile laboratory screw cap bottles. Next, PE fresh fruit juice extract was dried lyophilized technique. The PE lyophilized powder was kept at -40 $^{\circ}$ C to prevent the loss of antioxidant properties until use. A stock solution of 10 mg/mL of PE was freshly prepared by dissolving 10 mg PE lyophilized powder in 1 mL sterile nano water Type I and a 1.5 mL microcentrifuge tube containing PE stock solution were vortexed for 5 min until the solution dissolved.

3.2.3 Ferric reducing antioxidant power (FRAP) assay

Based on the potential of antioxidants in natural products to reduce ferric ions. The basic principle of FRAP assay in this study, the ferric-tripyridyltriazine complex (Fe (III)-TPTZ) is reduced by antioxidants to a navy-blue chromogen ferrous-tripyridyltriazine complex (Fe (II)-TPTZ), which has an absorbance at 593 nm. The increase in the absorbance value of the FRAP solution mixture indicates the high power of antioxidants within the chemical reaction system. Briefly, FRAP reagent was freshly

made by mixing 10 mM TPTZ with 300 mM acetate buffer, TPTZ (10 mM) dissolved in HCl (40 mM), and $\text{FeCl}_3 \cdot 6\text{H}_2\text{O}$ 20 (mM) dissolved in 40 mM HCl, which mix as the ratio 10:1:1, respectively. $\text{Fe (II)SO}_4 \cdot 7\text{H}_2\text{O}$ and ascorbic acid (ASC) reference standards were diluted to various concentrations consisting of 1.25, 2.50, 5.00, 12.50, 25.00, and 50.00 μM . Moreover, PE samples were prepared to the concentration of 0.39, 0.78, 1.56, 3.13, 6.25, 12.50, 25.00 and 50.00 $\mu\text{g/mL}$. The ten microlitres of standards and samples were added into each well of 96 well plates. Then, FRAP reagent (200 μL) was also added to 96 well plates. Next, 96 well plates contained solution was immediately detected absorbance at 593 nm using a spectrophotometer. This assay was conducted independently of three experiments. Data were expressed as FRAP value (FeSO_4 equivalent, μM) by calculation from a comparison between sample absorbance value and standard FeSO_4 curve. Furthermore, FRAP was also calculated FRAP value from Linear regression equation $y = ax + b$; where y is the dependent variable, a is the slope, x is the independent variable and b is the y-intercept.

3.2.4 Oxygen radical absorbance capacity (ORAC) assay

The 2,2'-azobis (2-amidino-propane) dihydrochloride (AAPH) is oxidized by oxygen at 37 °C, which generates free radicals. The peroxy radical reacts with fluorescein leading to quenching of fluorescence intensity. Meanwhile, antioxidants can inhibit decreasing of fluorescence intensity and attenuation of peroxy radicals. Due to involvement in fluorescence experiments, all steps of this assay were performed without the light. Briefly, the freshly prepared 10 nM fluorescein solution was added to each well of 96 well-plate, at the volume of 150 μL per well. Next, the serial dilution of PE samples (0.10, 0.20, 0.39, 0.78, 1.56 and 3.13 $\mu\text{g/mL}$) and Trolox reference standard (0.39, 0.78, 1.56, 3.13, 6.25 and 12.50 $\mu\text{g/mL}$), which dissolve in 75 mM PB, pH 7.4 were placed to individual well. For the blank well, 75 mM PB, pH 7.4 was used. The 96 well plate containing solution was incubated for 10 min at 37 °C in the microplate reader machine. At the finish time, 165 mM AAPH in 75 mM PB, pH 7.4 was added into 96 well microplate containing standards and samples to start the reaction. Next, 96 well-plate was then measured with the kinetic fluorescence with an excitation wavelength at 485 nm and an

emission wavelength 528 nm for 60 min, and the time interval was set at 1 min. The data from the microplate reader shown as an area under the curve (AUC). Net AUC was responded for antioxidant capacity of standard or sample which can calculate following this equation: $\text{Net AUC} = \text{AUC}_s - \text{AUC}_b$; Where AUC_s is the area under the curve of sample or standard (the complete reaction consists of PE sample or Trolox standard at the different concentration) and AUC_b is an area under the curve of blank (the reaction mixture containing only fluorescein, AAPH, and 75 mM PB, pH 7.4 without sample or standard). From net AUC data, the Trolox reference antioxidant standard curve was created. Moreover, PE sample ORAC value was expressed as the Trolox equivalent by calculating from the Trolox standard curve or linear regression equation.

3.2.5 Determination of hydroxyl radical scavenging activity

The hydroxyl radical scavenging activity was performed by a combination of two reactions including the Fenton reaction and Thiobarbituric acid-reactive substances (TBARS) reaction. In the Fenton reaction, sodium L-ascorbate reduces iron (III) to iron (II). Iron (II) reacts with hydrogen peroxide (H_2O_2) to produce iron (III), hydroxyl (OH^\cdot), and hydroxyl radical (OH^\cdot). For the TBARS reaction principle, the generation of hydroxyl radical (OH^\cdot) by Fenton reaction has interacted with 2-Deoxy-D-ribose which generated malonaldehyde (MDA). MDA reacts with thiobarbituric acid (TBA) to form a pink chromogen (MDA-TBA adduct) which can easily detect absorbance at 532 nm. Whereas antioxidant compounds from PE or standard Trolox compete with 2-Deoxy-D-ribose to react with Hydroxyl radical (OH^\cdot) and generate stable compounds. The decreasing of MDA-TBA adduct by antioxidant in the natural product indicates the hydroxyl radical scavenging activity of PE or standard Trolox. This method procedure was slightly adjusted from Mandal et al. protocol (124). First, the assay reaction mixture contained 0.2 mM EDTA, 0.1 mM FeCl_3 , 1.12 mM 2-Deoxy-D-ribose, 0.2 mM H_2O_2 and 9 mM PB (pH 7.4) as a final concentration. Second, the various concentrations of PE samples (final concentration at 20, 40, 80, 160 and 320 $\mu\text{g}/\text{mL}$) and Trolox standard (final concentration at 5, 10, 20, 40, 80 and 160 $\mu\text{g}/\text{mL}$) were clearly dissolved and diluted in 100 mM PB (pH 7.4). After finish preparation, all of the prepared reagents in

this assay were performed in a 1.5 mL microcentrifuge and mixed in order. The standard or sample and the assay reaction mixture were mixed. Then 0.02 mM sodium L-ascorbate was added to the solution mixture. The dry bath was set at 50 °C for 20 min and the solutions were incubated. At the end of incubation, 1.12% (w/v) TCA to stop reaction and 0.4% (w/v) TBA in 0.5% (w/v) NaOH to generate the chromogen were added. The microcentrifuge tube contained solution mixtures were boiled at 95 °C for 15 min in a dry bath and cooled at room temperature. The 200 µL of solutions were transferred to 96 well-plate and measured absorbance at 532 nm using a spectrophotometer. This assay was performed on triplicated independent experiments. The percentage of inhibition of hydroxyl radical scavenging activity was expressed by optical density (OD) value from spectrophotometer and calculated according to the equation: % inhibition = $(OD_B - OD_S) / (OD_B) \times 100$; Where OD_B is optical density value of blank (the reaction mixture with TCA and TBA without sample or standard), OD_S is optical density value of sample or standard (All of the solution mixture with sample or standard). Moreover, hydroxyl radical scavenging activity was also demonstrated as 50% inhibitory concentration or IC_{50} by calculation from Linear regression equation $y = ax + b$; where y is the dependent variable, a is the slope, x is the independent variable and b is the y-intercept or interpolation from Trolox standard curve.

3.2.6 Determination of superoxide scavenging activity

Following the oxidation reaction, NADH was oxidized and lost an electron. PMS oxidizing reagent gained an electron from NADH and produced PMS reduced form. When 2 molecules of oxygen react with PMS reducing agent leading to generates $O_2^{\cdot-}$, which is a highly reactive molecule. Finally, the Redox reaction between NBT and $O_2^{\cdot-}$ produced formazan, the chromogenic reagent can detect absorbance at 560 nm. The decrease in absorbance of the solution mixture indicates the appearance of antioxidants within the chemical reaction system and increasing in superoxide anion scavenging activity. The superoxide anion scavenging activity of PE was modified from Oliveira et al. method description (125). The reaction mixture for 1 assay tube containing 90 µM of NADH dissolved in 19 mM PB, pH 7.4, and 77.4 µM NBT in 19 mM PB (pH

7.4). PE samples (final concentration at 3.9, 7.8, 15.6 and 31.3 $\mu\text{g}/\text{mL}$) or Trolox standard (final concentration at 125, 250, 500, and 1000 $\mu\text{g}/\text{mL}$) were dissolved and diluted in 19 mM PB (pH 7.4) and then added to the reaction mixture each microcentrifuge tube. Next step, 30 μL of 9 μM PMS in 19 mM PB, pH 7.4 was mixed with a previous solution mixture to generate superoxide anion within the system. The solutions were vortexed before being incubated for three minutes at room temperature. A spectrophotometer was used to assess the absorbance at 560 nm. All these experiments were performed in triplicate independent experiments. The superoxide anion scavenging activity was defined as a percentage of inhibition which shown as optical density (OD) value from the spectrophotometer and calculated following to this equation: % inhibition = $(\text{OD}_B - \text{OD}_S) / (\text{OD}_B) \times 100$; Where OD_B is the optical density value of blank (the reaction mixture with PMS without PE sample or reference compound), OD_S is optical density value of PE samples or Trolox reference standard (All of the solution mixtures with PE sample or Trolox standard). Furthermore, superoxide anion scavenging activity was also represented as 50% inhibitory concentration or IC_{50} by calculation from Linear regression equation $y = ax + b$; where y is the dependent variable, a is the slope, x is the independent variable and b is the y-intercept or interpolation from the Trolox standard curve.

3.2.7 Determination of hydrogen peroxide scavenging activity

Non-fluorescent HVA monomer is reduced by H_2O_2 to fluorescent HVA dimer, which reacts to HRP as a mediator. This fluorescent HVA dimer product can detect the fluorescent excitation spectrum at 320 nm and the fluorescent emission spectrum at 420 nm. The procedure is in line with a variation of Paital et. al., with some adjustments (126). The reaction mixture containing 125 μM of HVA in nano water type I and 0.2 Unit of HRP dissolved in 0.1% BSA in 50 mM PB (pH 6.0) were prepared. Trolox at the concentration 0.2, 0.4, 0.6, 0.8 and 1.0 $\mu\text{g}/\text{mL}$ were used for reference standard. The 96 well-plate was filled with 100 μL of PB, pH 7.4. Each PE sample (0.63, 1.25, and 2.5 $\mu\text{g}/\text{mL}$) or standard (20 μL) was added to each well. Then, 40 μL of the prepared reaction mixture was added into wells and followed with 20 μL of H_2O_2 to start the

reaction. 96 well-plate was protected from light and gently shaken on the shaker for 60 min at room temperature. Afterward, the solution was measured absorbance at excitation wavelength 320 nm and an emission wavelength of 420 nm. For blank well contained HVA and HRP, without H_2O_2 and, sample or standard to check the background signals, which generates from chemical constituents within the system. Whereas control well was added with all of the reagents without sample or standard. The percentage of inhibition of hydrogen peroxide scavenging activity was represented by the absorbance value from the spectrophotometer. Then, absorbance was calculated according to the equation: % inhibition = $100 - ((RFU_s - RFU_b) / (RFU_c - RFU_b)) \times 100$; Where RFU_s is the absorbance value of sample or standard (All of solution mixture with sample or standard), RFU_b is the absorbance value of blank (the reaction mixture containing HVA and HRP, without H_2O_2 and, sample or standard), RFU_c is the absorbance value of control (the reaction mixture containing HVA, HRP and H_2O_2 , and without sample or standard). Furthermore, hydrogen peroxide scavenging activity was also expressed as 50% inhibitory concentration or IC_{50} by calculation from Linear regression equation $y = ax + b$; where y is the dependent variable, a is the slope, x is the independent variable and b is the y -intercept or interpolation from Trolox standard curve.

3.2.8 Cell culture

The immortalized human keratinocytes cell line, HaCaT cells were obtained from the Cell line service (passage number 32). Cells were grown in DMEM culture medium supplemented with 10% fetal bovine serum (FBS) and 1% 100 U/mL penicillin-streptomycin at 37 °C in CO_2 water-jacketed incubator containing 5% CO_2 . HaCaT cells were seeded in 96-well plates, 35-mm dish, or 60-mm dish depending on each assay and incubated overnight. Cells were passaged every 5 days or reached 90% confluence. Only the early passage (<50) was used to perform the experiments. HaCaT cells were adjusted to the concentration of 1×10^6 cells/mL and then counted using a glass hemocytometer under a microscope. The cell number was calculated following this equation: Cell number = $[(\text{Number of cells in 4 squares})/4] \times \text{dilution factor} \times 10,000$. For the HaCaT cell freezing, HaCaT cells were trypsinized and centrifuged at 300 g for 3

min. Afterward, the supernatant was discarded and cell pellets were transferred to freezing media containing 50% completed cell culture medium, 40% FBS, and 10% DMSO. HaCaT cells at the concentration of 2.5×10^6 cells/cryotube were rapidly kept in the freezing container to control the temperature overnight in a -20 °C refrigerator. Each cryotube was labeled the cell information consisting of cell passage, date of collection, name of the cell, and the concentration of cells. After incubation, HaCaT cells in cryotubes were transferred into a liquid nitrogen tank for long-term storage. For the HaCaT cells thawing, cells were carefully brought from the liquid nitrogen tank put in a 37 °C water circulating bath for 1 min. Then, cells were immediately transferred to fresh media and centrifuged at 300 g for 3 min to remove the freezing media. Cells were grown in T75-flask with complete media overnight. In the morning, HaCaT cells were changed to fresh media and checked the cell healthy under a microscope. All experiments were performed at least triplicate independent experiments.

3.2.9 PE treatment for keratinocytes

The PE stock concentration of 10 mg/mL was used to treat HaCaT cells. Cells were treated with different concentrations of PE in cell culture media and added at a final concentration of 10 , 50 , or 100 μ g/mL to each well. Cells were incubated with PE for 6 h. However, control groups of Non-UVB and UVB well were treated with the cell culture medium only and incubated in the same condition. The PE extract treatment pattern for keratinocytes was used for all cell culture assays in this project.

3.2.10 UVB treatment

The 96-well plates or dishes were divided into two groups including Non-UVB and UVB groups, which each group contained with or without PE treatment. The 96 well plates or dish were labeled as Non-UVB (CTRL), Non-UVB + PE10, Non-UVB + PE50, Non-UVB + PE100, UVB, UVB + PE10, UVB + PE50 and UVB + PE100. Before UVB irradiation, a plate or dish was discarded from the media and washed with PBS 2 times. PBS was added to cover the cells. For the UVB group, cells with or without PE pretreatment were exposed to 40 mJ/cm^2 of UVB radiation and incubated for 18 h using UV incubator BIO SUN Ultra violets. The Non-UVB group containing keratinocyte cells

was conducted with the same washing procedures as the UVB group, while the cells were kept in the dark and were not exposed to UVB.

3.3.11 Optimal dose of UVB by MTT assay

The high amount of UVB can cause extreme DNA damage, which fails to recover the DNA damage by cellular mechanism results in severe apoptosis. In contrast, the low amount of UVB decreases the production of proteins involved in inflammation and apoptosis. Thus, it is very important to find the optimal dose of UVB that moderates stimulate DNA damage and apoptosis in keratinocytes. The HaCaT cells were seeded at 20,000 cells/well in 96-well plates overnight. The cell culture media covering HaCaT cells were discarded. The cells were washed twice with cold-PBS, then the cells were irradiated with UVB at different doses including 0, 20, 40, 80, and 100 mJ/cm². The cells were incubated for 18 h. At the end of incubation time, 10 µL of MTT reagent was added to the media at a final concentration of 0.25 mg/mL. Next, the cells were incubated for 3 hours in the CO₂ incubator. The cell culture media containing the MTT solution was carefully removed. Formazan crystals at the bottom of 96-well plates appeared. The 100 µL of 100% DMSO was added to the individual well to dissolve the formazan crystals into the purple solution with gently shaking in the shaker. The absorbance was then measured at 550 nm. The data from the microplate reader was expressed as optical density value which can calculate the percentage of cell viability of HaCaT cells induced by UVB following this equation: Relative percentage of cell viability = $[(OD_{UVB} - OD_B)/(OD_C - OD_B)] \times 100$; Where OD_{UVB} is the optical density value of UVB treated group (HaCaT cells treated with various concentration of UVB radiation, MTT solution and 100% DMSO), OD_B is the optical density value of blank (HaCaT cells treated with 100 µL of 100% DMSO without MTT solution to determine the baseline of an experiment) and OD_C is the optical density value of control (HaCaT cells kept in the dark without UVB treatment, MTT solution and 100% DMSO). All experiments were performed at least triplicate independent experiments.

3.2.12 Cytotoxicity and photoprotective of PE by MTT assay

For the checking of cytotoxicity of PE in HaCaT cells, the 15,000 cells of keratinocytes were seeded in each well of 96-well plates and treated with the various

concentrations of PE. After incubation for 6 h, the cell culture media was removed, and cells were continuously grown in fresh completed media for 18 h. At the end of incubation, the MTT assay was performed. For the determination of the photo-protective effect of PE, HaCaT cells were pretreated with various concentrations of PE for 6 h and then irradiated with 40 mJ/cm² of UVB irradiation. After 18 h of incubation, MTT assay was conducted, assay procedure and relative percentage of cell viability calculation as the previous method described.

3.2.13 Determination of intracellular ROS generation

Detection of intracellular ROS by using 2',7'-Dichlorodihydrofluorescein diacetate fluorescent probe is one of the best methods to measure redox unbalance occurring from exorbitant ROS production in many cells. Moreover, 2',7'-Dichlorodihydrofluorescein diacetate is also easy to manage with high sensitivity and low-priced chemicals suitable for the detection of intracellular free radicals. Cells can uptake 2',7'-Dichlorodihydrofluorescein diacetate to the intracellular. The non-fluorescent 2',7'-Dichlorodihydrofluorescein diacetate is cleaved by esterases to fluorescent 2',7'-Dichlorodihydrofluorescein. Meanwhile, the 2',7'-Dichlorodihydrofluorescein speedily react with ROS or RNS within the cells producing 2',7'-Dichlorofluorescein. An increase in the gathering of fluorescent dye in the cells can be detected by flow cytometry at emission 530 nm and excitation at 485 nm. HaCaT cells (8×10^5 cells) were grown in a 60-mm dish and pretreated with PE for 6 h. After incubation, cells were exposed to 40 mJ/cm² UVB radiation. Cell culture media was changed and incubated in the fresh media for 18 h. Next, cells were performed through flow cytometry. The 5 mg/mL stock solution of 2',7'-Dichlorodihydrofluorescein diacetate was prepared by dissolving in 100% DMSO. The stock solution of 2',7'-Dichlorodihydrofluorescein was then dissolved in complete DMEM without phenol red at the final concentration of 25 µg/mL. HaCaT cells were washed twice with warm-PBS (start from this procedure needed to protect from light to prevent fluorescent fading). Media containing fluorescent probe was added to the 60-mm dishes (2 mL/dish) for 30 min at 37 °C in the CO₂ incubator. Afterward, cells were washed with PBS, trypsinized,

and washed twice with PBS using centrifugation (at 4 °C, 300 g for 3 min). The cells were adjusted to a concentration of approximately 400-600 cells/ μ L and stored on ice. The individual cell was examined for the intensity of fluorescence using the flow cytometer and InCyte software analysis. The flow cytometer was cleaned with bleach and distilled water before and after experimenting. For the acquisition parameters, the sample name, a total count of 10,000 events, count gate for all events, cells concentration 500 cells/ μ L, and volume 20 μ L were set in sample information before running the machine. Furthermore, Unstained is an untreated fluorescent dye, PE, or UVB cells that are used for gating the ROS criteria in plot graphs. Data from the flow cytometer were expressed as mean intensity. The percentage of mean intensity was calculated according to this equation: % Mean intensity = $(MI_S/MI_{NC}) \times 100$; Where MI_S is the mean intensity of sample (HaCaT cells treated with various doses of PE with/without UVB irradiation) and MI_{NC} is the mean intensity of negative control (HaCaT cells treated with neither PE nor UVB irradiation)

3.2.14 Detection of Hydrogen Peroxide Release assay

Amplex[®] Red Hydrogen Peroxide/Peroxidase Assay Kit was used to detect the releasing amount of H_2O_2 from HaCaT cells. The 10-acetyl-3,7-dihydroxy phenoxazine or Amplex[®] Red, an electron and hydrogen donor is cleaved by HRP and reacts with H_2O_2 to a red fluorescent product, Resorufin. At excitation wavelengths of 530-260 nm and emission wavelengths of 590 nm, which can effectively detect fluorescent intensity. Besides, H_2O_2 receives electrons from Amplex[®] red and produces the water (H_2O), which is also converted by HRP through the reduction reaction. For this experiment, HaCaT cells were cultured in 96 well plates, incubated for 16 h in an incubator and pretreated with PE, and then irradiated with UVB radiation. At 30 min after UVB irradiation, the 96 well-plate containing different treated groups of HaCaT cells were added with a 1X reaction mixture containing 50 μ M Amplex[®] Red reagent and 0.1 U/mL HRP and left at room temp for 5 min. The reaction was protected from light until the experiment ended. Moreover, the stock solution of 20 mM H_2O_2 was freshly prepared and used within only 1 h by preparing approximately 3.0% (0.88 M) H_2O_2 in 1X Reaction

Buffer. The stock solution of 20 mM H_2O_2 was then diluted into different concentrations consisting of 0.125, 0.250, and 0.500 μM . The 1X Reaction buffer without H_2O_2 was used as a blank or negative control. Finally, the fluorescence intensity was measured using a microplate reader at excitation wavelength 571 nm and an emission wavelength of 585 nm. The data from a microplate reader was shown as relative fluorescence units (RFU). H_2O_2 standard curve was generated. All test sample data from each group were subtracted from the blank or negative control. To find the total amount of H_2O_2 released from cells, the absolute RFU of samples was interpolated from the H_2O_2 standard curve using Graph Prism software.

3.2.15 Detection of superoxide release assay

Dihydroethidium (DHE) has been widely used to determine the accumulation of superoxide within the cells. DHE is penetrated through the cell membrane and oxidized resulting in uncharged DHE changing to positively charge 2-Hydroxy ethidium. This red fluorescent product can insert at the double strand of DNA in the nucleus of cells and observe the excitation filter at 490 and emission filter at 590 nm. For this experiment, The HaCaT cells were grown in 96 well plates and treated with PE for 6 h. Afterward, cells were irradiated under 40 mJ/cm^2 of UVB, replaced with fresh medium, and incubated for 18 h. Further, cells were probed with 10 μM of DHE dissolving in sterile type I nano water for 30 min and protected from light. Cells were washed with PBS twice and added the 100 μL PBS to cover cells. Fluorescent intensity was detected under the fluorescence microplate reader with an emission wavelength of 488 nm and an excitation wavelength of 610 nm. The data from a microplate reader was shown as relative fluorescence units (RFU). All data from each group were subtracted blank. Superoxide releasing from cells was calculated as relative control non UVB.

3.2.16 Catalase activity assay

Catalase is an antioxidant enzyme that is present in living cells. CAT can convert harmful molecules H_2O_2 to O_2 and H_2O . At the same time, CAT catalyzes methanol to formaldehyde and then formaldehyde reacts with a colorless chromogen called Purpald (4-amino-3-hydrazino-5-mercapto-1,2,4-triazole) under alkaline conditions. The colorless Purpald is oxidized by potassium periodate to the purple color

product. This oxidation product can easily detect at the absorbance wavelength of 540 nm. The catalase activity based on Purpald reagent is a simple and rapid method for the evaluation of catalase activity in the sample. HaCaT cells were seeded in 6 well culture plates nearly 90% confluent overnight. Cells were treated following PE and UVB treatment protocol. After 18 h of incubation, cell culture media were removed from 6 well plates. Cells were washed twice with cold-PBS and added 500 μ L of 50 mM potassium phosphate buffer (pH 7) contained with 1 mM EDTA. A cell scraper was used to remove cells from the bottom of the plate. Cell lysate solutions were placed into a 1000 μ L microtube, sonicated on the ice at 35% amplitude for 1 min (pulse on for 10 sec and pulse off for 10 sec), and centrifuged at 12000 rpm for 10 min using a pre-cooled centrifuge. The clear supernatant was transferred to the new microcentrifuge tube and kept in the cold refrigerator to freshly conduct catalase activity measurement. Protein cell lysates were measured protein concentration using Bradford solution before performing this assay. The cell lysate samples and formaldehyde standard series (5, 10, 20, 40, 60, 80, 120, and 240 μ M) were freshly diluted with 100 mM potassium phosphate buffer (pH 7.5) containing 0.1% BSA and 1 mM EDTA and kept on ice. For this assay procedure, a 100 μ L test buffer (100 mM potassium phosphate buffer, pH 7.0 containing methanol in ratio 7:3) was firstly added to each well of 96 well plates. The prepared various formaldehyde standard concentrations and cell lysate samples were then added to labeled well in 96 well plates which conduct triplicate well per sample or standard. The H_2O_2 dissolved in Nano water type I was quickly added to start the reaction using a multichannel mechanic pipette and incubated for 20 min at room temperature on the shaker (protect from light). At the end of incubation, 50 μ L Purpald in 0.5 M potassium hydroxide was added to generate chromogenic substances and incubated for 10 min at room temperature on a shaker. The 10 μ L Potassium periodate in 0.5 M KOH was immediately filled to each well to stop the reaction. Catalase activity was measured by increasing the absorbance at 540 nm using a microplate reader. The absorbance of formaldehyde standards was used for plotting the standard curves and the Formaldehyde of samples were calculated according to this equation: Formaldehyde of

$\text{samples} = [A_s - (\text{y-intercept})/\text{slope}] \times [V_T - V_s(0.17 \text{ mL})/V_s(0.02 \text{ mL})]$; Where A_s is the absorbance of sample, V_T is a volume of all reagent added in this reaction except the volume of Purpald and V_s is the volume of sample or standard. Moreover, Catalase activity of the PE samples was calculated from the standard curve of formaldehyde by the following equation: $\text{CAT activity (nmol/min/mL/mg protein)} = [(F_s (\mu\text{mol/L})/C_s (\text{mg protein}))]/[T_{R(20\text{min})}] \times (\text{Sample dilution})$; Where $F_s (\mu\text{M})$ is the concentration of formaldehyde of PE samples (μM), $C_s (\text{mg protein})$ is protein concentration of PE samples (mg/mL) and $T_{R(20\text{min})}$ is the reaction time in this assay which detect at 20 min.

3.2.17 Superoxide dismutase activity assay

Superoxide dismutase is an antioxidant enzyme that converts the superoxide radical into hydrogen peroxide and an oxygen molecule. The principle of an assay, Tetrazolium (NBT) is reacted with WST-1 and xanthine oxidase generates WST-1 formazan, determines by a colorimetric method. HaCaT cells were grown overnight in 6 well plates at a density of 1×10^6 cells/plate. Cells were treated with or without PE and UVB radiation. After 18 h of UVB irradiation, cell culture media were removed from 6 well plates. Cells were washed twice with cold-PBS and then added 500 μL of 50 mM potassium phosphate buffer (pH 7). Cells were detached from the plate using a cell scraper. Cell lysates solutions were collected in a 1000 μL microtube and sonicated at 35 % amplitude for 1 min (pulse on for 10 sec and pulse off for 10 sec) on ice. Cell lysate solutions were centrifuged at 12000 rpm for 10 min at 4 $^{\circ}\text{C}$. The clear supernatant was transferred to the new microcentrifuge tube and kept at the -80 $^{\circ}\text{C}$ refrigerator to perform the SOD activity assay. The protein cell lysates were measured protein concentration using Bradford solution before performing SOD activity assay to prevent the freezing and thawing cycle. For starting the assay, protein lysate samples of PE and various concentrations of SOD standards (0.001, 0.01, 0.05, 0.1, 1, 5, 10, 20, 50, 100, and 200 U/mL) were added into 96 well plates to each labeled well. The Nano water type I was used instead as a sample in a blank well. Then the WST working solution was added to all well and the 96 well plate was mixed. Furthermore, a 20 μL enzyme working solution was added to the sample well, standard well, and blank 1 well. Whereas a 20 μL

dilution buffer was added to blank 2 well and blank 3 well and completely mixed using a shaker. The plate was incubated for 20 min at 37 °C. The total amount of each well equaled 240 μ L per well. After the end incubation, WST-1 formazan was detected by a decrease in absorbance at 450 nm using a microplate reader by kinetic measurement setting. SOD standard was set as a standard inhibition curve and SOD activity of the PE samples were calculated by the following equation: $\text{SOD activity} = [(A_{B1} - A_{B3}) - (A_S - A_{B2})] / (A_{B1} - A_{B3}) \times 100$; Where A_{B1} is the absorbance of reaction solution contained with Nano water type I, WST working solution and enzyme working solution. A_{B2} is the absorbance of the reaction solution consisting of the sample solution, WST working solution, and dilution buffer. A_{B3} is the absorbance of reaction solution comprising of Nano water type I, WST working solution, and dilution buffer. A_S is the absorbance of reaction solution containing sample or standard solution, WST working solution, and enzyme working solution.

3.2.18 Glutathione peroxidase activity assay

HaCaT cells (1×10^6 cells/plate) were grown in 6 well plates and incubated overnight. Cells were treated with or without PE for 6 h and UVB radiation for 18 h. The cell culture plate was covered with cold-PBS after incubation and washed twice with cold-PBS. Cells were collected using a cell scraper and cell lysates were centrifuged at 12000 rpm for 10 min at 4 °C. The proteins were kept at the -80 °C refrigerator to perform GPx activity assay within a week. The protein cell lysates were quantified protein concentration using Bradford solution and proteins were adjusted to 1 mg/mL before performing the assay. To start the reaction, these solutions or reagents were added following the sample or standard, GPx assay buffer (50 mM Tris-HCl buffer containing 1 mM EDTA (pH 7.4), GPx, Co-substrate mixer, and cumene hydroperoxide, respectively. In blank well, 120 μ L GPx assay buffer was added to 96 well plates following the 50 μ L Co-substrate mixer (0.4 mg/mL GSH, 0.6 mg/mL NADPH and 5 units/mL GR) to each well. For a sample or standard well, 20 μ L samples or standards in sample buffer (50 mM Tris-HCl buffer, pH 7.4, containing 1 mM EDTA and 1 mg/mL BSA) were added to each well following the 100 μ L GPx assay buffer and 50 μ L Co-

substrate mixer with gentle shaking. Then, 20 μL of freshly prepared 15 mM cumene hydroperoxide was quickly added to the well. The absorbance was immediately read the kinetic detection at wavelength 340 nm every 1 min for 30 min using a microplate reader. This equation was used to measure the difference in absorbance per minute: $\Delta A_{340}/\text{min} = [\Delta A_{340}(\text{Time}_2) - \Delta A_{340}(\text{Time}_1)]/(\text{Time}_2 - \text{Time}_1)$; where $\Delta A_{340}(\text{Time}_2)$ is the absorbance at 340 nm of time 2 and $\Delta A_{340}(\text{Time}_1)$ is the absorbance at 340 nm of time 1 to subtract 2 points for determination changing in absolute absorbance. Then, GPx activity was calculated following the equation: $\text{GPx activity} = (\Delta A_{340}/\text{min} \times V_T \times \text{Conversion factor})/(\epsilon_{\text{NADPH}} \times V_S)$; Where V_T is the total volume of this assay (0.19 mL), ϵ_{NADPH} is the molar extinction coefficient of NADPH. V_S is the sample volume of this assay (0.02 mL).

3.2.19 Apoptotic analysis by Hoechst 33342

A blue fluorescent dye, Hoechst 33342 dye is widely used to detect nuclear transformation in living cells. This fluorescent dye is water-soluble and non-toxic to the cells. Furthermore, Hoechst 33342 dye can easily diffuse through the cell membrane and specific binding to double-strand DNA that appears bright blue fluorescent using fluorescent microscopes. Briefly, HaCaT cells were plated at a density of 4×10^5 cells/dish in a 35-mm dish overnight and then treated with different concentrations of PE for 6 hours. Hoechst 33342 dye stock solution was prepared at the concentration of 10 $\mu\text{g}/\text{mL}$ by dissolving Hoechst 33342 dye in Milli-Q[®] Type 1 Ultrapure Water, which can store in the refrigerator for several months. After 13 h UVB irradiation, cells were washed with PBS and then added PBS containing 1 $\mu\text{g}/\text{mL}$ of Hoechst 33342 dye for 10 min and protected from light. PBS containing Hoechst 33342 dye solution was discarded from cells. Moreover, cells were washed and replaced with PBS to cover the cells. The cells were observed under a fluorescence microscope. The analysis program, ImageJ software was used to calculate the percentage of apoptotic cells.

3.2.20 Prostaglandin E_2 detection

Prostaglandin E_2 (PGE_2) is synthesized from arachidonic acid by prostaglandin synthetase enzymes such as COX-2. The increase in PGE_2 can induce

a pathological mechanism such as inflammation and cancer. To detect the PGE₂, HaCaT cells were grown, treated with PE for 6 h, and incubated after UVB irradiation for 18 h. The medium was collected for PGE₂ detection by using Prostaglandin E₂ Parameter Assay Kit (R&D Systems). To start the procedure, 200 μ L of Calibrator Diluent RD5-56 was added to the NSB (non-specific binding) wells. A 150 μ L of Calibrator Diluent RD5-56 was added to the zero standards (B₀) wells. PGE₂ standard was prepared by dissolving PGE₂ standard in sterile Milli-Q[®] Type 1 Ultrapure Water at the stock solution concentration 25,000 pg/mL and diluted with Calibrator Diluent RD5-56 to the working concentrations (78, 156, 313, 625, 1250, and 2500 pg/mL). A 150 μ L of standard or samples were added to each well. Then, 50 μ L of the Primary Antibody Solution was added to each well (excluding the NSB wells). The stripped plate was covered with a sealer to protect nonspecifically and incubated for 1 h at room temperature on a shaker. At the end of incubation, 50 μ L of PGE₂ Conjugate was added to each well (excluding the NSB wells). The plate was covered and incubated for 2 h at room temperature on the shaker. The plate was discarded and washed with a 400 μ L Wash Buffer for 4 times. A 200 μ L of Substrate Solution was added to each well, protected from light, and incubated for 30 min at room temperature on the benchtop. At finishing time, 100 μ L of Stop Solution was added to each well and gently mixed the plate. The blue color in the wells was changed to yellow. The absorbance was determined at 450 nm. PGE₂ standard was generated and the PGE₂ level in samples was interpolated from the standard curve.

3.2.21 Preparation of cell lysates

Western blot time-course analysis, HaCaT cells were grown in 60-mm dishes for 16 h. The cells were treated with 40 mJ/cm² UVB and changed to fresh media. The cells were collected at various times such as 0, 15, 30, 60, and 120 min to perform a western blot time course of NF- κ B, β -actin, phospho-c-Jun, phospho-Akt, Akt, phospho-p38, and p38 protein detection. Moreover, cells were also harvested at 0, 6, 12, 18, and 24 h to conduct a western blot time course of COX-2, Cytochrome c, and β -actin. Western blot analysis, HaCaT cells were seeded in 60-mm dishes. The cells

were pretreated with various doses of PE (0, 10, 50, and 100 µg/mL). The cells were then exposed to UVB and incubated with fresh media. The peak time of protein expression after UVB irradiation were selected at 30 min for phospho-Akt, Akt, phospho-p38 and p38 protein detection, 2 h for NF- κ B, and phospho-c-Jun) and 24 h for COX-2 and Cyt c protein detection. Finished each incubation time, old media were discarded from cell culture dishes, and cells were washed twice with cold-PBS. The cold PBS was added to 60-mm dishes. Cell lysates were harvested using blade wide 13 mm cell scraper and kept on ice. The cell lysates were transferred to 1.5 mL pre-cooled microcentrifuge tubes and centrifuged 600 g for 5 minutes at 4 °C. The whole lysates were extracted from HaCaT cells using RIPA lysis buffer (50 mM Tris-HCL, 100 mM NaCl, 0.1% Triton X-100, 0.1% sodium deoxycholate, 0.1% sodium dodecyl sulphate (SDS), 1 mM sodium orthovanadate (Na_2HPO_4), 1 mM sodium fluoride (NaF), 1 mM EDTA, 1 mM EGTA, 1% protease inhibitor and 1% phosphatase inhibitor) and a nuclear extraction kit was used to harvest nuclear lysates (Cayman No.10009277). The supernatants were removed from the cell pellet and then 150 µL cold-RIPA lysis buffer or 50 µL cold-nuclear extraction kit was added to each microcentrifuge tube. Cell lysate solutions were mixed every 5 min using a vortex. Afterward, the cell lysates were incubated for 20 mins and centrifuged at 12,000 rpm for 10 mins at 4 °C to separate protein from cell debris. The clear supernatant was transferred to a sterile microcentrifuge tube and stored at -80 °C refrigerator until used. The whole protein concentrations were quantified using the Bradford solution. The whole protein lysates were diluted at 1:4 with RIPA lysis buffer. The 10 µL of each diluted protein sample was added to 96 well plates following by 200 µL Bradford solution. The 0, 0.05, 0.1, 0.2, 0.4 and 0.8 mg/mL BSA were prepared and added to 96 well plate. Bradford solution (200 µL) was added to each well. The 96-well plate was shaken on the shaker for 5 mins. The absorbance was measured at 595 nm. Bovine serum albumin (BSA) was used for protein standard calibration curves. The total amount of protein in the sample was evaluated by calculating from the BSA standard curve.

3.2.22 Western blot analysis

The whole protein lysates were separated using SDS-PAGE. A 10% sodium dodecyl sulfate-polyacrylamide gel electrophoresis (SDS-PAGE) was prepared by mixing DI water, 30% acrylamide gel, 15 M Tris, pH 8.8, 10% SDS, 10% Ammonium persulphate, and N,N,N',N'-tetramethyl ethane-1,2-diamine (TEMED). Moreover, the stacking gel was prepared. The electrode assembly, gel cassettes, green gaskets, and clamping frame were set. The electrode module was put into the tank. 1X running buffer (25 mM Tris base, 192 mM glycine, and 0.1% SDS) was filled to the chamber. Protein samples were prepared by mixing with 6x-dye and buffer to adjust to equal amounts of protein. Protein mixtures were boiled at 95 °C for 5 mins using a dry bath. At the end of incubation, 20 µL protein mixtures were shortly centrifuged and loaded into a 15-well comb of separating gel. The 2 µL of molecular weight markers were loaded together. The proteins were run at 100 V for 90 mins. 1X running buffer (25 mM Tris base, 192 mM glycine, and 0.1% SDS) was filled to the chamber. Protein samples were prepared by mixing with 6x-dye and water to adjust to equal amounts of protein. Protein mixtures were boiled at 95 °C for 5 mins using a dry bath. At the end of incubation, protein mixtures were shortly centrifuged and loaded into a 15-well comb of separating gel. Proteins from polyacrylamide gel were transferred to Amersham Hybond 0.45 µM PVDF membrane. The membrane was activated in absolute methanol for 5 mins and then rehydrated in 1x cold-transfer buffer (48 mM Tris, 39 mM glycine, and 20% methanol, pH 9.2) for 15 mins. polyacrylamide gel, foam pad, and filter paper were soaked in 1x cold-transfer buffer for 15 mins. Then, foam pad, filter paper, polyacrylamide gel, PVDF membrane, filter paper, and foam pad were assembled in cassette, respectively. After finish preparation, the gel sandwich and ice pack were placed into the transfer tank with a 1x cold-transfer buffer. A protein transfer set mini-PROTEAN Tetra system was connected to the power supply and set to 100 V to start running for 2 h. After finish protein transferring, the membranes were rinsed with Tris-buffered saline with Tween 20 buffer, TBST (20 mM Tris-HCl, 150 mM NaCl and 0.1% Tween 20) and blocked by using blocking buffer (5% BSA or 5% skim milk in TBST depending on each antibody

recommendation) for 1 hour with gentle shaking to block nonspecific. The membranes were then incubated with 1:1000 primary antibodies concentration including phospho-Akt, Akt, phospho-p38, p38, NF- κ B, phospho-c-Jun, COX-2, cytochrome c, and β -actin antibodies overnight at 4 °C. After incubation, the membranes were washed with TBST 3 times for 15 mins and probed with mouse or rabbit HRP-conjugated secondary antibodies at the dilution factor 1:3000 in 5% skim milk in TBST for 1 h at room temperature. Then membranes were developed with ECL prime chemiluminescent detection reagent and captured protein bands using gel documentation. Protein band intensity was analyzed using ImageJ software. Furthermore, the membranes were stripped using a stripping buffer (1.5% glycine, 0.1% SDS, and 1% Tween 20, pH 2.2), blocked with a blocking buffer, and reprobed again.

3.2.23 Statistical analysis

All data were reported as mean \pm SEM for three or more replications. Statistical was operated using GraphPad Prism software. The means \pm SEM was compared by one-way analysis of variance (ANOVA) analyzed by the Dunnet test.

CHAPTER 4

RESULT

4.1 Identification of phytochemical constituents in PE

A high-performance liquid chromatographic technique was found to be precise, specific, reproducible, and rapidly used to detect and analyze chemical constituents in the PE. In this study, ascorbic acid, ellagic acid, gallic acid, chlorogenic acid, quercetin, and phyllanthin were used as a chemical marker for the determination of quantification and qualification in PE crude extract. The maximum absorption wavelength of ascorbic acid, ellagic acid, gallic acid, chlorogenic acid, quercetin, and phyllanthin was 243, 270, 253, 325, 255, and 280 nm which present UV spectrum graph of each compounds from the UV-VIS photodiode array detector. To identify composition compounds in PE, the two chromatographic criteria including retention time and specific UV absorption spectrum graph were used to compare between reference standard and sample. The results show that the chromatographic peak shapes of compounds analysis were symmetric peak shapes which located purity of chromatographic system and no interference of solvents from the mobile phase. The retention time between each sample and standard showed a similar retention time which confirmed ascorbic acid, ellagic acid, gallic acid, chlorogenic acid, quercetin, and phyllanthin chemical constituents found in PE. Moreover, the concentration of chemical content in PE was calculated from the standard calibration curve for each compound. The linear range for standards calibration curves was between 6.25 and 200 $\mu\text{g}/\text{mL}$ depending on each standard concentration. The correlation coefficient (R^2) of standard ascorbic acid, ellagic acid, gallic acid, chlorogenic acid, quercetin, and phyllanthin were 0.9999, 1.0000, 0.9998, 0.9987, 1.0000, and 0.9992, respectively (Table 1). After calculation comparison with the standard calibration curve, the ascorbic acid, gallic acid, ellagic acid, chlorogenic acid, and quercetin concentration contents present in PE was found to be 1.589 (% w/w), 0.625 (% w/w), 0.370 (% w/w), 0.015 (% w/w), and 0.001 (% w/w), respectively. Table 3 shows that the determination of chemical constituents in PE indicated that ascorbic acid

is a major compound that is found in PE. Besides PE fruit juice extract was not found in the phyllanthin although it was found in the Phyllanthus genus plants. (Figure 13)

Table 3 The summary content of compound analytes in PE

Compounds	The retention time of standards (min)	R ² of standard	The wavelength of detection (nm)	Content (%w/w)	mg/g DW of PE
Ascorbic acid	9.806	0.9999	243	1.589 ± 0.03	15.89 ± 0.26
Gallic acid	4.949	1.0000	270	0.370 ± 0.01	3.70 ± 0.08
Ellagic acid	4.993	0.9998	253	0.625 ± 0.00	6.25 ± 0.00
Chlorogenic acid	8.626	0.9987	325	0.015 ± 0.00	0.15 ± 0.00
Quercetin	12.677	1.0000	255	0.001 ± 0.00	0.01 ± 0.00
Phyllanthin	17.187	0.9992	280	N/D	N/D

N/D, not detectable

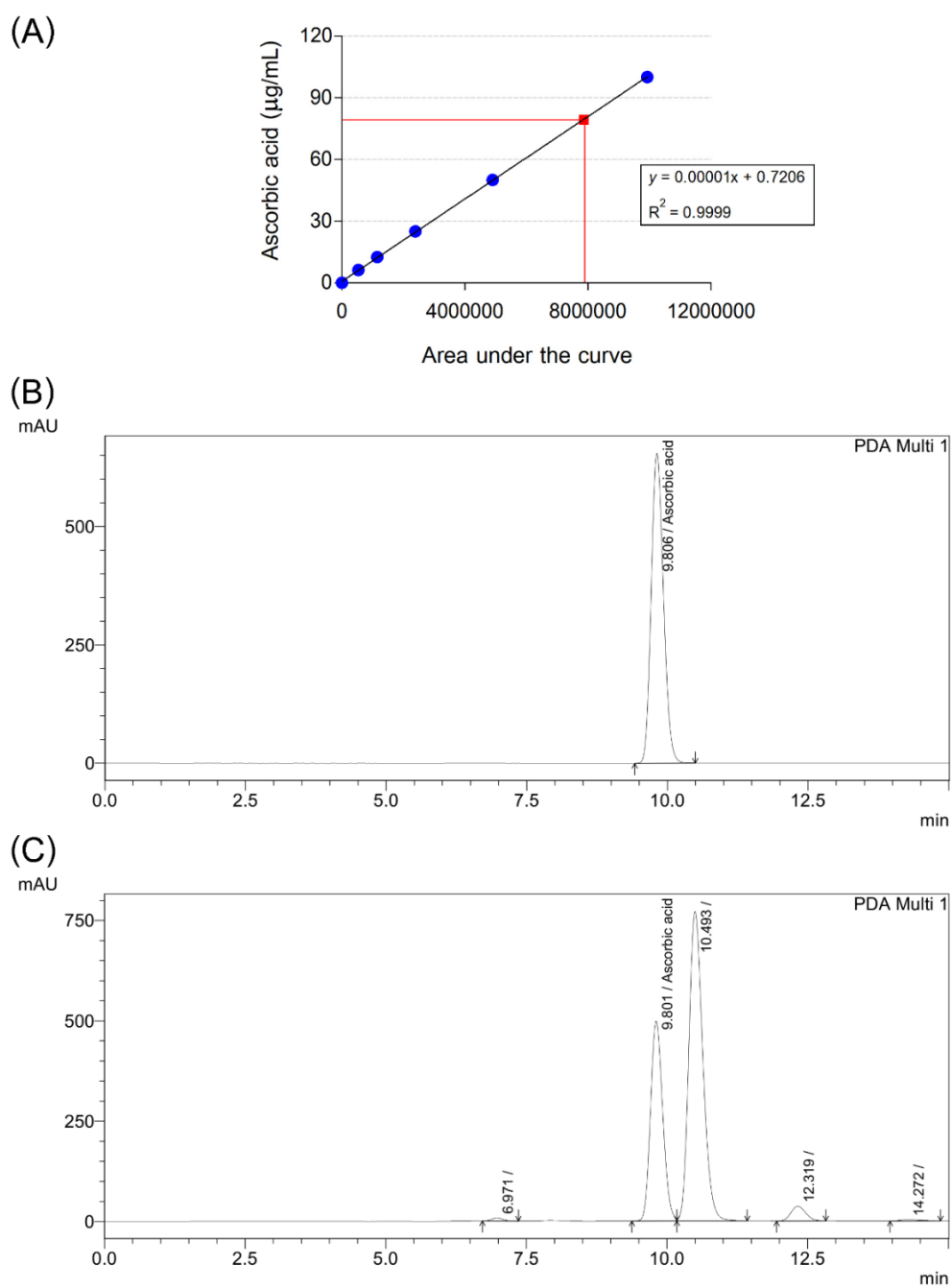


Figure 8 A representative of HPLC analysis of ascorbic acid detected at 243 nm.

(A) standard calibration curve of standard ascorbic acid at the concentration of 0-100 $\mu\text{g/mL}$. (B) HPLC chromatogram of standard ascorbic acid and retention time for standard ascorbic acid was 9.806 mins (C) HPLC chromatogram of ascorbic acid content in PE fruit extract at the retention time 9.801 mins.

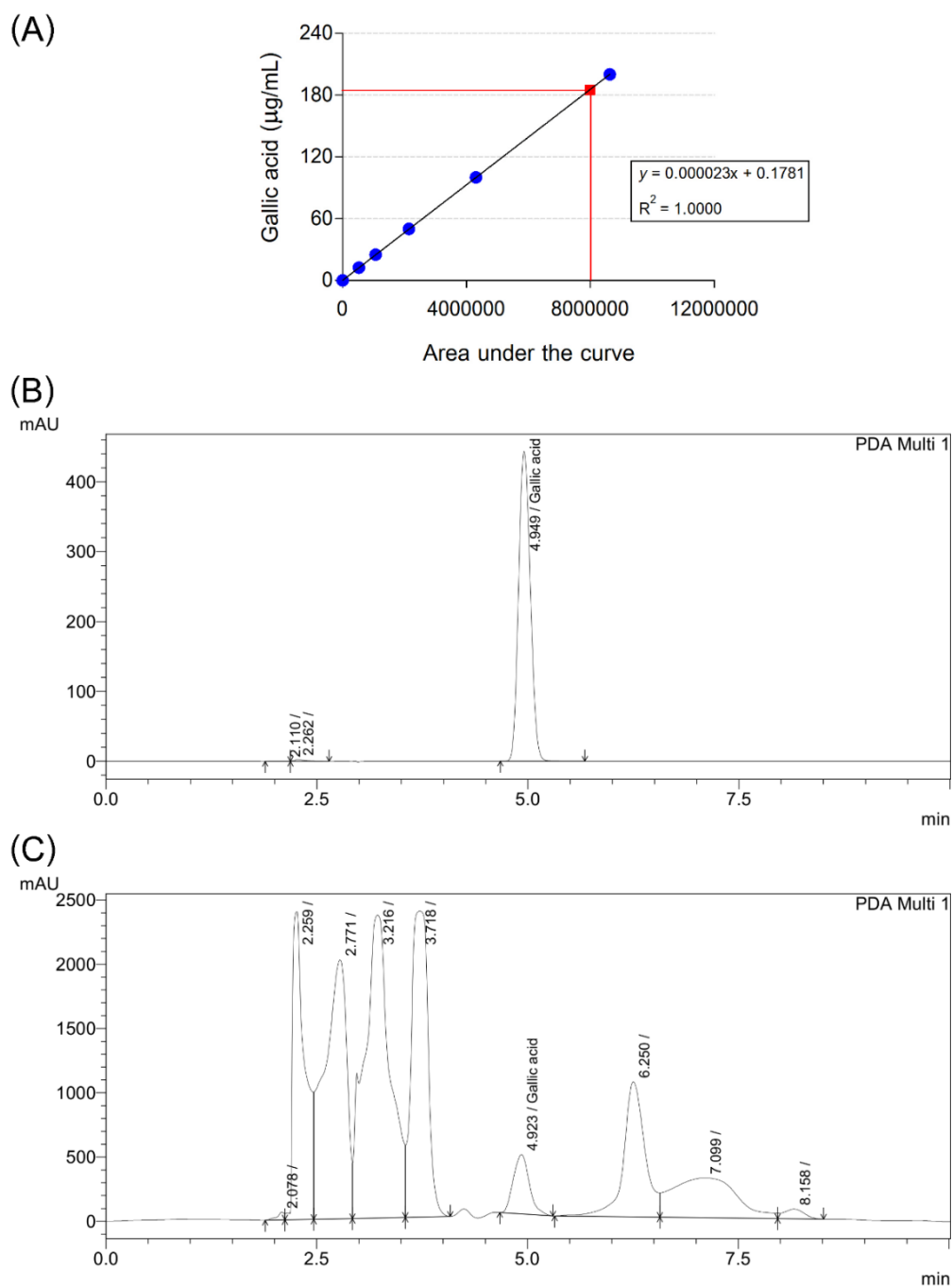


Figure 9 A representative of HPLC analysis of gallic acid detected at 270 nm.

(A) standard calibration curve of standard gallic acid at the concentration of 0-200 $\mu\text{g/mL}$. (B) HPLC chromatogram of standard gallic acid and retention time for standard gallic acid was 4.949 mins (C) HPLC chromatogram of gallic acid content in PE fruit extract at the retention time 4.923 mins.

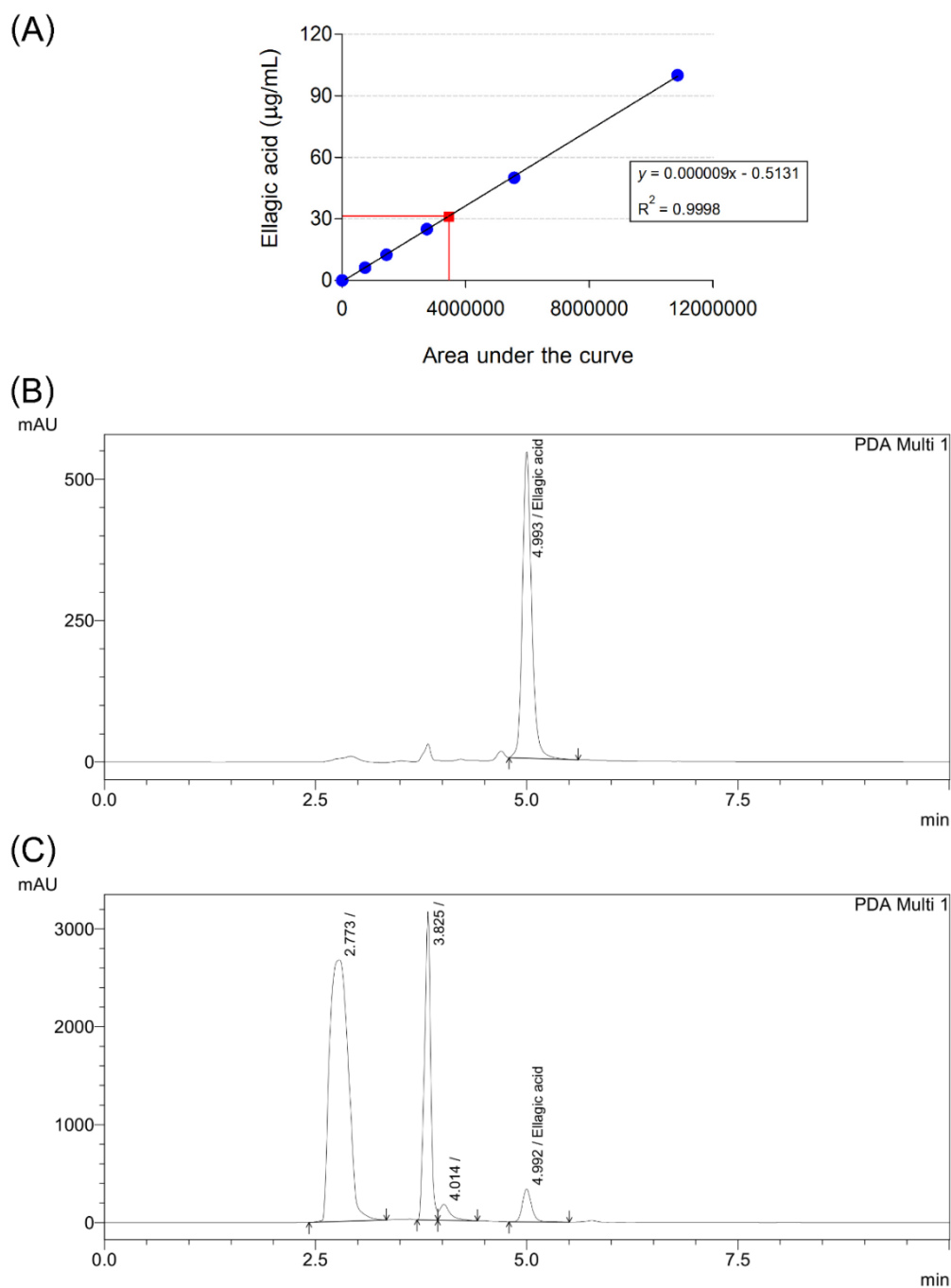


Figure 10 A representative of HPLC analysis of ellagic acid detected at 253 nm.

(A) standard calibration curve of standard ellagic acid at the concentration of 0-100 $\mu\text{g/mL}$. (B) HPLC chromatogram of standard ellagic acid and retention time for standard ellagic acid was 4.993mins (C) HPLC chromatogram of ellagic acid content in PE fruit extract at the retention time 4.992 mins.

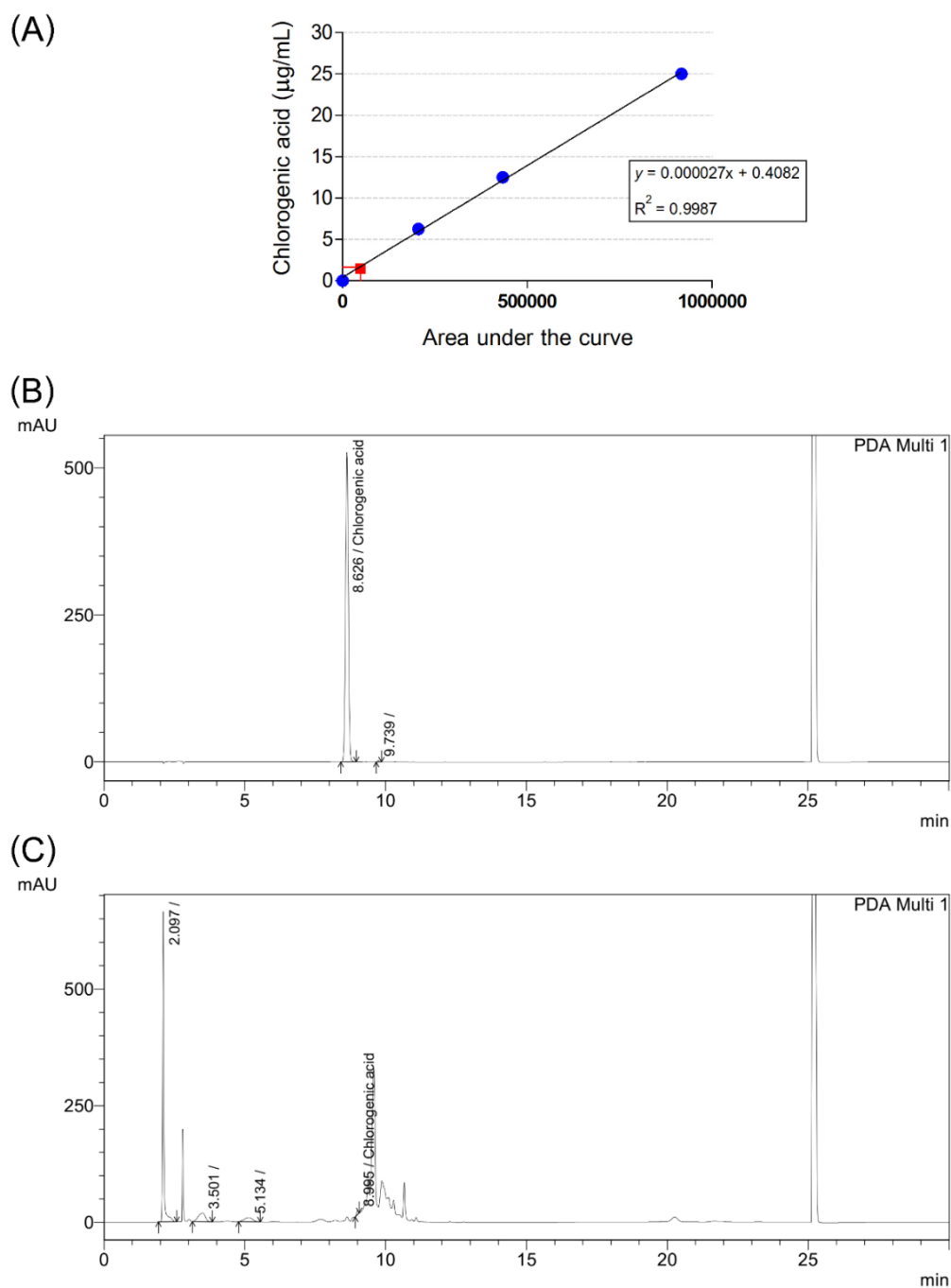


Figure 11 A representative of HPLC analysis of chlorogenic acid detected at 325 nm. (A) standard calibration curve of standard chlorogenic acid at the concentration of 0-25 $\mu\text{g/mL}$. (B) HPLC chromatogram of standard chlorogenic acid and retention time for standard chlorogenic acid was 8.626 mins (C) HPLC chromatogram of chlorogenic acid content in PE fruit extract at the retention time 8.995 mins.

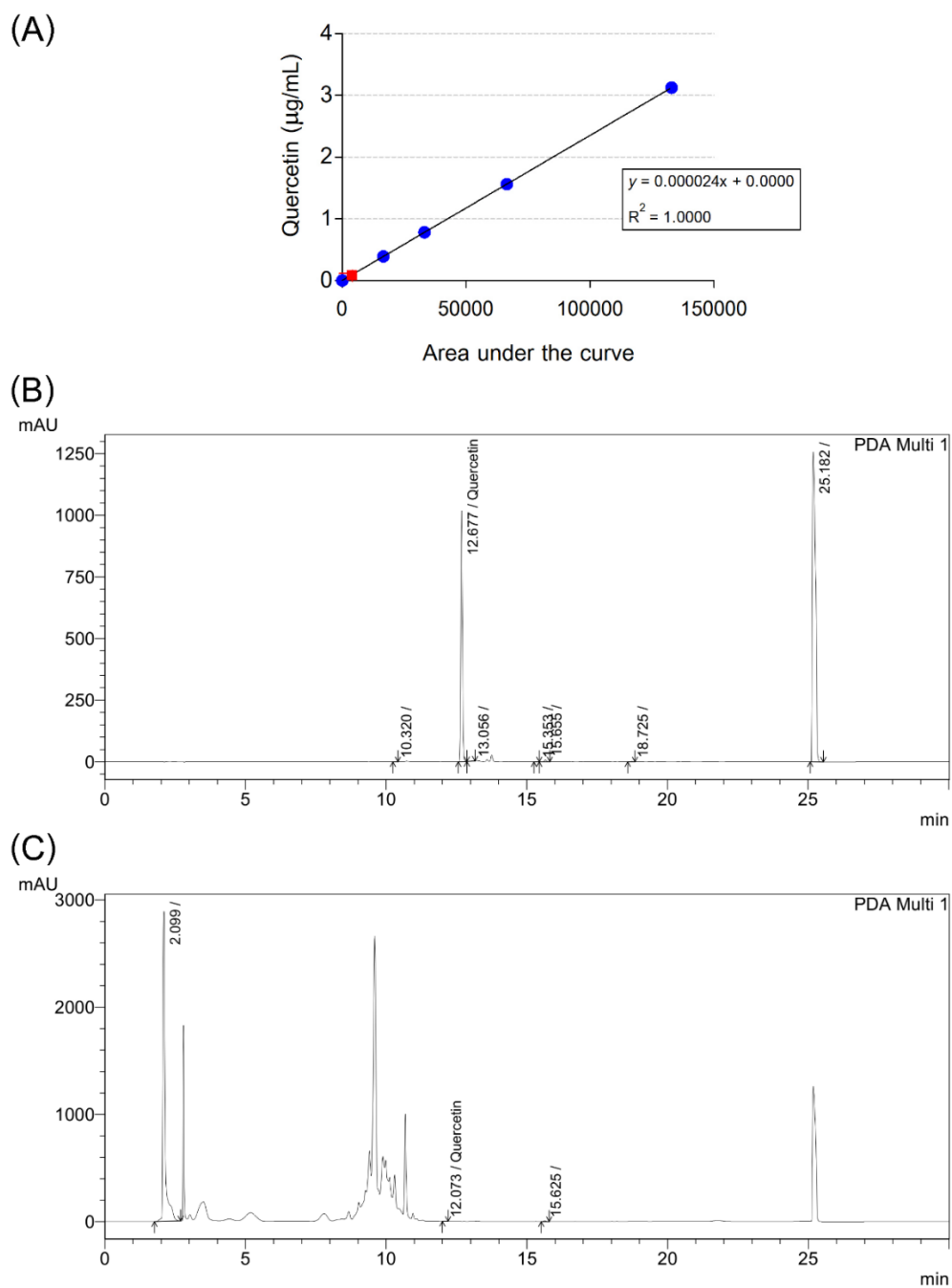


Figure 12 A representative of HPLC analysis of quercetin was detected at 255 nm. (A) standard calibration curve of standard quercetin at the concentration of 0-3.25 $\mu\text{g/mL}$. (B) HPLC chromatogram of standard quercetin and retention time for standard quercetin was 12.677 mins (C) HPLC chromatogram of quercetin content in PE fruit extract at the retention time 12.073 mins.

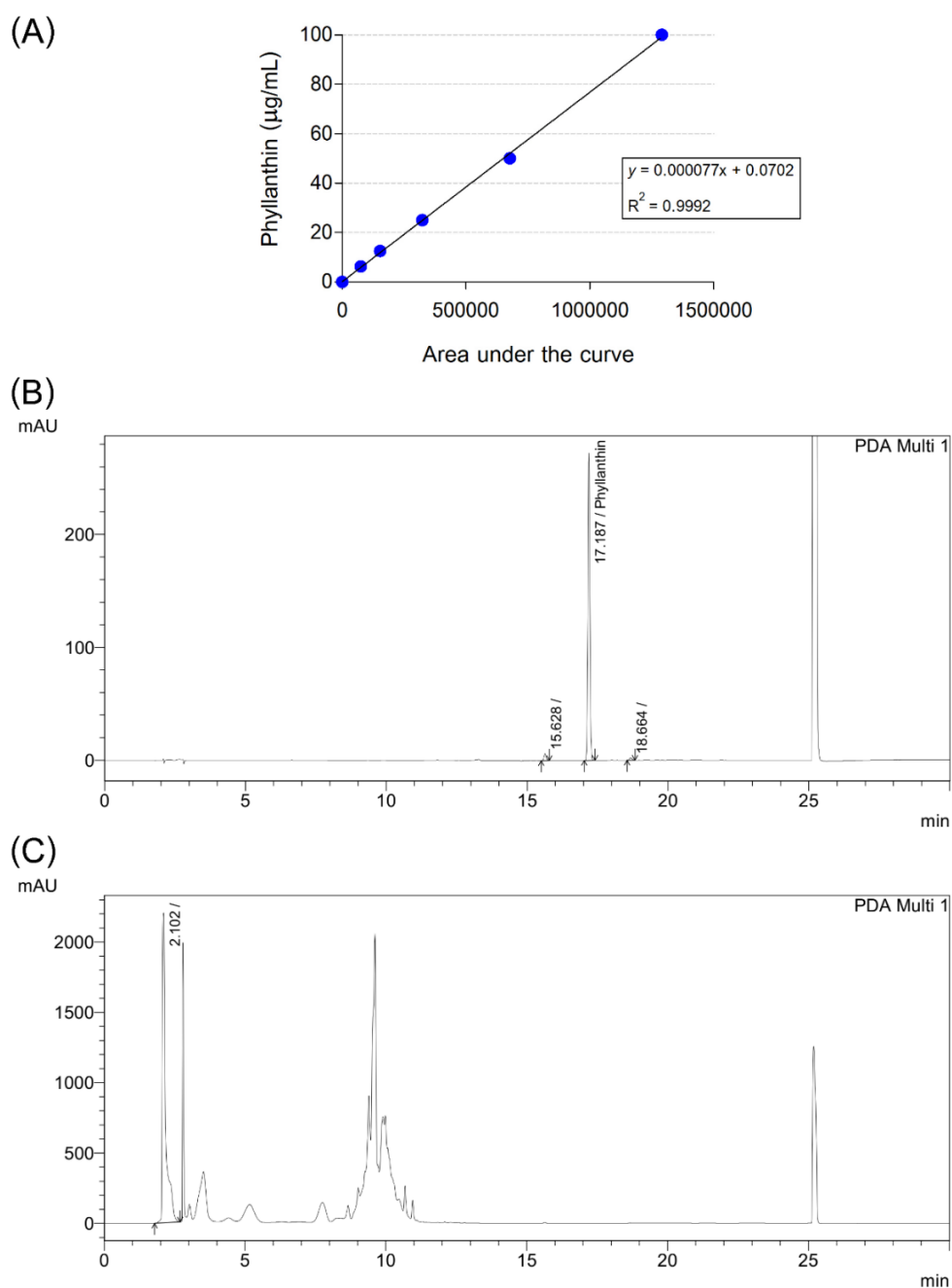


Figure 13 A representative of HPLC analysis of phyllanthin was detected at 280 nm.

(A) standard calibration curve of standard phyllanthin at the concentration of 0 to 100 $\mu\text{g/mL}$. (B) HPLC chromatogram of standard phyllanthin and retention time for standard phyllanthin was 17.187 mins (C) HPLC chromatogram of phyllanthin content in PE fruit extract.

4.2 Antioxidant capacity of PE

4.2.1 Ferric-reducing antioxidant power (FRAP)

The ferric reducing antioxidant power of standard ASC and PE extract was shown in Figure 14. The FeSO_4 standard curve was measured at an absorbance of 593 nm and FeSO_4 at the concentration 0 to 50 μM shown a good linear standard curve with $R^2 = 0.9978$ (Figure 14A). The FRAP values of standard ASC and PE extract were found from the linear regression to the concentration of standard ASC in the range from 0 to 500 $\mu\text{g}/\text{mL}$ and PE in the range from 0 to 250 $\mu\text{g}/\text{mL}$. Moreover, the increase in a dose dependent of FRAP value of standard ASC and PE extract appeared in an excellent linear regression graph with $R^2 = 0.9964$ and $R^2 = 0.9969$, respectively (Figure 14B and 14C). The antioxidant capacity from Table 1, FRAP value of standard ASC and PE were $2.39 \pm 0.12 \mu\text{mol}/\text{mg}$ and $4.28 \pm 0.27 \mu\text{mol}/\text{mg}$, respectively. PE has shown antioxidant capacity higher than standard ASC.

Table 4 The antioxidant capacities of PE

Antioxidant capacity			
FRAP	Standard ASC	2.39 ± 0.12	Linear regression equation $y = 2.072x + 14.69$
	PE	4.28 ± 0.27	$y = 4.217x + 24.50$
ORAC		Trolox equivalent (mmol TE/g)	Linear regression equation
	PE	5.480 ± 0.55	$y = 3.799x + 10.51$

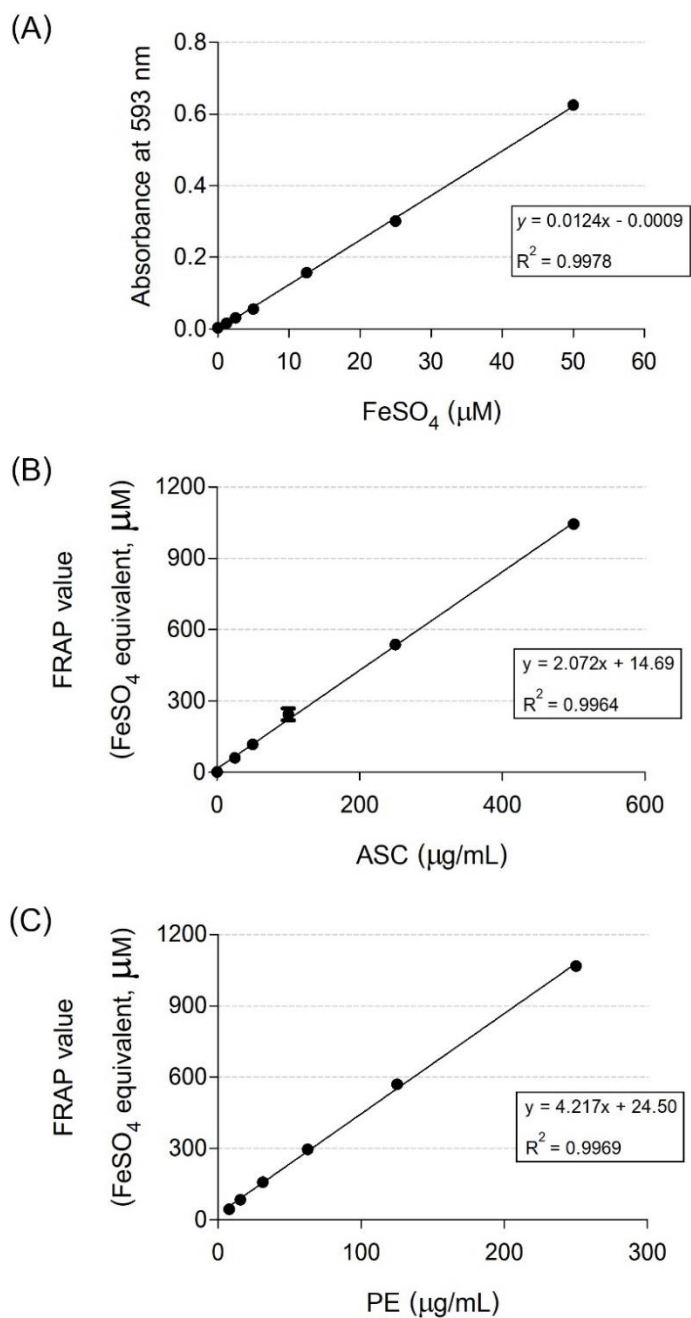


Figure 14 FRAP antioxidant capacities of ASC reference standard and the PE fruit extract are expressed in FeSO_4 equivalent.

(A) The ferrous standard curve was detected at an absorbance of 593 nm. (B) FRAP value of ASC at the concentration of 0 - 500 $\mu\text{g/mL}$. (C) FRAP value of PE extract at the concentration 0 - 250 $\mu\text{g/mL}$.

4.2.2 Oxygen radical absorbance capacity (ORAC)

The oxygen radical absorbance capacity of standard Trolox was demonstrated in Figure 15. The 1:2 serial dilution of Trolox kinetic curves were ranged from 0 to 100 μM . The kinetic curve showed decreasing in the fluorescent intensity of the individual concentration of Trolox depending on time. Moreover, the fluorescent intensities were represented as a relative fluorescent unit (RFU) with normalized to 100% of control (Figure 15A). The oxygen radical absorbance capacity of standard Trolox concentrations was presented as the net area under the curve (AUC), and the linear regression of the Trolox standard dose-response curve shown a good linear standard curve with $R^2 = 0.9843$ (Figure 15B). Moreover, the various dose of PE extracts kinetic curves ranging from 0 to 25 μM also showed in Figure 16A. After interpolation with the Trolox standard dose-response curve, the linearity of the Trolox equivalent of PE extract at the different concentrations was expressed (Figure 16B) and the correlation coefficient was 0.9643. The oxygen radical absorbance capacity of PE indicated a Trolox equivalent value of 5.480 ± 0.55 mmol TE/g (Table 4).

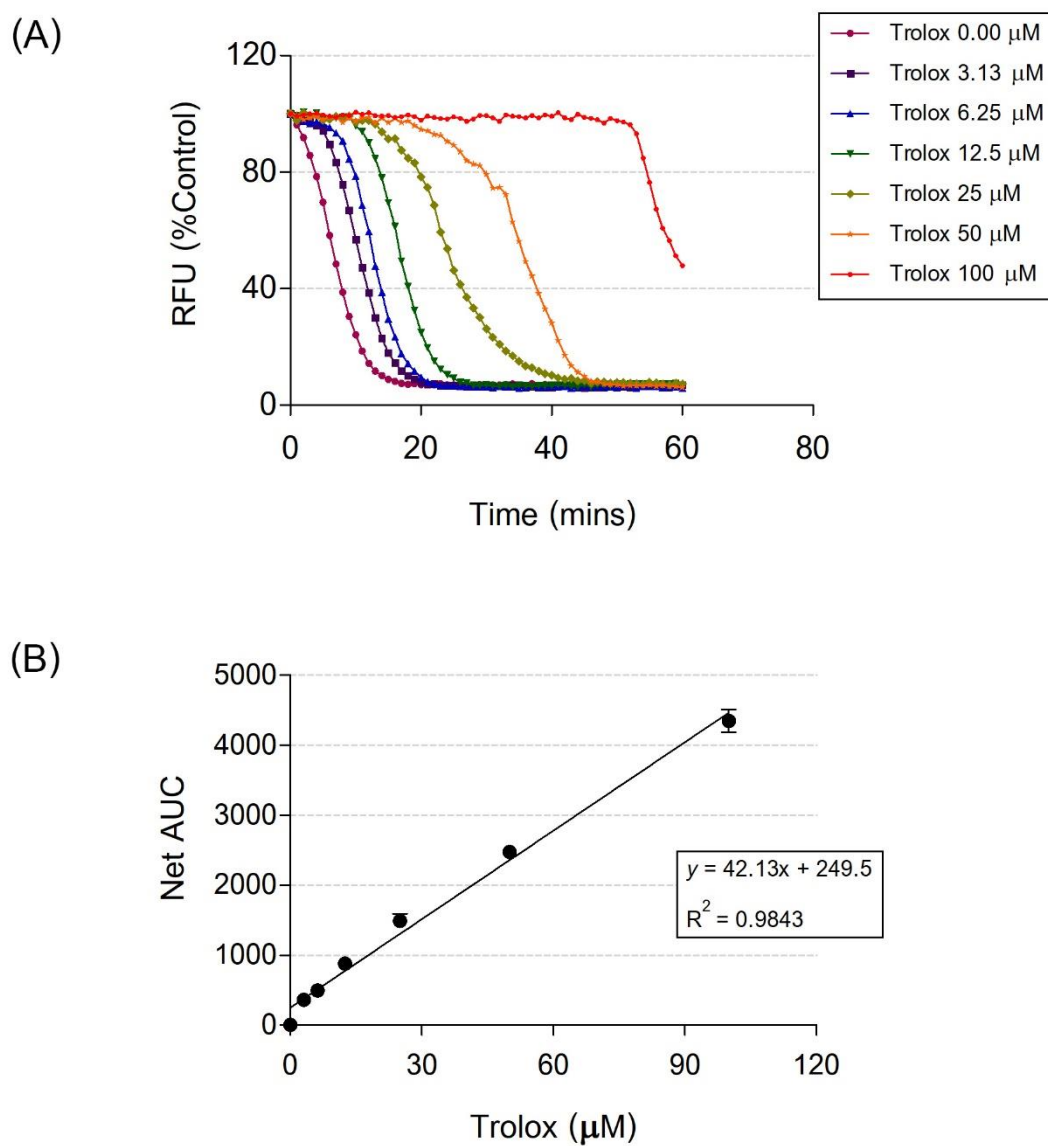


Figure 15 Determination of ORAC assay of Trolox

(A) Trolox kinetic curves with different concentrations from 0 to 100 μM . (B) The linear regression of the Trolox standard dose-response curve.

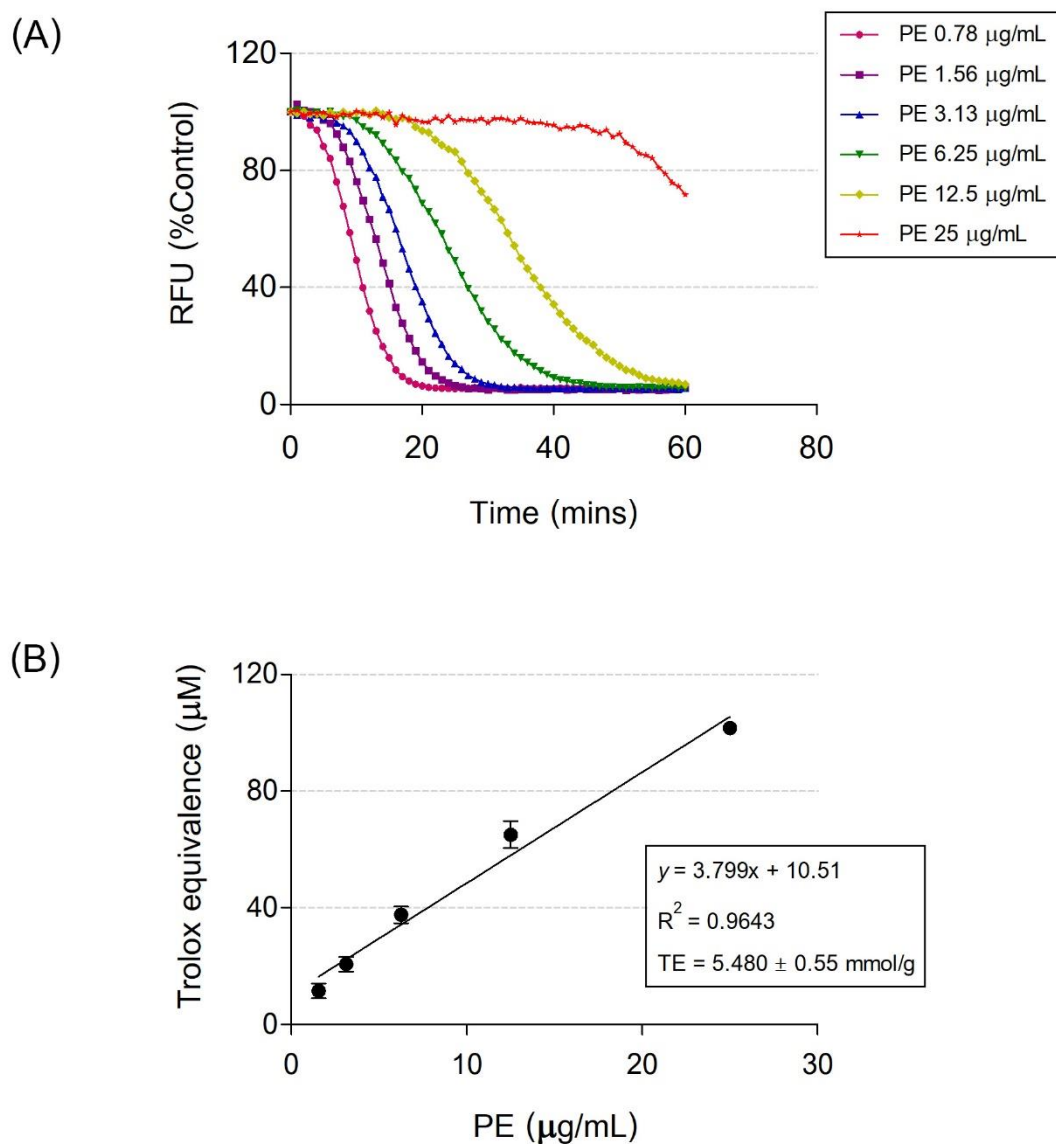


Figure 16 Determination of ORAC assay of PE extract

(A) PE extract kinetic curves with serial dilutions ranging from 0 to 25 µM. (B) The linear regression of the Trolox equivalent of PE extract.

4.3 Antioxidant scavenging activity

4.3.1 Hydroxyl radical scavenging activity

The results of the Hydroxyl radical scavenging activities of the Trolox reference compound and PE extract were shown in Figure 17. The Trolox standard

inhibition curve was measured at an absorbance at 532 nm and plot with the two-fold serial dilution of Trolox ranging from 125 to 1000 $\mu\text{g/mL}$. The standard curve has shown great linearity with $R^2 = 0.9811$ (Figure 17A). Also, in Figure 17B, The PE extract inhibition curve against Hydroxyl radical scavenging activities expressed good linearity with $R^2 = 0.9216$. The IC_{50} value of the standard Trolox and PE extract was 45.83 ± 3.23 $\mu\text{g/mL}$ and 282.49 ± 17.59 $\mu\text{g/mL}$, respectively. These results can indicate that the IC_{50} value of PE extract was higher than the IC_{50} value of the standard Trolox. This indicated that PE has an antioxidant activity lower than standard Trolox.

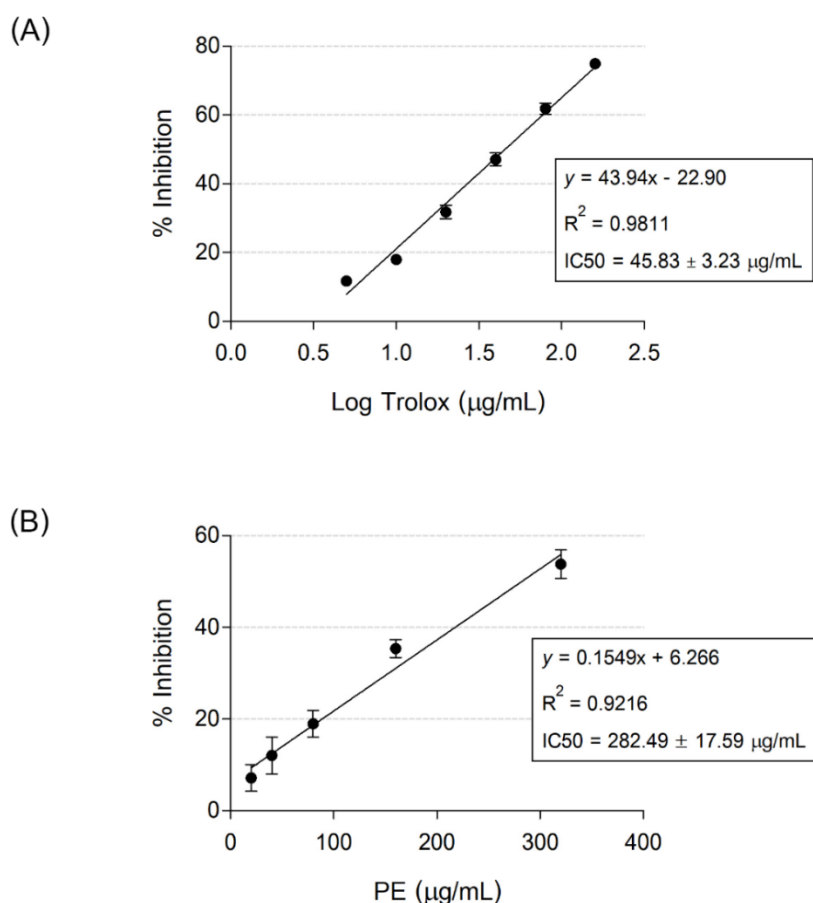


Figure 17 Hydroxyl radical scavenging activities of the Trolox reference and PE extract. (A) Percentage of inhibition curve of standard Trolox. (B) Percentage of inhibition curve of PE extract.

4.3.2 Superoxide anion scavenging activity

Superoxide anion scavenging activities of the Trolox standard and PE extract were shown in Figure 18. The standard curve from superoxide anion scavenging activities represented great linearity with $R^2 = 0.9731$ (Figure 18A). The PE extract inhibition curves with the various dose (0 – 31.25 $\mu\text{g/mL}$) expressed a good linear regression with $R^2 = 0.9797$ which is shown in Figure 18B. The IC_{50} value of the standard Trolox and PE extract were $337.66 \pm 18.90 \mu\text{g/mL}$ and $14.94 \pm 0.15 \mu\text{g/mL}$, respectively. These results showed that the IC_{50} value of PE extract was less than the IC_{50} value of the standard Trolox. PE has a higher antioxidant activity than reference Trolox, according to this result.

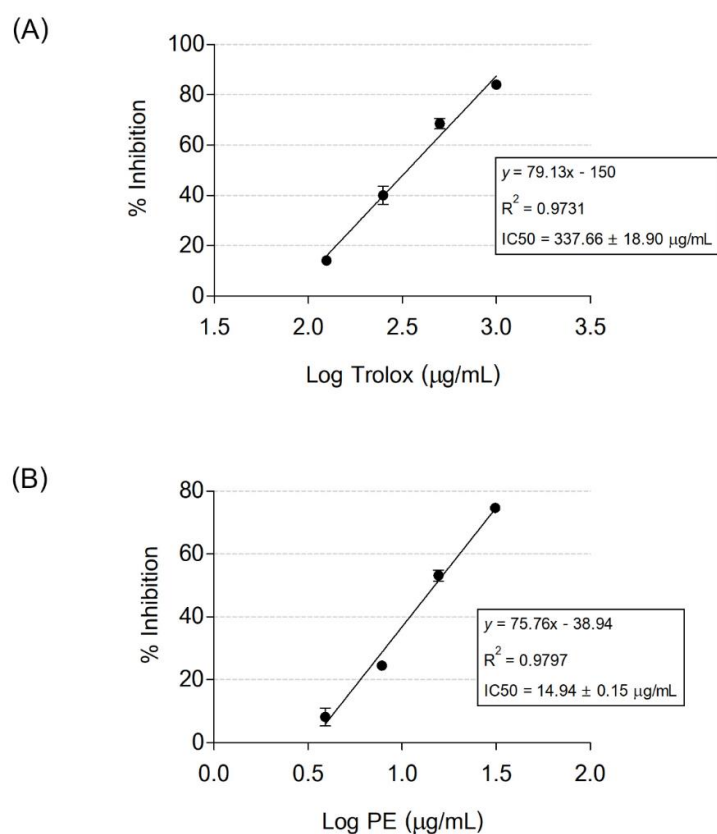


Figure 18 Superoxide anion scavenging activities of the Trolox standard and PE extract. (A) Percentage of inhibition curve of standard Trolox. (B) Percentage of inhibition curve of PE extract.

4.3.3 Hydrogen peroxide scavenging activity

Hydrogen peroxide scavenging activities of the Trolox reference standard and PE extract were demonstrated in Figure 19. The standard curve of superoxide anion scavenging activities represented great linearity with $R^2 = 0.9734$ (Figure 19A). The PE extract inhibition curves with the various dose expressed a good linear regression with $R^2 = 0.9375$ which was shown in Figure 19B. The IC_{50} value of the standard Trolox and PE extract were $0.55 \pm 0.03 \mu\text{g/mL}$ and $1.46 \pm 0.37 \mu\text{g/mL}$, respectively. These results showed that the IC_{50} value of PE extract was higher than the IC_{50} value of the standard Trolox. This suggested that PE has an antioxidant activity lower than standard Trolox.

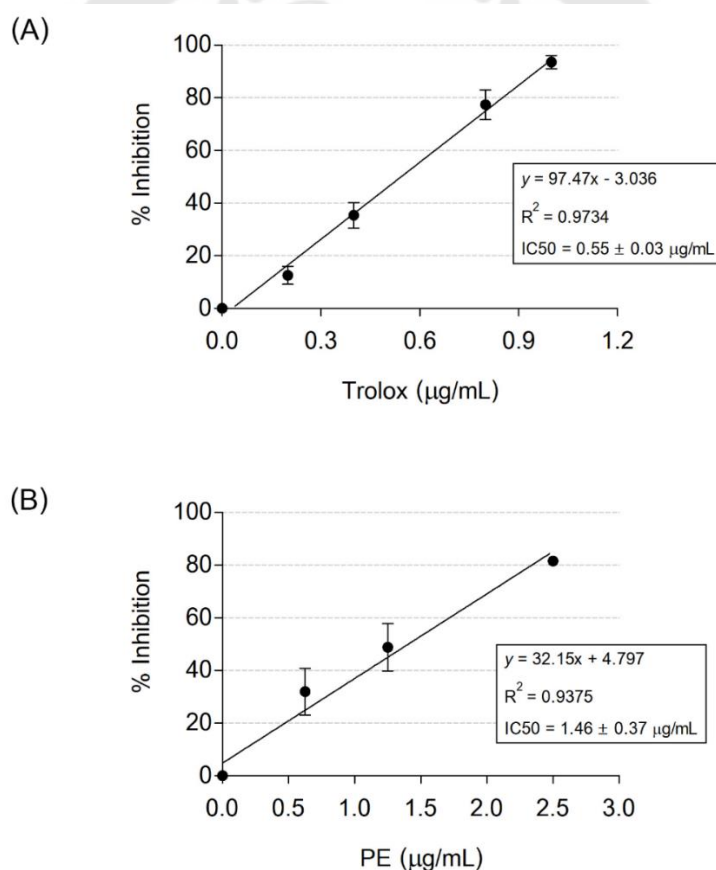


Figure 19 Hydrogen peroxide scavenging activities of the Trolox standard and PE extract.

(A) Percentage of inhibition curve of standard Trolox. (B) Percentage of inhibition curve of PE extract.

4.4 Effect of UVB on keratinocyte cell viability

The colorimetric MTT assay was globally used to detect cell viability, cytotoxicity, and cell proliferation. The HaCaT cell viability and cytotoxicity were measured at 18 h after UVB irradiation as shown in Figure 20. The effect of various dosages of UVB irradiation on cell viability in HaCaT cells, UVB radiation was gradually decreasing HaCaT cell viability in a dose-dependent manner. After HaCaT cells were treated with different dosages of UVB; 20, 40, 60, 80, and 100 mJ/cm². The HaCaT cell viability was reduced to 89%, 76%, 60%, 45% and 31%, respectively, compared to 100% viability in non-UVB treated control. (n= 4) Whereas, HaCaT cells after 20, 40, 60, 80 and 100 mJ/cm² UVB irradiation, were dead at 11%, 24%, 39%, 55%, and 69%, respectively. Thus, 40 mJ/cm² UVB irradiation which dead cells approximately 24% cell viability were selected to optimal dose UVB radiation to perform another experiment in this project.

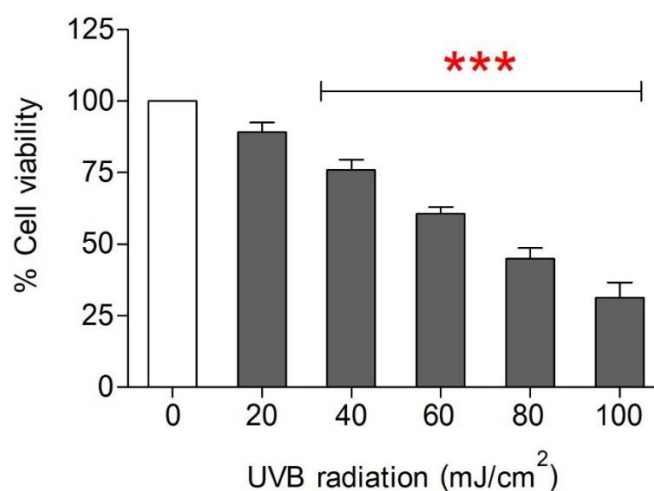


Figure 20 Relative cell viability of HaCaT cells after exposure to various doses of UVB. Cytotoxic effect of UVB on the relative percentage of HaCaT cell viability induced with various doses of UVB (20, 40, 60, 80, and 100 mJ/cm²). Error bars represent the mean \pm S.E.M. four independent experiments conducted in triplicate. ***P < 0.001, compared UVB-irradiated group with control non-UVB.

4.5 Effect of PE on UVB-induced keratinocyte cell viability

In Figure 21, HaCaT cells were pretreated with PE at the different concentrations (0.01, 0.1, 1, 10, 50, 100 and 1,000 $\mu\text{g}/\text{mL}$) for 6 h. In the dark, the cell was incubated with fresh media for another 18 hours. After pretreatment of various doses of PE, there were no significant differences in cell viability of HaCaT cells.

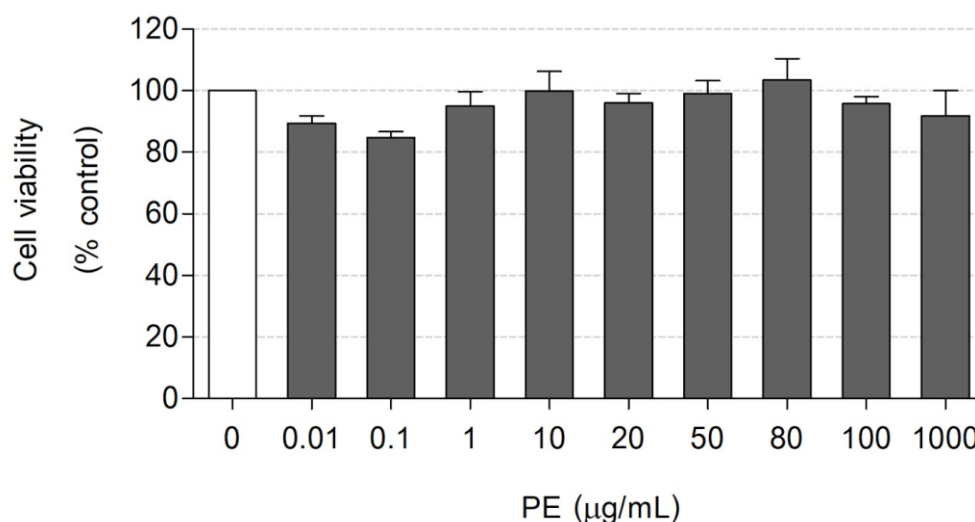


Figure 21 Cytotoxicity of PE on HaCaT cells viability.

Data are expressed as mean \pm SEM (n = 4).

Whereas cell viability was decreased by 40 mJ/cm^2 UVB irradiation to 76% consisting of 24% dead cells. However, pretreatment with PE at the different concentrations (0.01, 0.1, 1, 10, 20, 50, 80, 100 and 1,000 $\mu\text{g}/\text{mL}$) combined exposure with 40 mJ/cm^2 UVB irradiation, PE tended to increase cell viability (74% , 75% , 78% , 80% , 81% , 94% , 86% , 87% and 69%, respectively) when compared to UVB irradiation group (76%). Especially, PE at the concentration 50 $\mu\text{g}/\text{mL}$ significantly increased cell viability to 94% in HaCaT cells. Thus, PE at the concentrations 10, 50 and 100 $\mu\text{g}/\text{mL}$ were chosen for further experiments.

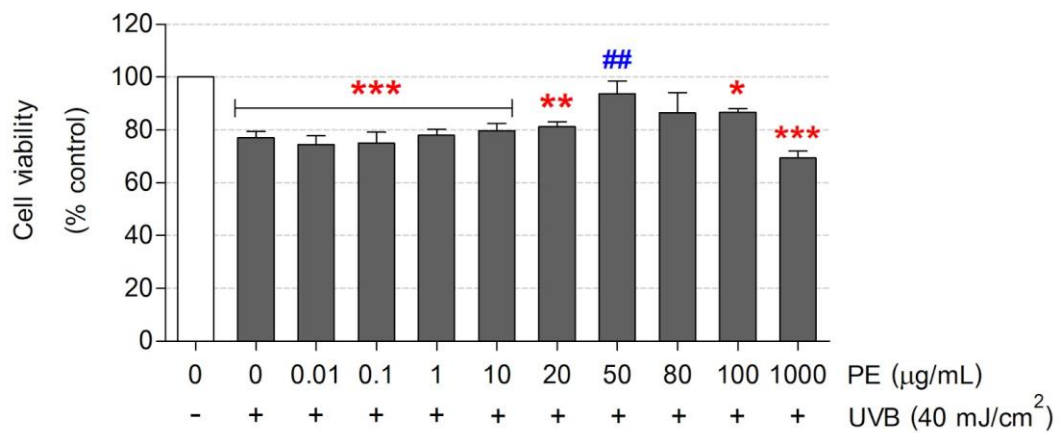


Figure 22 Protective effect of PE on HaCaT cells viability stimulated with 40 mJ/cm² UVB irradiation.

Data are represented as mean \pm SEM (n = 4). *P<0.05, **P<0.01, ***P<0.001 compared with control non-UVB; ##P<0.01 comparison between PE treatment combined with UVB irradiation and control UVB.

4.6 Effect of PE on UVB-induced intracellular ROS production

After 18 h UVB exposure, cells were analyzed intracellular ROS by flow cytometer data represented as dot-plot and histogram plots in Figure 23. Unstained were analyzed to identify the location of the HaCaT cells population and to test the background fluorescence level without 2',7'-Dichlorodihydrofluorescein diacetate probe. The HaCaT cell population of PE pretreatment with the different concentrations located outside ROS gating and almost closed with an unstained area compared to control non-UVB cell population. PE treatments alone did not affect intracellular ROS. Moreover, an intracellular ROS of the HaCaT cell population has the same level as control of the non-UVB cell population. The HaCaT cell population of UVB irradiation is located on the ROS channel. However, HaCaT cells with PE pretreatment before exposure to UVB radiation, cell population shift into the left of the x-axis (log scale) of dot-plot and histogram plots which mean the intracellular ROS is less than the right of x-

axis compared to UVB irradiation cell population. The shifting of dot-plot and histogram plots correlate with doses of PE in a dependent manner. After analysis by Guava InCyte software, the intracellular ROS was expressed as a percentage of mean fluorescence intensity (Figure 24). The results showed that ROS generation within the cell was not affected by pretreatment with PE at the different concentrations compared to control non-UVB. The relative percentage of mean intensity of ROS basal level of control non-UVB in the cells was 100% whereas PE pretreatment at the concentrations 10, 50, and 100 $\mu\text{g}/\text{mL}$ were 108% , 107% , and 96% , respectively. UVB radiation was found to strongly induce intracellular ROS generation to 255% ($P < 0.001$). PE demonstrated dose-dependent inhibition of ROS generation induced by UVB irradiation. Our results demonstrate that PE at the concentrations 10, 50, and 100 $\mu\text{g}/\text{mL}$ was attenuated intracellular ROS to 252% , 208% , and 181% , respectively. Especially, 100 $\mu\text{g}/\text{mL}$ PE significantly reduced ROS production in HaCaT cells to 181% ($P < 0.05$) compared to control UVB.

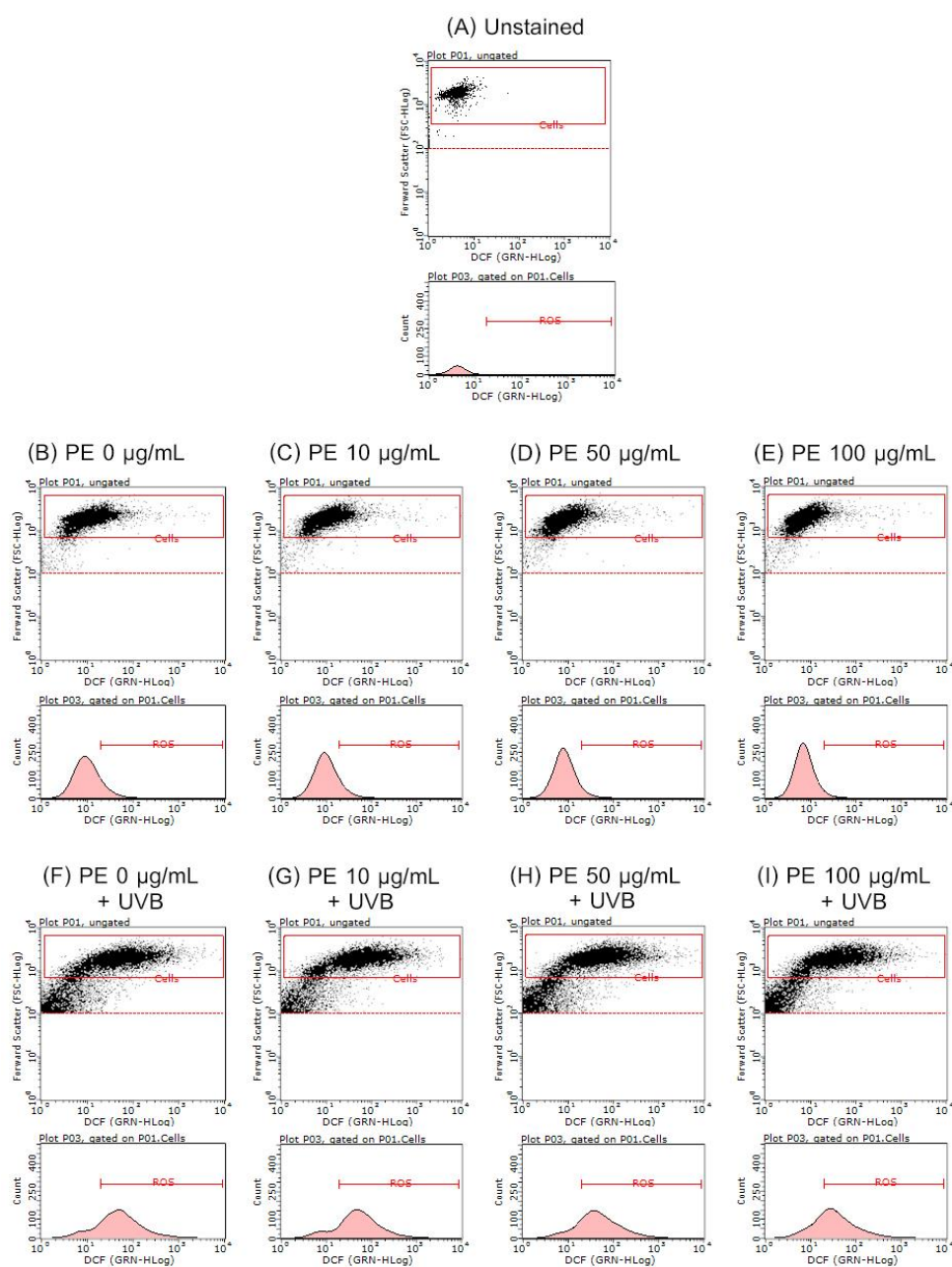


Figure 23 The dot-plot and histogram plots of intracellular ROS via flow cytometer (a) Unstained control of HaCaT cells population. HaCaT cells were treated with PE at the concentrations (b) 0, (c) 10, (d) 50, and (e) 100 $\mu\text{g/mL}$ and probed with 2',7'-Dichlorodihydrofluorescein diacetate. HaCaT cells were combined with treatment between 40 mJ/cm^2 UVB and PE at the concentrations (f) 0, (g) 10, (h) 50, and (i) 100 $\mu\text{g/mL}$ and stained with 2',7'-Dichlorodihydrofluorescein diacetate.

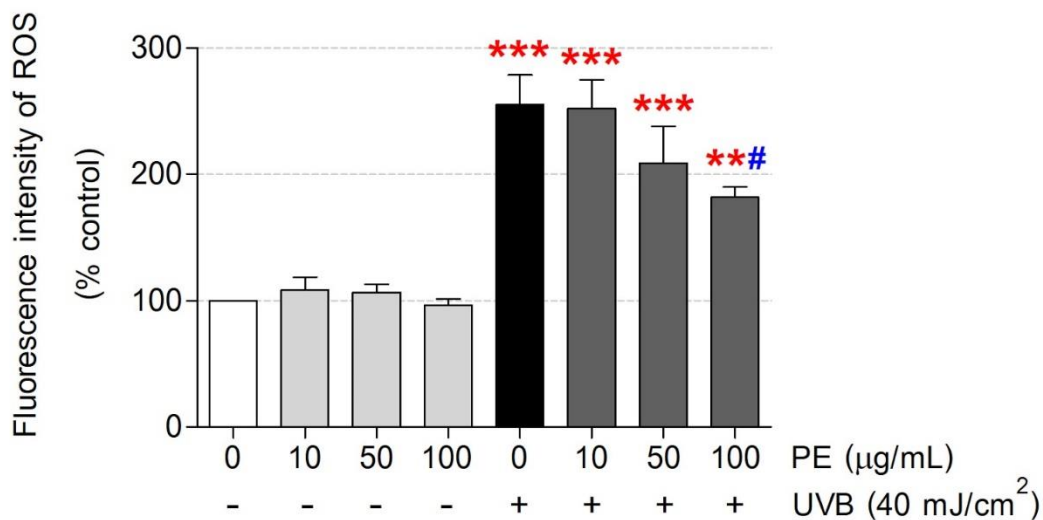


Figure 24 The fluorescent mean intensity of intracellular ROS is detected by a flow cytometer.

Data are expressed as mean \pm SEM (n = 4). **P<0.01, ***P<0.001 significantly different compared to control non-UVB, #p<0.05 significant comparison between HaCaT cells treated with UVB alone and UVB in combination with PE.

4.7 Effect of PE on UVB-induced intracellular superoxide production

We found that PE alone (10, 50, 100 µg/ mL) significantly decreased the superoxide level to 90% (P<0.05), 80% (P<0.001) and 69 % (P<0.01), respectively. While intracellular superoxide was increased by UVB irradiation to 125% when compared with control non-UVB. Pretreatment with PE combined with UVB exposure tended to decrease superoxide production in HaCaT cells at the concentration of 10, 50, 100 µg/mL 102%, 91%, and 82%, respectively, when compared to UVB alone (Figure 25).

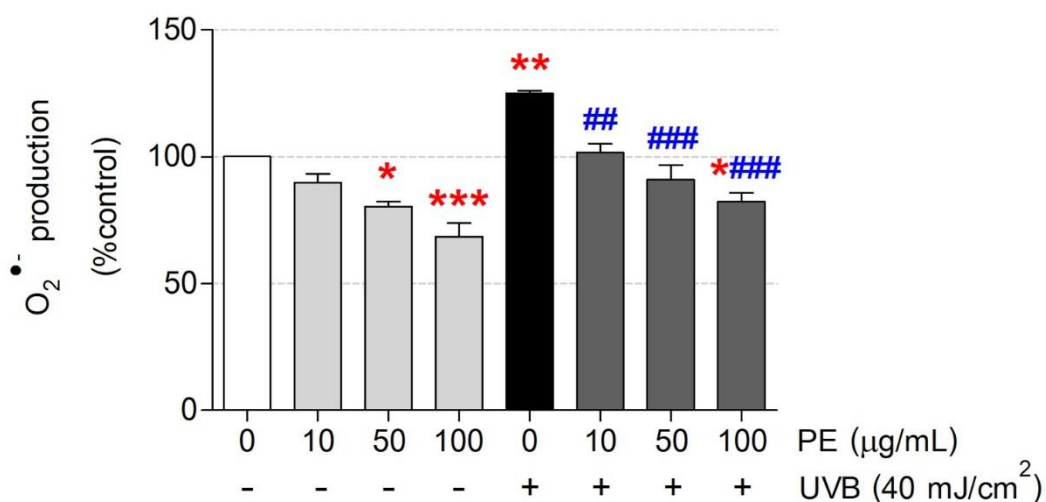


Figure 25 Relative superoxide production in HaCaT cells after treatment with or without UVB irradiation.

Data are shown as mean \pm S.E.M. * $P < 0.05$, ** $P < 0.01$, *** $P < 0.001$ significantly different compared to control non-UVB, ## $P < 0.01$, ### $P < 0.001$ significantly different compared to the control UVB exposure.

4.8 Effect of PE on UVB-induced hydrogen peroxide production

An Amplex red kit was used to detect the accumulation of H_2O_2 in the cells based on fluorescent reactions. The H_2O_2 production of HaCaT cells were 77%, 73%, and 71% after pretreatment with PE alone at the concentration 10, 50, 100 µg/mL, respectively, compared with control non UVB. Although, the increase of H_2O_2 level up to 129% was affected by UVB irradiation. Pretreatment with PE (10, 50, 100 µg/mL) combined with exposure to UVB radiation significantly decreased the level of H_2O_2 within the cells to 110%, 90%, and 73%, respectively (Figure 26).

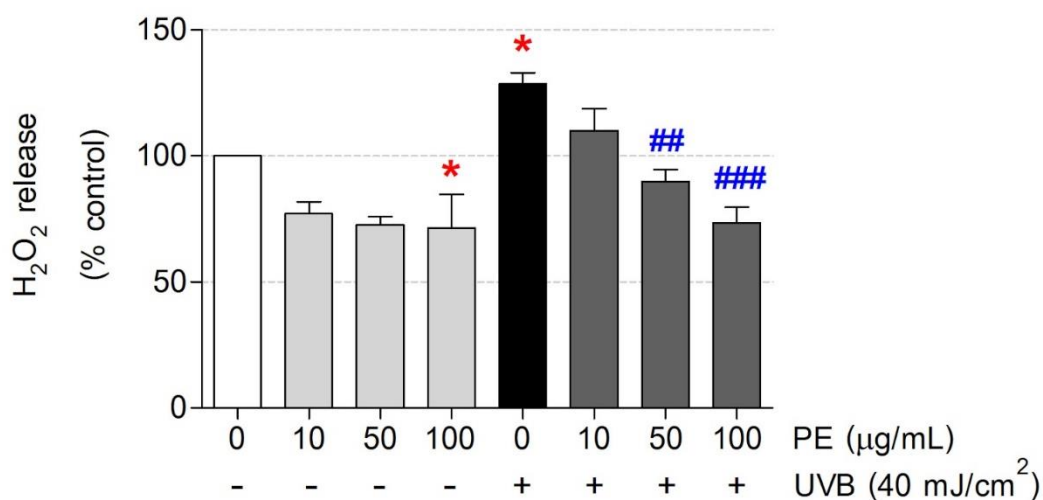


Figure 26 The intracellular H₂O₂ production in HaCaT cells.

Data are represented as mean \pm SEM (n = 3). *p<0.05 significant compared with HaCaT cells untreated with UVB or PE (control group); ##p<0.01, ###p<0.01 significant comparison between HaCaT cells treated with UVB alone and UVB in combination with PE.

4.9 Effect of PE on UVB-induced CAT enzyme antioxidant activity

After calculation and generation of standard curve of formaldehyde at the absorbance 540 nm, linear regression equation is $y = 0.00192x - 0.0017$ and $R^2 = 0.9758$. CAT enzyme activity of PE at the concentration 10, 50, 100 μg/mL were not changed (48, 50 and 44 nmol/min/mL/mg protein, respectively) when compared with the control non-UVB (53 nmol/min/mL/mg protein). UVB radiation showed inhibition of CAT enzyme activity of HaCaT cells by decreasing in CAT enzyme activity to 43 nmol/min/mL/mg protein (p<0.05), whereas CAT enzyme activity was increased by PE pretreatment combined with UVB irradiation in a dose-dependent manner. CAT activity of PE at the various concentration 10, 50, 100 μg/mL in combination with concentration 10, 50, 100 μg/mL exposure were 44, 50 and 58 nmol/min/mL/mg protein, respectively (Figure 27).

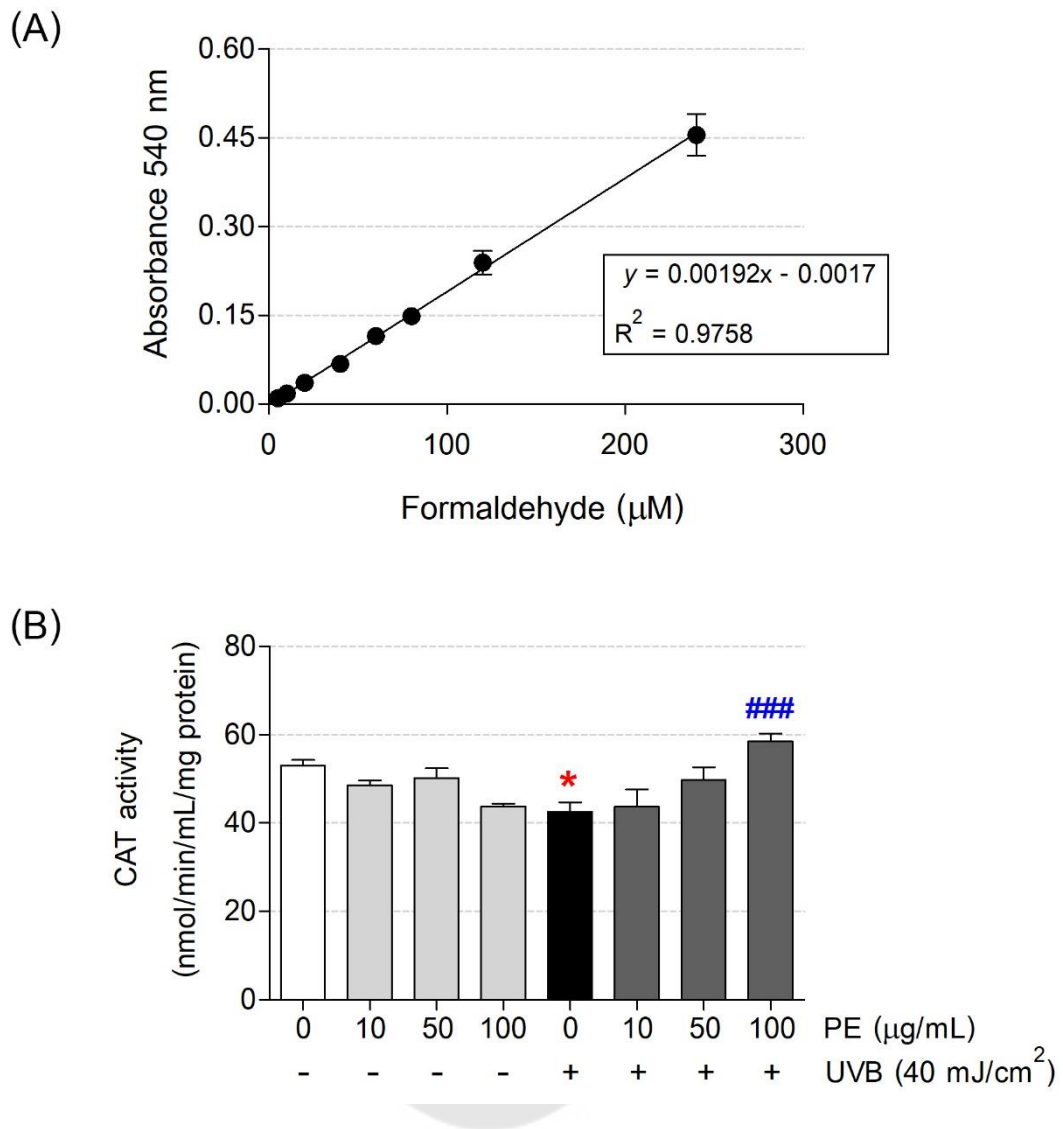


Figure 27 The CAT activity in HaCaT cells after induced with UVB radiation.

(a) standard formaldehyde curve of CAT activity. (b) CAT activity. Data are represented as mean \pm SEM ($n = 3$). * $p < 0.05$ significant compared with HaCaT cells untreated with UVB or PE (control group); ### $p < 0.01$ significant comparison between HaCaT cells treated with UVB alone and UVB in combination with PE.

4.10 Effect of PE on UVB-induced SOD enzyme antioxidant activity

Standard SOD activities of various concentrations were plot as a percentage of inhibition in Figure 28A. The linearity of the standard SOD activity inhibition graph showed a great standard with correlation coefficient (R^2) = 0.9545 (Figure 28B). There was no change in the SOD activity among PE pretreatment alone groups and control non UVB. SOD activity of PE at the different concentrations 10, 50, and 100 mg/mL were 0.75, 0.75 and 0.70 Unit/mL/mg protein, respectively, when compared with control non UVB that SOD activity was 0.69 Unit/mL/mg protein. UVB radiation significantly induced SOD activity (1.65 unit/mL/mg protein, $p < 0.05$) in HaCAT cells when compared with control non UVB. Moreover, PE pretreatment in combination with UVB irradiation trended to increase SOD activity in a dose-dependent manner, but not significantly changed when compared with control UVB. SOD activity of HaCaT cells exposed with UVB and treated with PE at the concentrations 10, 50, and 100 ug/mL was 1.92, 1.77, and 2.13 unit/mL/mg protein, respectively (Figure 28C).

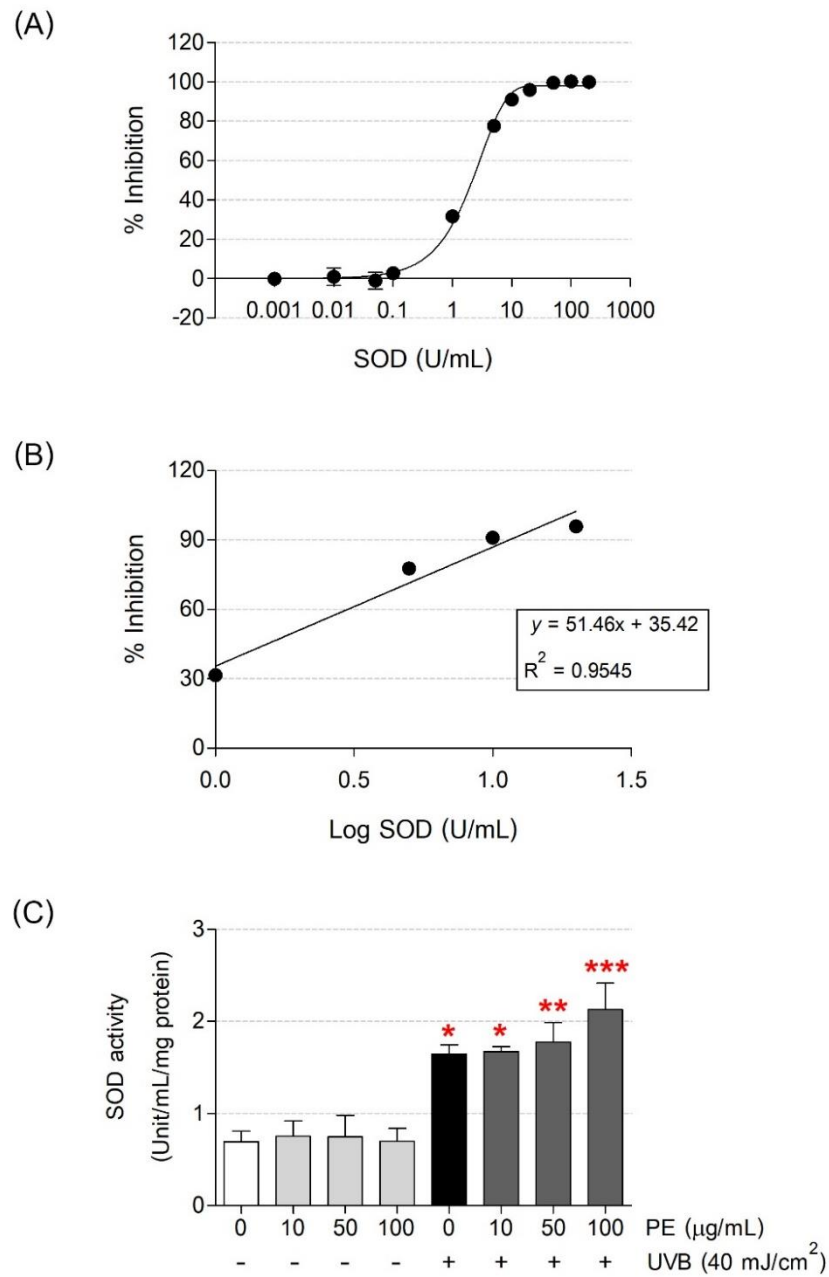


Figure 28 The SOD activity in HaCaT cells.

(A) Inhibition curve of standard SOD (B) Linear regression of standard SOD and (C) SOD activity of HaCaT cells induced with UVB radiation. Data are represented as mean \pm SEM ($n = 3$). * $p < 0.05$ significant compared with HaCaT cells untreated with UVB or PE (control group); ** $p < 0.01$, *** $p < 0.001$ significant comparison between HaCaT cells treated with UVB alone and UVB in combination with PE.

4.11 Effect of PE on UVB-induced GPx enzyme antioxidant activity

No significant differences between GPx activity were found in HaCaT cells pretreated with PE and combined with, or without UVB radiation (Figure 29).

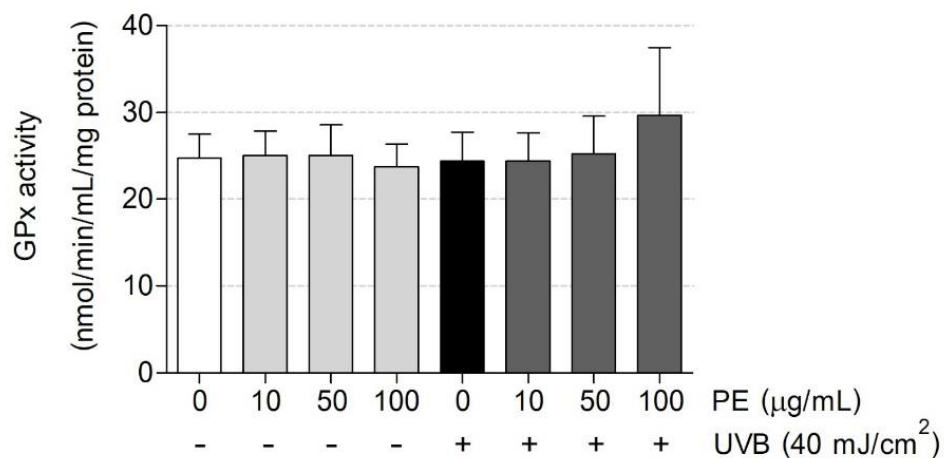


Figure 29 The GPx activity in HaCaT cells induced with UVB radiation.

Data are shown as mean \pm SEM of three independent experiments.

4.12 Effect of PE on UVB-induced apoptosis in HaCaT cells

There was no significant difference among the percentage of apoptotic cells in the control non UVB and PE treatment alone group which percentage of apoptotic cells of control non UVB and PE at the concentration 10, 50 and 100 ug/ mL were approximately 3%. While treatment HaCaT cells with UVB alone showed 20% ($p < 0.001$) of apoptotic cells. Pretreatment HaCaT cells with PE and UVB radiation significantly reduced apoptotic cells to 16, 10, and 8%, respectively (Figure 30).

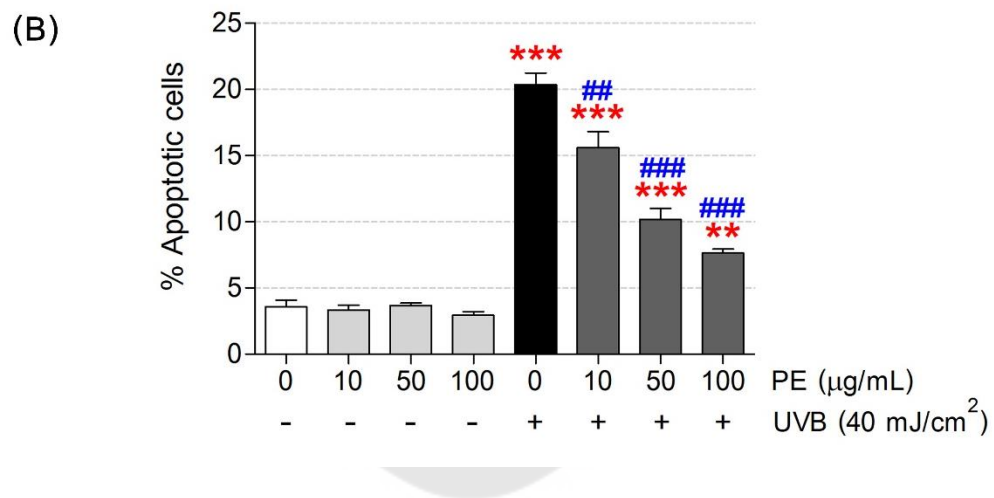
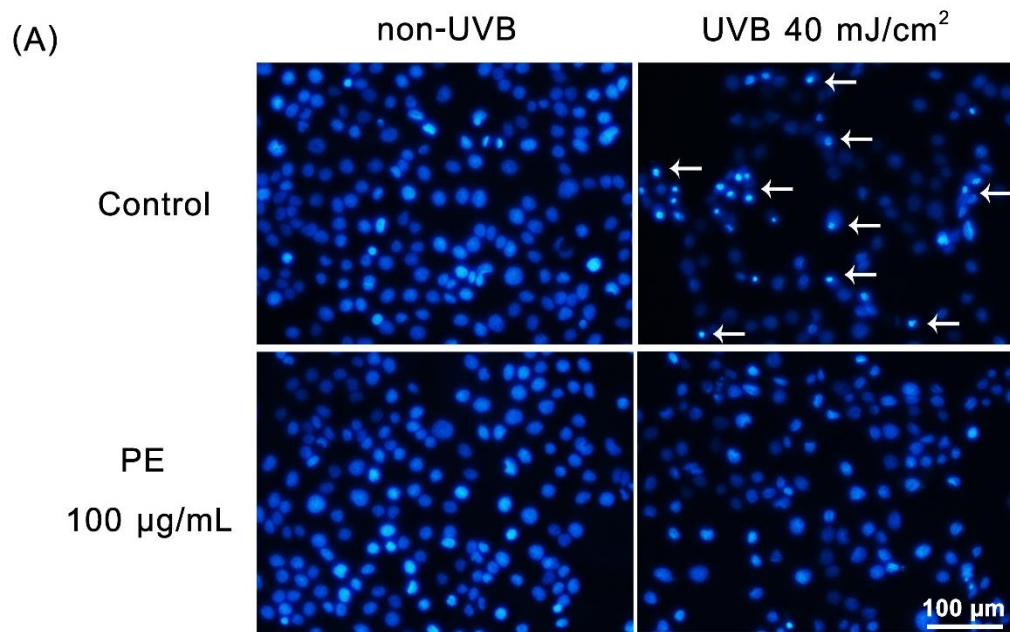


Figure 30 Cell apoptosis in HaCaT cells by Hoechst staining.

(A) Fluorescent microscopic images of Hoechst stained HaCaT cells (B) Representative of percentage apoptotic HaCaT cells after exposure to UVB radiation and protective effect of PE treatment on HaCaT cells which reduced apoptotic cells. The data presented as mean \pm SEM ($n = 3$). ** $p < 0.01$ and *** $p < 0.001$ significant comparisons between HaCaT cells treated with UVB radiation and control group; ## $p < 0.01$ and ### $p < 0.01$ significant comparison between HaCaT cells treated with UVB alone and UVB in combination with PE.

4.13 Effect of PE on UVB-induced PGE₂ production

PGE₂ production was not affected by PE pretreatment at the various concentrations when compared with control non UVB. Whereas PGE₂ production in HaCaT cells was increased by UVB radiation to 1,423 pg/mL. The pretreatment with different concentrations of PE (10, 50, and 100 µg/mL) in combination with UVB irradiation significantly decreased PGE₂ production to 784, 615, and 356 pg/mL when compared with the control UVB-irradiated group (Figure 31).

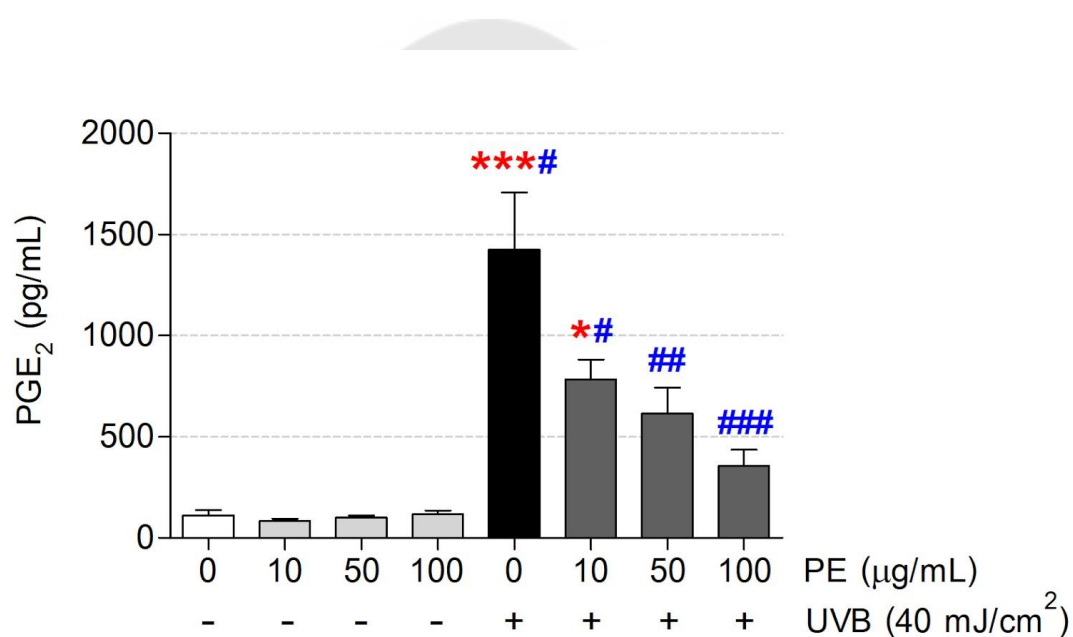
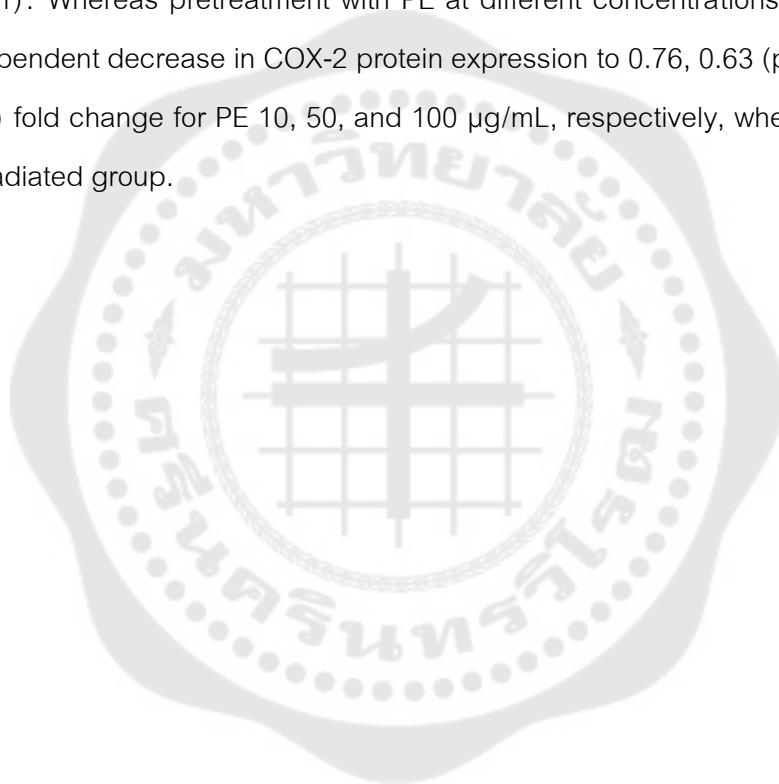


Figure 31 Representative of PGE₂ releasing in HaCaT cells.

The data expressed as mean \pm SEM (n = 3). *p<0.05 and ***p<0.001 significant comparisons between HaCaT cells treated with UVB radiation and control group; #p<0.05, ##p<0.01 and ###p<0.01 significant comparison between HaCaT cells treated with UVB alone and UVB in combination with PE.

4.14 Effect of PE on UVB-induced COX-2 protein expression

Figure 32A, UVB showed the increase of COX-2 protein expression depending on time after exposure to UVB radiation. At 6 hours, UVB slightly increased the protein expression of COX-2. Whereas 12, 18, and 24 hours, UVB significantly induced COX-2 expression to 1.95, 2.39, and 2.42 fold ($p < 0.001$) when compared with control non-UVB, respectively. From Figure 32B, the comparison between UVB irradiation and non-UVB also showed a high expression of COX-2 in the UVB-irradiated group to 3.52 fold ($p < 0.001$). Whereas pretreatment with PE at different concentrations, demonstrated a dose-dependent decrease in COX-2 protein expression to 0.76, 0.63 ($p < 0.05$), and 0.65 ($p < 0.05$) fold change for PE 10, 50, and 100 $\mu\text{g/mL}$, respectively, when compared with UVB- irradiated group.



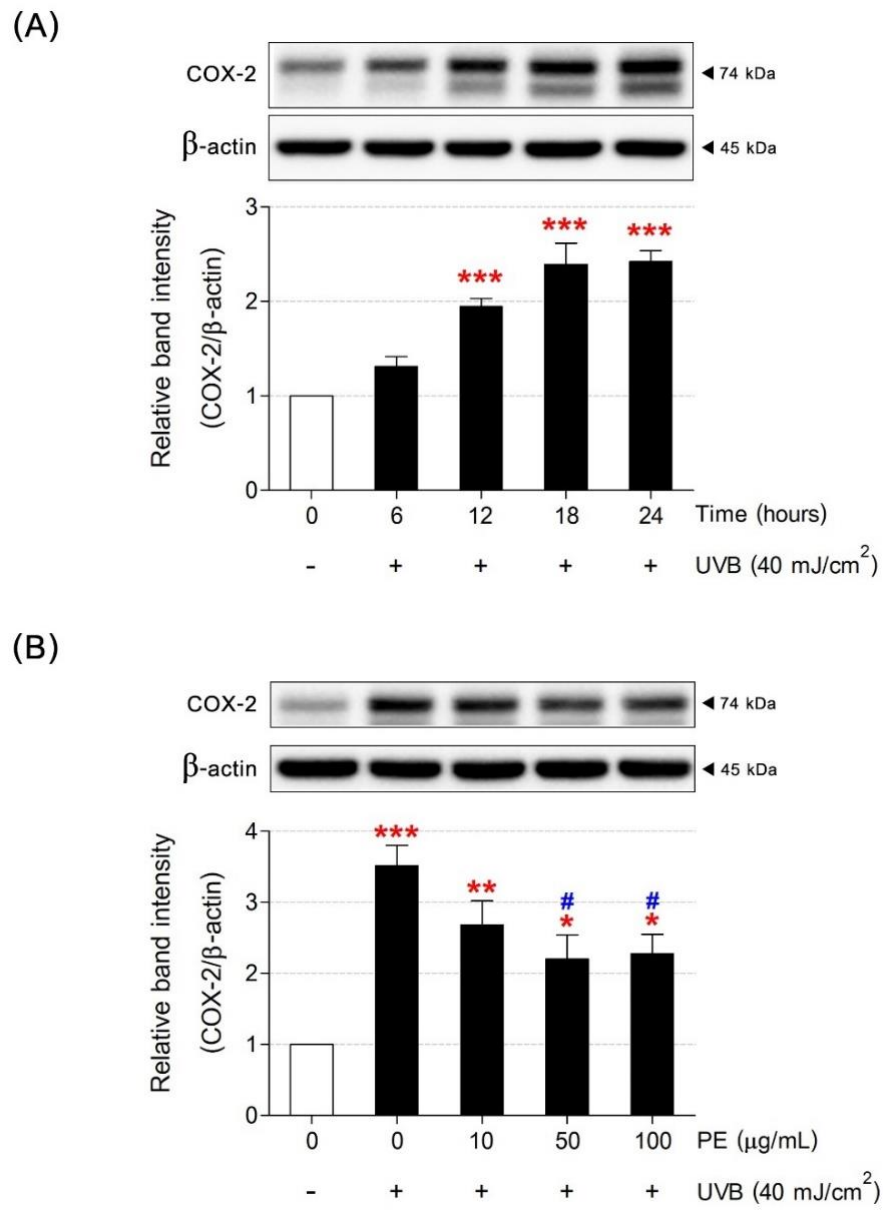


Figure 32 Western blot analysis of COX-2 expression in HaCaT cells induced by UVB.

(A) Western blot analysis showing the time course of COX-2 protein expression at times

6, 12, 18, and 24 hours. (B) The effect of PE on UVB radiation-induced inflammation in

HaCaT cells. Western blot results of three independent protein samples. Error bars

indicate mean ± S.E.M. *P<0.05, **P<0.01, and ***P<0.001 significantly different

compared to control non-UVB, #p<0.05 significant comparison between HaCaT cells

treated with UVB alone and UVB in combination with PE.

4.15 Effect of PE on UVB-induced NF- κ B protein expression

UVB exposure increases NF- κ B protein expression depending on time. UVB irradiation significantly increases NF- κ B protein expression at 15, 30, 60, and 120 mins to 1.17, 1.25 ($p < 0.05$), 1.26 ($p < 0.05$) and 1.45 ($p < 0.001$) fold changed when compared with relative control non-UVB, respectively (Figure 33). From Figure 33B, the comparison between UVB irradiation increases the expression of NF- κ B to 1.50 fold changed ($p < 0.001$) when compared with the vehicle-treated group. Whereas preincubation of PE with 100 μ g/mL showed attenuated NF- κ B protein expression down to 1.18 ($p < 0.05$) fold changed when compared with the UVB-irradiated group.



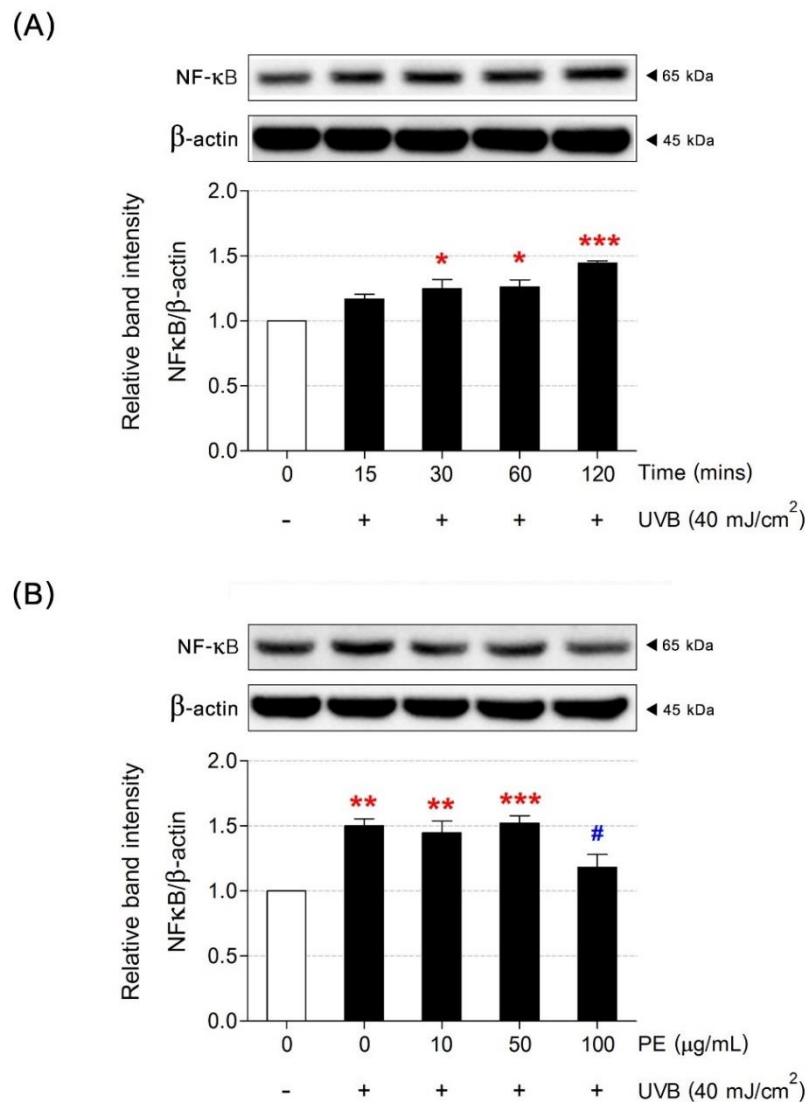


Figure 33 Western blot analysis of NF-κB expression in HaCaT cells induced by UVB.

(A) The representative of western blot analysis showing the time course of NF-κB protein expression at times 15, 30, 60, and 120 mins. (B) The effect of PE on UVB radiation-induced NF-κB expression levels in HaCaT cells. Western blot results of three independent protein samples. Data showed mean ± S.E.M. * $p < 0.05$, ** $p < 0.01$, and *** $p < 0.001$ significantly different compared to non-irradiated, # $p < 0.05$ significant comparison between HaCaT cells treated with UVB alone and UVB in combination with PE.

4.16 Effect of PE on UVB-induced Akt protein expression

The results in Figure 34 showed that UVB-exposed significantly increases phosphorylation of Akt at 30, 60, and 120 mins to 2.41 ($p < 0.05$), 3.32 ($p < 0.001$), and 3.15 ($p < 0.001$) fold changed when compared with the vehicle-treated group, respectively. The representative of Figure 34B shows a significant increase in pAkt/Akt (1.42 fold changed) when compared with the non-exposure group. PE pretreatment at concentrations 10, 50, and 100 $\mu\text{g}/\text{mL}$ significantly decreased signaling of the Akt pathway to 0.88 ($p < 0.01$), 0.80 ($p < 0.01$), and 0.63 ($p < 0.001$) fold changed when compared with the UV-exposed group, respectively.



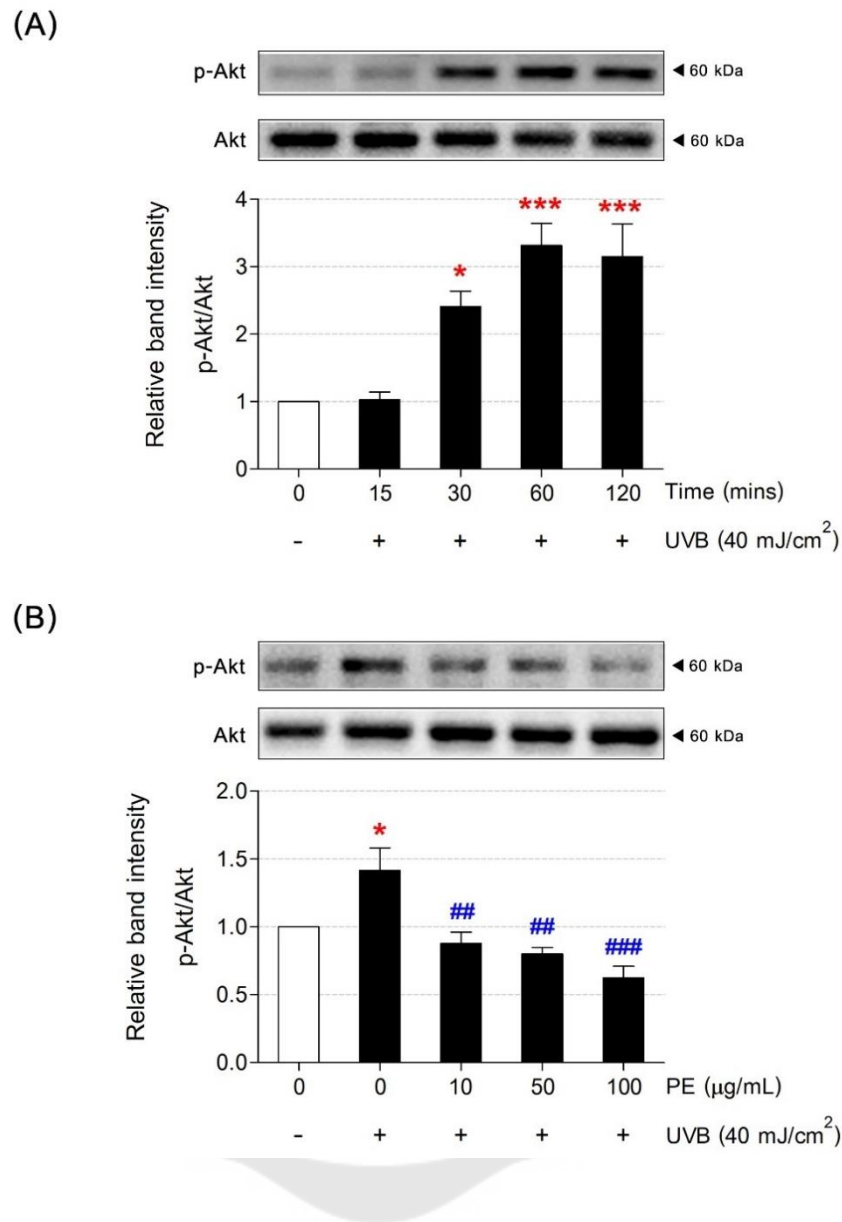


Figure 34 Western blot analysis of Akt expression in HaCaT cells induced by UVB ray. (A) The representative of western blot analysis showing the time course of Akt protein expression at times 15, 30, 60, and 120 mins. (B) The effect of PE on UVB radiation-induced p-Akt/Akt ratio in HaCaT cells. Western blot results of three independent protein samples. Data showed mean \pm S.E.M. * $p < 0.05$ and *** $p < 0.001$ significantly different compared to control non-UVB, ## $p < 0.01$ and ### $p < 0.001$ significant comparisons between HaCaT cells treated with UVB alone and UVB in combination with PE.

4.17 Effect of PE on UVB-induced p38 protein expression

UVB irritation significantly increases phosphorylation of p38 of all the time at 15, 30, 60, and 120 mins to 5.69, 14.18, 8.67, and 9.51 (** * $p < 0.001$) fold-changed, respectively. Especially, the highest p-p38 protein expression was 30 mins (Figure 35). Figure 35B, However, UVB radiation can induce HaCaT cells p-p38 protein expression but no significant changes in p-p38 levels for all the PE pretreatment groups were found when compared with the UVB-treated group.



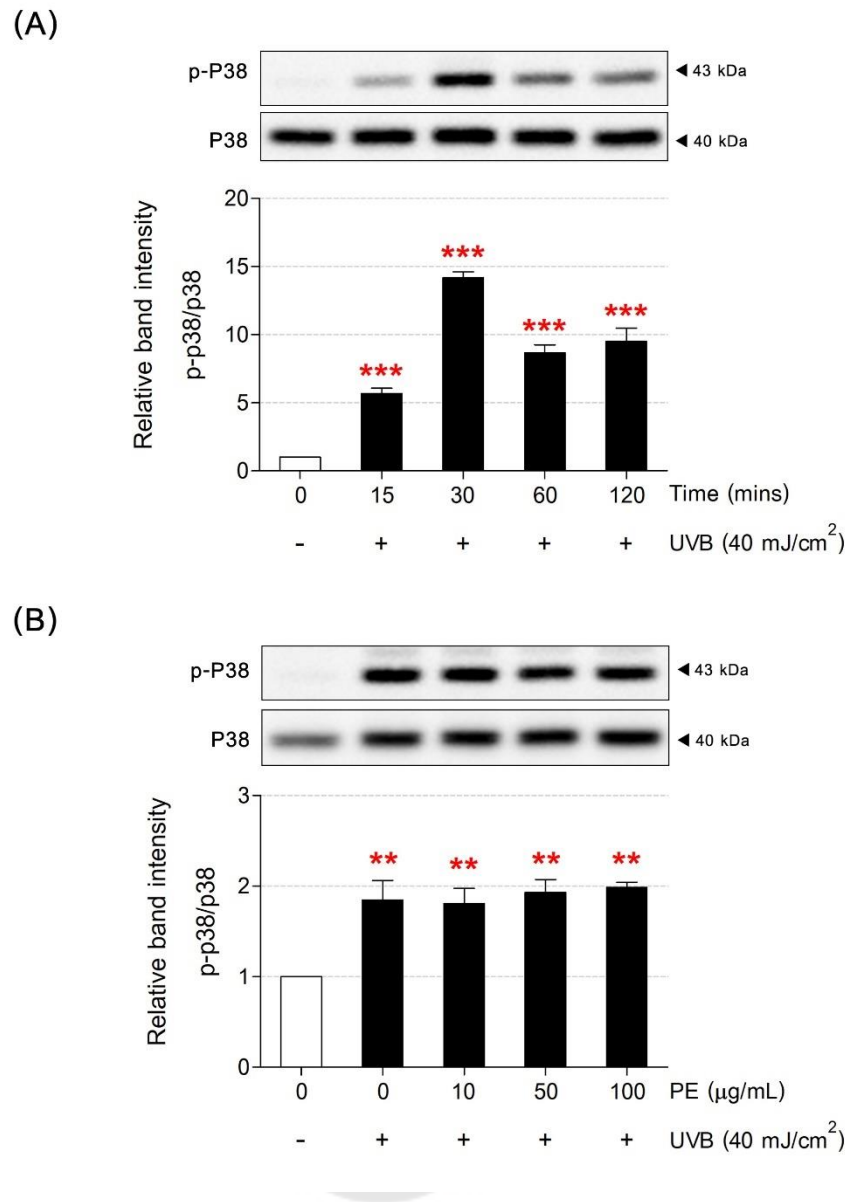
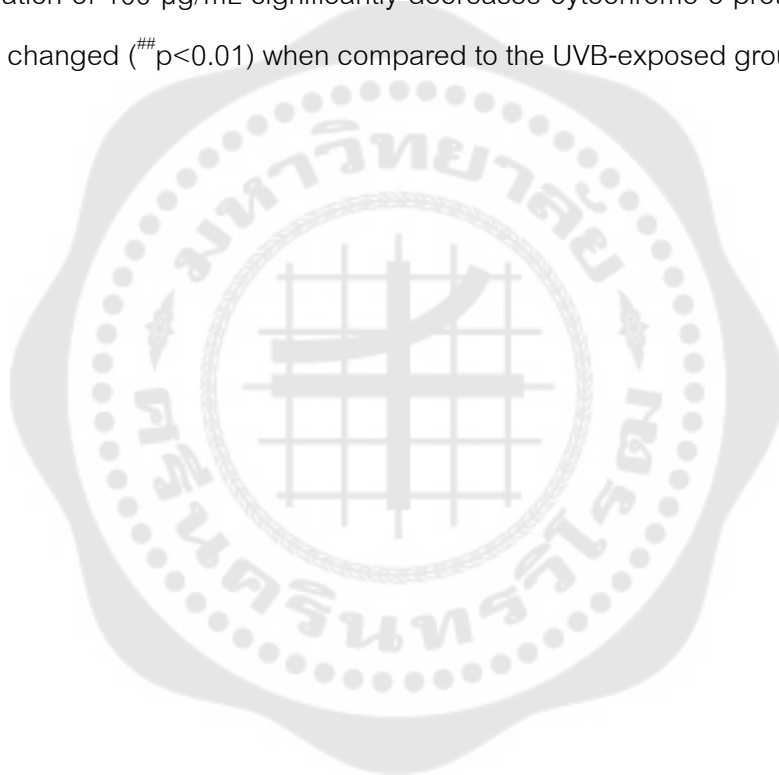


Figure 35 Western blot analysis of p38 expression in HaCaT cells induced by UVB ray.

(A) The representative of western blot analysis showing the time course of p-p38/p38 protein ratio at times 15, 30, 60, and 120 mins. (B) Relative fold change of western blot band intensity of PE on UVB radiation-induced p-p38 expression in HaCaT cells. Data expressed as mean \pm S.E.M. (n=3) **p<0.01 and ***p<0.001 significantly different compared to control non-UVB.

4.18 Effect of PE on UVB-induced cytochrome c protein expression

Figure 36A, cytochrome c expression band intensity presented at 14 kDa of the blotting membrane. After various times of UVB exposure (6, 12, 18, and 24 hours), the highest protein levels of cytochrome c expression were 1.64 fold changed (** $p < 0.01$) at 24 hours on UVB-irradiated HaCaT cells, when compared with vehicle control. Also in Figure 36B, UVB radiation-induced cytochrome c activation up to 1.77 fold changed (** $p < 0.01$), compared with relative control non UVB. However, pretreatment of PE at a concentration of 100 $\mu\text{g}/\text{mL}$ significantly decreases cytochrome c protein expression to 1.42 fold changed ([#] $p < 0.01$) when compared to the UVB-exposed group.



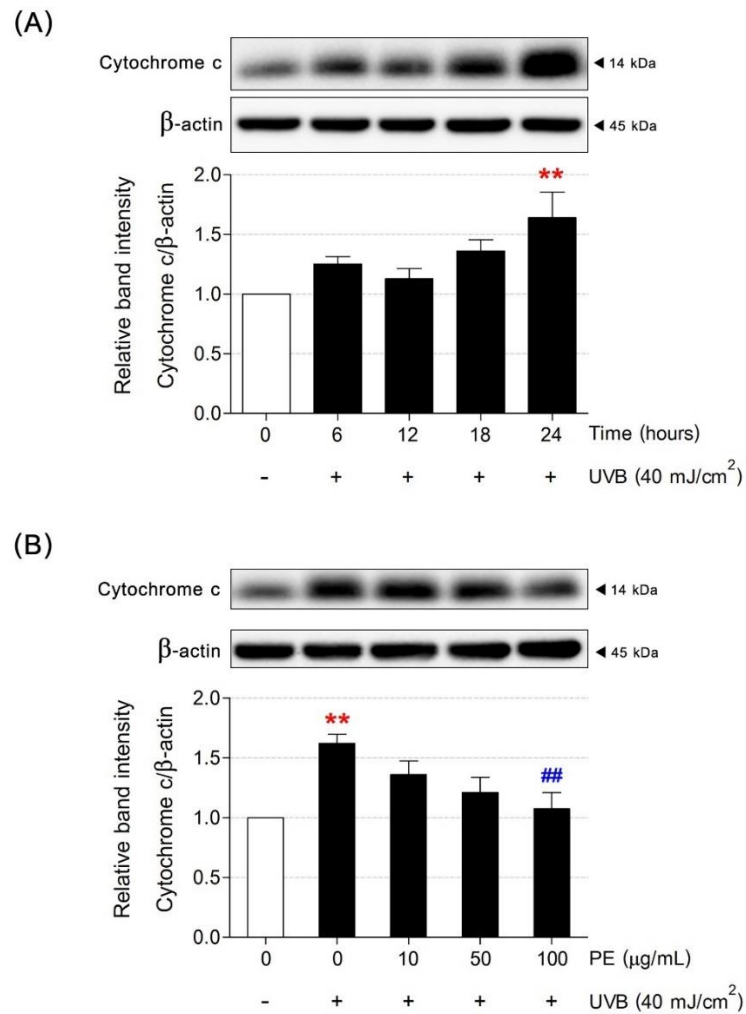


Figure 36 Western blot analysis of cytochrome c expression in HaCaT cells induced by UVB radiation.

(A) The quantification of western blot analysis showing the time course of cytochrome c protein expression at times 6, 12, 18, and 24 hours. (B) The effect of PE on UVB radiation-induced cytochrome c/β-actin ratio in HaCaT cells. Western blot results of three independent protein samples. Data showed mean ± S.E.M. **p<0.01 significantly different compared to control non-UVB, ##p<0.01 significant comparison between HaCaT cells treated with UVB alone and UVB in combination with PE.

4.19 Effect of PE on UVB-induced c-Jun protein expression

The p-c-Jun expression levels were significantly increased to 4.01 (** $p < 0.01$), 4.24 (** $p < 0.001$), and 6.05 (** $p < 0.001$) fold change in a dose-dependent manner when HacaT cells exposed to UVB radiation at 30, 60, and 120 mins, respectively (Figure 37A). Nevertheless, 100 $\mu\text{g}/\text{mL}$ of PE preincubation showed a significant decrease of phosphorylation c-Jun levels to 0.76 ($^{\#}p < 0.05$) fold changed when compared with the relative UVB-treated group (Figure 37B).



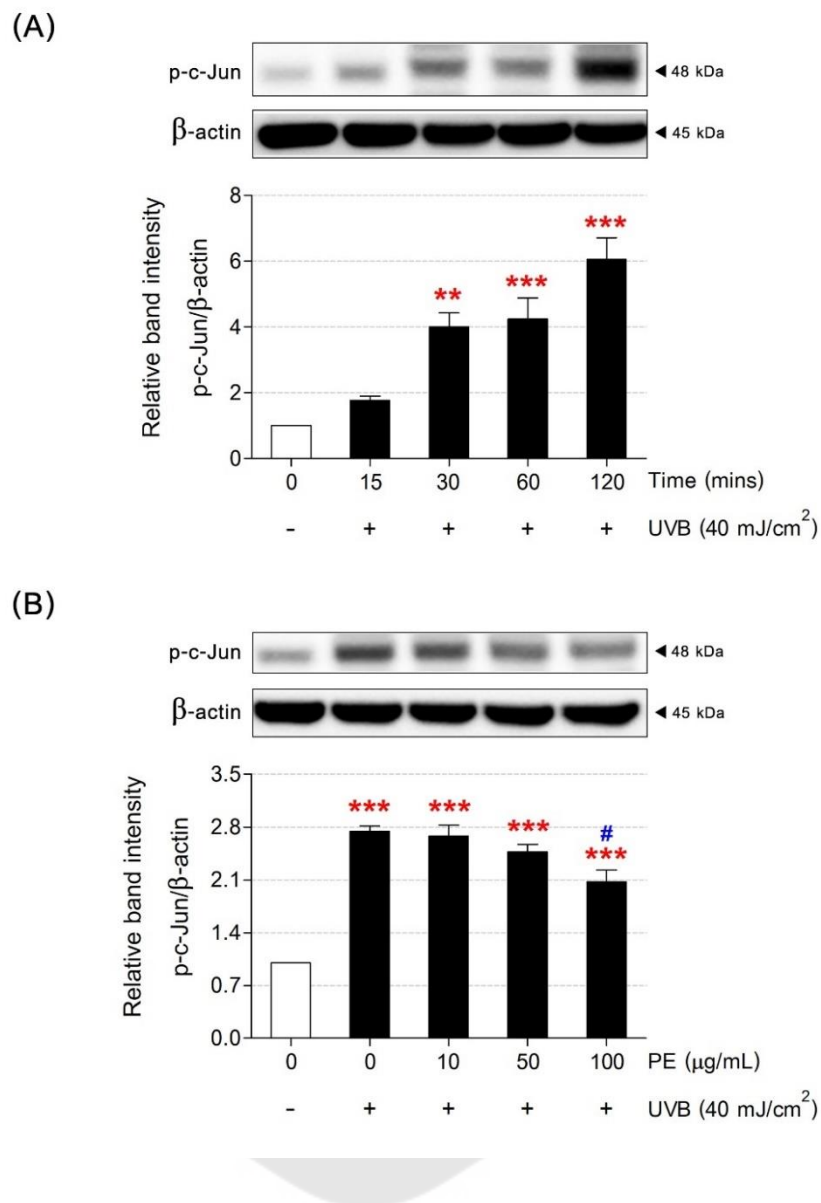


Figure 37 western blot analysis of p-c-Jun expression in HaCaT cells induced by UVB. (A) The western blot band and quantification data of cytochrome c protein activation at the times 0, 15, 30, and 120 mins after UVB irradiation. (B) The effect of PE on UVB radiation-induced p-c-Jun activation in HaCaT cells. Data showed the mean \pm S.E.M of three independent experiments. ** $p < 0.01$ and *** $p < 0.001$ significantly different compared to control non-UVB, # $p < 0.1$ represent significant differences compared with UVB-treated group.

CHAPTER 5

SUMMARY DISCUSSION AND SUGGESTION

Almost the whole energies of the earth come from the sun, especially in the photosynthesis of plants. In humans, the skin epidermis synthesizes vitamin D by the activation of UV rays from sunlight (127). Apart from sunlight benefits, overexposure to UV rays also causes human skin damage, injury, and inflammation leading to skin photoaging and skin cancer (24). UVB-induced damage to keratinocytes can be separated into two main mechanisms. First, UVB penetrates and directly damages cellular DNA to form CPD formation, leading to mutation and apoptosis. Second, UVB indirectly induces ROS production causing cell damage and inflammation through survival (Akt and ERK), inflammatory (NF- κ B), and death signaling pathway (apoptotic, JNK/AP-1, and p38), leading to human skin diseases (128). Finding the perfectly mimic model of UVB exposure on skin is beneficial to studies and design the preventive effect of natural compounds sources. The first objective of this study, we optimized the condition for UVB radiation induced-skin damage by performing the MTT assay to find the optimal dose of UVB radiation. We found that UVB irradiation at 40 mJ/cm² significantly decreases HaCaT cells viability. Therefore, inducing the HaCaT cells with 40 mJ/cm² of UVB radiation is the perfect condition for the model of UVB-induced keratinocyte damage that mimics the actual absorption condition of UVB on human skin. Moreover, this model was used to investigate the protective effect of PE on UVB-induced cellular oxidative damage, inflammation, and cell death mechanism. The results of this study showed that PE pretreatment on UVB-irradiated HaCaT cells had a high antioxidant and scavenging effect to control ROS levels, while enzymatic antioxidants consisting of CAT was restored by PE pretreatment after eliminating the production of ROS by UVB induction. The reduction of intracellular ROS by PE improves cell viability and decreases cell apoptosis of UVB-exposed cells which corresponds to the decreases of cytochrome c. The decrease of Akt survival of PE pretreatment on UVB-exposed HaCaT cells showed the improvement of the cell to homeostasis via restoration

of the cellular homeostasis. In inflammatory pathways, UVB exposure increases the secretion of PGE₂ in surrounding media that correspond to the signal transduction of inflammatory cascade including NF-**KB**, COX-2, and c-Jun. PE preincubation decreases these inflammatory factors to reduce cell inflammation and death. Our results proved that PE had a high antioxidant effect to protect UVB-induced HaCaT cell inflammation and death.

Oxidative stress condition is induced by the imbalance between intracellular oxidant molecules and antioxidants which have high levels of ROS damaging biomolecules and signaling cascades leading to cell inflammation and death (129). Antioxidants play crucial roles to control ROS levels and cell homeostasis which natural antioxidant consumption can improve oxidative damage cells. PE is a high natural antioxidants source containing a high concentration of vitamins, carotenoids, and polyphenols (phenolic and flavonoids) . Our study found that PE is composed of ascorbic acid, gallic acid, ellagic acid, chlorogenic acid, and quercetin, which are high-capacity natural antioxidant compounds. However, we did not find Phyllantin, a specific compound found in many *Phyllanthus* species likely the previous study reported by Ramanujam et. al., (130) and Liu et. al., (131). Phyllantin is likely to dissolve in a non-aqueous phase in which our PE was extracted using the aqueous extraction method due to Phyllantin not found. PE showed high antioxidant potential on FRAP, which is higher than standard ascorbic acid because of it containing many antioxidant compounds. PE also has a high antioxidant capacity in ORAC assay. Moreover, its capacity is also highly effective to scavenge on specific ROS including H₂O₂, O₂^{•-} and OH⁻ as well as its effect on intracellular ROS of UVB-exposed HaCaT cells in the flow cytometry method. These ROS were decreased when UVB-absorbed cell pretreatment with PE. The improvement of high ROS levels by antioxidants maintains cell homeostasis to reduce risks of cell inflammation and death (132). Besides, the cellular antioxidant mechanism via the production of enzymatic antioxidants including SOD, GPX, and CAT is also important to eliminate intracellular ROS (37). UVB exposure showed an increase of SOD enzyme activity whereas a decrease of CAT but not effect on GPX. ROS especially

superoxide had high production under UVB-induced mitochondrial dysfunction leading to an increase of SOD to high activity earlier for scavenger excess of $O_2^{\bullet-}$ (133). $O_2^{\bullet-}$ converted to H_2O_2 , SOD is recovered to active levels whereas CAT and GPX activity is active to eliminate the excess of converted- H_2O_2 . Eventually, CAT and GPX were used for scavenging H_2O_2 leading to impaired of its activity and restored to basal levels after the long procedure. PE pretreatment increased SOD activity from an active base after UVB exposure, while CAT activity was restored. This phenomenon demonstrated that PE directly scavenges intracellular ROS and maintains cell homeostasis. CAT plays a pivotal role in responding to H_2O_2 due to low GPX activity in UVB-induced H_2O_2 production (134). Therefore, PE is a high antioxidant scavenger that can improve intracellular ROS levels of UVB exposure in HaCaT cells to reduce cell inflammation and death.

Excluding the induction of oxidative stress, UVB also induces HaCaT cell inflammation via ROS generation and their signaling cascades. PGE_2 is an important inflammatory mediator responding to cell inflammation induced by stimuli such as UVB irradiation. When cells respond to inflammatory stimuli, the COX-2 enzyme is produced via activation of the NF- κ B pathway, which cleaves arachidonic acid into PGE_2 , and finally PGE_2 . Secretion of PGE_2 induces cell and surrounding tissue damage and inflammation (135). Our study also showed the same event that UVB exposure on HaCaT cells increases the releasing of PGE_2 and the production of COX-2 and NF- κ B levels. PE pretreatment decreases the secretion of PGE_2 levels in surrounding media as well as COX-2 and NF- κ B levels in UVB-exposed cells, proving that this medical plant extract has a high potential to reduce UVB-induced cell inflammation. Furthermore, UVB also affects MAPK/AP-1 which is an important inflammatory signaling pathway (136, 137). Similarly, in the NF- κ B inflammatory pathway, PE pretreatment decreases AP-1 levels on UVB-induced HaCaT cells inflammation. Other antioxidants such as N-Acetylcysteine (NAC), which has an antioxidant effect directly eliminated ROS, and decreases NF- κ B and AP-1 pathways (134). The overall events proved that PE had excellent antioxidant and anti-inflammation effects to improve HaCaT cells damaged by

UVB irradiation, which affects decreasing of UVB-induced skin cell death. UVB irradiation directly attacks cell DNA and induces the production of ROS due to cell survival (Akt) and death cascades (p38, JNK, and apoptosis) activation (138, 139).

In the MTT experiment, UVB activation decreased cell viability and also increased the percent of apoptotic cells in Hoechst staining. The p38, JNK/AP-1, Akt, and apoptotic pathways are all elevated following UVB irradiation. ROS-induced oxidative stress can activate p38 and JNK pathways signaling to their downstream protein due to the induction of the apoptotic pathway via releasing of cytochrome c. The activation of the JNK/AP-1 cascade by UVB also has positive feedback sensing to p38/p53 apoptotic pathway (140). PE had an inhibitory effect on UVB-induced excess of intracellular ROS leading to the reduction of cytochrome c level via down-regulation of p38 and JNK/AP-1 pathway. These circumstances correspond to the increases in cell survival and decreases of percent apoptotic cell death in our study on MTT and Hoechst staining assay, respectively. Also, UVB exposure induces high expression of Akt protein, which activates cell survival from the effect of stimuli (141). PE pretreatment on UVB exposure facilitates the elimination of the production of ROS and improves cell homeostasis due to the reduction of Akt protein levels as well as the decreases of NF- κ B inflammatory pathway, which can be sensed by Akt (142). Therefore, this study proved that PE is a medical herb to prevent UVB-induced skin cell damage via scavenging of ROS, inflammation, and cell death. PE could be a candidate for an ingredient of traditional medical cosmetics to improve and protect skin from sunlight or UV rays.

Following summary in Figure 38, UVB exposure induces the excessive production of intracellular ROS, H_2O_2 , and $O_2^{\cdot-}$, ROS-induced phosphorylation of p38 and Akt cascades activates the NF- κ B and AP-1 pathways. The translocation of these pathways encourages the development of inflammatory mediators (COX-2) and the production of PGE_2 . Due to reduced cell viability after UVB exposure, PGE_2 secretion facilitates cell inflammation and apoptosis. Furthermore, ROS destroys mitochondria directly, allowing cyt c to leak into the cytosol and causing apoptosis. PE demonstrated

high antioxidant properties in both antioxidants scavenging activity and capacity assay. Correspondingly, pretreatment of PE on UVB exposure cells directly decreases intracellular ROS. PE-related ROS reduction improves cell survival and viability through the decreases of inflammatory and apoptotic cascades.

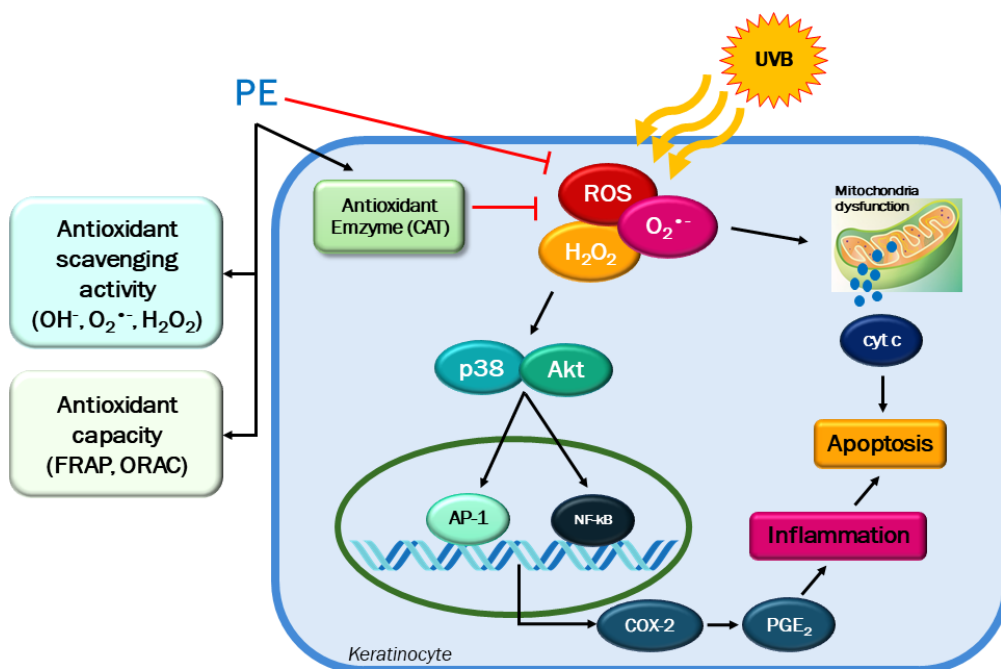


Figure 38 The preventive effect of PE on UVB-induced oxidative stress in keratinocytes.

REFERENCES

1. Pouloupoulos SG. Chapter 2 - atmospheric environment. In: Pouloupoulos SG, Inglezakis VJ, editors. *Environment and Development*. Amsterdam: Elsevier; 2016. p. 45-136.
2. Dugo MA, Han F, Tchounwou PB. Persistent polar depletion of stratospheric ozone and emergent mechanisms of ultraviolet radiation-mediated health dysregulation. *Reviews on environmental health*. 2012;27(0):103-16.
3. Cancer Registry Unit NCIT. *Cancer in Thailand*. Bangkok: New Thammada Press 2015. 222 p.
4. Dawes SM, Tsai S, Gittleman H, Barnholtz-Sloan JS, Bordeaux JS. Racial disparities in melanoma survival. *Journal of the American Academy of Dermatology*. 2016;75(5):983-91.
5. Brenneisen P, Sies H, Scharffetter-Kochanek K. Ultraviolet-B irradiation and matrix metalloproteinases. *Annals of the New York Academy of Sciences*. 2002;973(1):31-43.
6. Röck K, Grandoch M, Majora M, Krutmann J, Fischer JW. Collagen fragments inhibit hyaluronan synthesis in skin fibroblasts in response to ultraviolet B (UVB): New insights into mechanisms of matrix remodeling*. *Journal of Biological Chemistry*. 2011;286(20):18268-76.
7. Freitas-Rodríguez S, Folgueras AR, López-Otín C. The role of matrix metalloproteinases in aging: Tissue remodeling and beyond. *Biochimica et Biophysica Acta (BBA) - Molecular Cell Research*. 2017;1864(11, Part A):2015-25.
8. Bonnans C, Chou J, Werb Z. Remodelling the extracellular matrix in development and disease. *Nat Rev Mol Cell Biol*. 2014;15(12):786-801.
9. Sproul CD, Mitchell DL, Rao S, Ibrahim JG, Kaufmann WK, Cordeiro-Stone M. Cyclobutane pyrimidine dimer density as a predictive biomarker of the biological effects of ultraviolet radiation in normal human fibroblast. *Photochemistry and photobiology*. 2014;90(1):145-54.
10. Amar SK, Goyal S, Mujtaba SF, Dwivedi A, Kushwaha HN, Verma A, et al. Role of

type I & type II reactions in DNA damage and activation of caspase 3 via mitochondrial pathway induced by photosensitized benzophenone. *Toxicology letters*. 2015;235(2):84-95.

11. Ruszkiewicz JA, Pinkas A, Ferrer B, Peres TV, Tsatsakis A, Aschner M. Neurotoxic effect of active ingredients in sunscreen products, a contemporary review. *Toxicology Reports*. 2017;4(Supplement C):245-59.

12. Korać RR, Khambholja KM. Potential of herbs in skin protection from ultraviolet radiation. *Pharmacognosy Reviews*. 2011;5(10):164-73.

13. Variya BC, Bakrania AK, Patel SS. *Emblica officinalis* (Amla): A review for its phytochemistry, ethnomedicinal uses and medicinal potentials with respect to molecular mechanisms. *Pharmacological Research*. 2016;111:180-200.

14. D'Orazio J, Jarrett S, Amaro-Ortiz A, Scott T. UV radiation and the skin. *International Journal of Molecular Sciences*. 2013;14(6):12222-48.

15. Wickett RR, Visscher MO. Structure and function of the epidermal barrier. *American Journal of Infection Control*. 2006;34(10):S98-S110.

16. Boukamp P, Petrussevska RT, Breitkreutz D, Hornung J, Markham A, Fusenig NE. Normal keratinization in a spontaneously immortalized aneuploid human keratinocyte cell line. *The Journal of cell biology*. 1988;106(3):761-71.

17. Henseleit U, Zhang J, Wanner R, Haase I, Kolde G, Rosenbach T. Role of p53 in UVB-induced apoptosis in human HaCaT keratinocytes. *The Journal of investigative dermatology*. 1997;109(6):722-7.

18. Raj D, Brash DE, Grossman D. Keratinocyte apoptosis in epidermal development and disease. *The Journal of investigative dermatology*. 2006;126(2):243-57.

19. Griffin LL, Lear JT. Photodynamic therapy and non-melanoma skin cancer. *Cancers*. 2016;8(10).

20. Muzic JG, Schmitt AR, Wright AC, Alniemi DT, Zubair AS, Olazagasti Lourido JM, et al. Incidence and trends of basal cell carcinoma and cutaneous squamous cell carcinoma: A population-based study in Olmsted County, Minnesota, 2000 to 2010. *Mayo Clinic proceedings*. 2017;92(6):890-8.

21. Rogers HW, Weinstock MA, Feldman SR, Coldiron BM. Incidence estimate of nonmelanoma skin cancer (keratinocyte carcinomas) in the U.S. population, 2012. *JAMA dermatology*. 2015;151(10):1081-6.
22. Porceddu SV, Veness MJ, Guminski A. Nonmelanoma cutaneous head and neck cancer and merkel cell carcinoma: Current concepts, advances, and controversies. *Journal of Clinical Oncology*. 2015;33(29):3338-45.
23. Leiter U, Garbe C. Epidemiology of melanoma and nonmelanoma skin cancer--the role of sunlight. *Advances in experimental medicine and biology*. 2008;624:89-103.
24. Watson M, Holman DM, Maguire-Eisen M. Ultraviolet radiation exposure and its impact on skin cancer risk. *Semin Oncol Nurs*. 2016;32(3):241-54.
25. Gupta AK, Bharadwaj M, Mehrotra R. Skin cancer concerns in people of color: Risk factors and prevention. *Asian Pacific journal of cancer prevention*. 2016;17(12):5257-64.
26. Society AC. *Cancer facts & figures 2021*. American Cancer Society. 2021:1-67.
27. Walter FM, Birt L, Cavers D, Scott S, Emery J, Burrows N, et al. This isn't what mine looked like': a qualitative study of symptom appraisal and help seeking in people recently diagnosed with melanoma. *BMJ Open*. 2014;4(7):e005566.
28. Garcovich S, Colloca G, Sollena P, Andrea B, Balducci L, Cho WC, et al. Skin cancer epidemics in the elderly as an emerging issue in geriatric oncology. *Aging Dis*. 2017;8(5):643-61.
29. Knips A, Zacharias M. Both DNA global deformation and repair enzyme contacts mediate flipping of thymine dimer damage. *Scientific Reports*. 2017;7.
30. Gill SS, Anjum NA, Gill R, Jha M, Tuteja N. DNA damage and repair in plants under ultraviolet and ionizing radiations. *The Scientific World Journal*. 2015;2015.
31. Shah P, He YY. Molecular regulation of UV-induced DNA repair. *Photochemistry and photobiology*. 2015;91(2):254-64.
32. Lakin ND, Jackson SP. Regulation of p53 in response to DNA damage. *Oncogene*. 1999;18(53):7644-55.
33. Smith ML, Ford JM, Hollander MC, Bortnick RA, Amundson SA, Seo YR, et al. p53-mediated DNA repair responses to UV radiation: studies of mouse cells lacking p53, p21,

and/or gadd45 genes. *Molecular and cellular biology*. 2000;20(10):3705-14.

34. Tavana O, Benjamin CL, Puebla-Osorio N, Sang M, Ullrich SE, Ananthaswamy HN, et al. Absence of p53-dependent apoptosis leads to UV radiation hypersensitivity, enhanced immunosuppression and cellular senescence. *Cell cycle (Georgetown, Tex)*. 2010;9(16):3328-36.

35. Benjamin CL, Ananthaswamy HN. p53 and the pathogenesis of skin cancer. *Toxicology and applied pharmacology*. 2007;224(3):241-8.

36. Sharma P, Jha AB, Dubey RS, Pessarakli M. Reactive oxygen species, oxidative damage, and antioxidative defense mechanism in plants under stressful conditions. *Journal of Botany*. 2012;2012:26.

37. Nimse SB, Pal D. Free radicals, natural antioxidants, and their reaction mechanisms. *RSC Advances*. 2015;5(35):27986-8006.

38. Lu JM, Lin PH, Yao Q, Chen C. Chemical and molecular mechanisms of antioxidants: experimental approaches and model systems. *Journal of cellular and molecular medicine*. 2010;14(4):840-60.

39. Barrera G. Oxidative stress and lipid peroxidation products in cancer progression and therapy. *ISRN Oncology*. 2012;2012:21.

40. Song JL, Gao Y. Protective effects of *Lindera coreana* on UVB-induced oxidative stress in human HaCaT keratinocytes. *Iranian Journal of Pharmaceutical Research : IJPR*. 2014;13(4):1369-78.

41. Krishnaveni M, Mirunalini S. Therapeutic potential of *Phyllanthus emblica* (amla): the ayurvedic wonder. *Journal of basic and clinical physiology and pharmacology*. 2010;21(1):93-105.

42. Grimsrud PA, Xie H, Griffin TJ, Bernlohr DA. Oxidative stress and covalent modification of protein with bioactive aldehydes. *The Journal of biological chemistry*. 2008;283(32):21837-41.

43. Perluigi M, Di Domenico F, Blarzino C, Foppoli C, Cini C, Giorgi A, et al. Effects of UVB-induced oxidative stress on protein expression and specific protein oxidation in normal human epithelial keratinocytes: a proteomic approach. *Proteome science*.

2010;8:13.

44. Jena NR. DNA damage by reactive species: Mechanisms, mutation and repair. *Journal of biosciences*. 2012;37(3):503-17.
45. Cadet J, Wagner JR. DNA base damage by reactive oxygen species, oxidizing agents, and UV radiation. *Cold Spring Harbor Perspectives in Biology*. 2013;5(2).
46. Cavinato M, Jansen-Dürr P. Molecular mechanisms of UVB-induced senescence of dermal fibroblasts and its relevance for photoaging of the human skin. *Experimental Gerontology*. 2017;94:78-82.
47. Choi H-J, Alam MB, Baek M-E, Kwon Y-G, Lim J-Y, Lee S-H. Protection against UVB-Induced Photoaging by *Nypa fruticans* via Inhibition of MAPK/AP-1/MMP-1 Signaling. *Oxidative Medicine and Cellular Longevity*. 2020;2020.
48. Rabe JH, Mamelak AJ, McElgunn PJS, Morison WL, Sauder DN. Photoaging: Mechanisms and repair. *Journal of the American Academy of Dermatology*. 2006;55(1):1-19.
49. Lee CH, Wu SB, Hong CH, Yu HS, Wei YH. Molecular mechanisms of UV-induced apoptosis and its effects on skin residential cells: The implication in UV-based phototherapy. *International Journal of Molecular Sciences*. 2013;14(3):6414-35.
50. Wong RS. Apoptosis in cancer: from pathogenesis to treatment. *Journal of experimental & clinical cancer research : CR*. 2011;30:87.
51. Takasawa R, Nakamura H, Mori T, Tanuma S. Differential apoptotic pathways in human keratinocyte HaCaT cells exposed to UVB and UVC. *Apoptosis*. 2005;10(5):1121-30.
52. Lawrence T. The nuclear factor NF-kappaB pathway in inflammation. *Cold Spring Harbor Perspectives in Biology*. 2009;1(6):a001651.
53. Gilmore TD. Introduction to NF-kappaB: players, pathways, perspectives. *Oncogene*. 2006;25(51):6680-4.
54. Morgan MJ, Liu ZG. Crosstalk of reactive oxygen species and NF-kappaB signaling. *Cell research*. 2011;21(1):103-15.
55. Martins GR, Gelaleti GB, Moschetta MG, Maschio-Signorini LB, Zuccari DA.

Proinflammatory and anti-inflammatory cytokines mediated by NF-kappaB factor as prognostic markers in mammary tumors. *Mediators of inflammation*. 2016;2016:9512743.

56. Pino MS, Nawrocki ST, Cognetti F, Abruzzese JL, Xiong HQ, McConkey DJ. Prostaglandin E₂ drives cyclooxygenase-2 expression via cyclic AMP response element activation in human pancreatic cancer cells. *Cancer biology & therapy*. 2005;4(11):1263-9.

57. Fukai T, Ushio-Fukai M. Superoxide dismutases: role in redox signaling, vascular function, and diseases. *Antioxidants & redox signaling*. 2011;15(6):1583-606.

58. Punnonen K, Lehtola K, Autio P, Kiistala U, Ahotupa M. Chronic UVB irradiation induces superoxide dismutase activity in human epidermis in vivo. *Journal of photochemistry and photobiology B, Biology*. 1995;30(1):43-8.

59. Rezvani HR, Mazurier F, Cario-Andre M, Pain C, Ged C, Taieb A, et al. Protective effects of catalase overexpression on UVB-induced apoptosis in normal human keratinocytes. *The Journal of biological chemistry*. 2006;281(26):17999-8007.

60. Shindo Y, Witt E, Han D, Packer L. Dose-response effects of acute ultraviolet irradiation on antioxidants and molecular markers of oxidation in murine epidermis and dermis. *The Journal of investigative dermatology*. 1994;102(4):470-5.

61. Kansanen E, Kuosmanen SM, Leinonen H, Levonen AL. The Keap1-Nrf2 pathway: Mechanisms of activation and dysregulation in cancer. *Redox biology*. 2013;1:45-9.

62. Sykiotis GP, Bohmann D. Stress-activated cap'n'collar transcription factors in aging and human disease. *Science signaling*. 2010;3(112):re3.

63. Shih P-H, Yen G-C. Differential expressions of antioxidant status in aging rats: the role of transcriptional factor Nrf2 and MAPK signaling pathway. *Biogerontology*. 2007;8(2):71-80.

64. Huang C-Z, Tung Y-T, Hsia S-M, Wu C-H, Yen G-C. The hepatoprotective effect of *Phyllanthus emblica* L. fruit on high fat diet-induced non-alcoholic fatty liver disease (NAFLD) in SD rats. *Food & Function*. 2017;8(2):842-50.

65. Renaud E, Miccoli L, Zacal N, Biard DS, Craescu CT, Rainbow AJ, et al. Differential contribution of XPC, RAD23A, RAD23B and CENTRIN 2 to the UV-response in human cells. *DNA repair*. 2011;10(8):835-47.

66. de Laat WL, Jaspers NG, Hoeijmakers JH. Molecular mechanism of nucleotide excision repair. *Genes & development*. 1999;13(7):768-85.
67. Kimura S, Sakaguchi K. DNA repair in plants: *Chem. Rev.*; 2006. 753-66 p.
68. Schärer OD. Nucleotide excision repair in eukaryotes. *Cold Spring Harbor Perspectives in Biology*. 2013;5(10).
69. Munoz MJ, Nieto Moreno N, Giono LE, Cambindo Botto AE, Dujardin G, Bastianello G, et al. Major roles for pyrimidine dimers, nucleotide excision repair, and ATR in the alternative splicing response to UV irradiation. *Cell reports*. 2017;18(12):2868-79.
70. Hossini AM, Quast AS, Plotz M, Grauel K, Exner T, Kuchler J, et al. PI3K/AKT signaling pathway is essential for survival of induced pluripotent stem cells. *PloS one*. 2016;11(5):e0154770.
71. Ouyang W, Luo W, Zhang D, Jian J, Ma Q, Li J, et al. PI-3K/Akt pathway-dependent cyclin D1 expression is responsible for arsenite-induced human keratinocyte transformation. *Environmental Health Perspectives*. 2008;116(1):1-6.
72. Wang Y, Zhou Y, Graves DT. FOXO transcription factors: their clinical significance and regulation. *BioMed research international*. 2014;2014:925350.
73. Zhang X, Tang N, Hadden TJ, Rishi AK. Akt, FoxO and regulation of apoptosis. *Biochimica et biophysica acta*. 2011;1813(11):1978-86.
74. Altomare DA, Testa JR. Perturbations of the AKT signaling pathway in human cancer. *Oncogene*. 2005;24(50):7455-64.
75. Kim W, Yang HJ, Youn H, Yun YJ, Seong KM, Youn B. Myricetin inhibits Akt survival signaling and induces Bad-mediated apoptosis in a low dose ultraviolet (UV)-B-irradiated HaCaT human immortalized keratinocytes. *Journal of radiation research*. 2010;51(3):285-96.
76. Lee ER, Kim JY, Kang YJ, Ahn JY, Kim JH, Kim BW, et al. Interplay between PI3K/Akt and MAPK signaling pathways in DNA-damaging drug-induced apoptosis. *Biochimica et biophysica acta*. 2006;1763(9):958-68.
77. Nys K, Maes H, Andrei G, Snoeck R, Garmyn M, Agostinis P. Skin mild hypoxia enhances killing of UVB-damaged keratinocytes through reactive oxygen species-

- mediated apoptosis requiring Noxa and Bim. *Free radical biology & medicine*. 2012;52(6):1111-20.
78. Moriyama M, Moriyama H, Uda J, Kubo H, Nakajima Y, Goto A, et al. BNIP3 upregulation via stimulation of ERK and JNK activity is required for the protection of keratinocytes from UVB-induced apoptosis. *Cell death & disease*. 2017;8(2):e2576.
79. Wortzel I, Seger R. The ERK cascade: distinct functions within various subcellular organelles. *Genes & cancer*. 2011;2(3):195-209.
80. Zhang Y, Dong Z, Bode AM, Ma WY, Chen N, Dong Z. Induction of EGFR-dependent and EGFR-independent signaling pathways by ultraviolet A irradiation. *DNA and cell biology*. 2001;20(12):769-79.
81. Xu Y, Shao Y, Zhou J, Voorhees JJ, Fisher GJ. Ultraviolet irradiation-induces epidermal growth factor receptor (EGFR) nuclear translocation in human keratinocytes. *Journal of cellular biochemistry*. 2009;107(5):873-80.
82. Cuenda A, Rousseau S. p38 MAP-kinases pathway regulation, function and role in human diseases. *Biochimica et biophysica acta*. 2007;1773(8):1358-75.
83. López-Camarillo C, Ocampo EA, Casamichana ML, Pérez-Plasencia C, Álvarez-Sánchez E, Marchat LA. Protein kinases and transcription factors activation in response to UV-radiation of skin: implications for carcinogenesis. *International Journal of Molecular Sciences*. 2012;13(1):142-72.
84. Cavinato M, Waltenberger B, Baraldo G, Grade CVC, Stuppner H, Jansen-Dürr P. Plant extracts and natural compounds used against UVB-induced photoaging. *Biogerontology*. 2017;18(4):499-516.
85. Katz L, Baltz RH. Natural product discovery: past, present, and future. *Journal of Industrial Microbiology and Biotechnology*. 2016;43(2-3):155-76.
86. Vostalova J, Zdarilova A, Svobodova A. *Prunella vulgaris* extract and rosmarinic acid prevent UVB-induced DNA damage and oxidative stress in HaCaT keratinocytes. *Archives of dermatological research*. 2010;302(3):171-81.
87. Perianayagam JB, Narayanan S, Gnanasekar G, Pandurangan A, Raja S, Rajagopal K, et al. Evaluation of antidiarrheal Potential of *Embllica officinalis*.

Pharmaceutical Biology. 2005;43(4):373-7.

88. Chaphalkar R, Apte KG, Talekar Y, Ojha SK, Nandave M. Antioxidants of *Phyllanthus emblica* L. bark extract provide hepatoprotection against ethanol-induced hepatic damage: A comparison with silymarin. *Oxidative Medicine and Cellular Longevity*. 2017;2017:3876040.

89. Rose K, Wan C, Thomas A, Seeram NP, Ma H. Phenolic compounds isolated and identified from amla (*Phyllanthus emblica*) juice powder and their antioxidant and neuroprotective activities. *Natural Product Communications*. 2018;13(10):1934578X1801301019.

90. Gaire BP, Subedi L. Phytochemistry, pharmacology and medicinal properties of *Phyllanthus emblica* Linn. *Chinese Journal of Integrative Medicine*. 2014.

91. Zhang Y-J, Tanaka T, Yang C-R, Kouno I. New phenolic constituents from the fruit juice of *Phyllanthus emblica*. *Chemical and Pharmaceutical Bulletin*. 2001;49(5):537-40.

92. Li Y, Guo B, Wang W, Li L, Cao L, Yang C, et al. Characterization of phenolic compounds from *Phyllanthus emblica* fruits using HPLC-ESI-TOF-MS as affected by an optimized microwave-assisted extraction. *International Journal of Food Properties*. 2019;22(1):330-42.

93. Jain SK, Khurdiya DS. Vitamin C enrichment of fruit juice based ready-to-serve beverages through blending of Indian gooseberry (*Emblica officinalis* Gaertn.) juice. *Plant foods for human nutrition (Dordrecht, Netherlands)*. 2004;59(2):63-6.

94. Majeed M, Bhat B, Anand S, Sivakumar A, Paliwal P, Geetha KG. Inhibition of UV-induced ROS and collagen damage by *Phyllanthus emblica* extract in normal human dermal fibroblasts. *Journal of cosmetic science*. 2011;62(1):49-56.

95. Chen TS, Liou SY, Wu HC, Tsai FJ, Tsai CH, Huang CY, et al. Efficacy of epigallocatechin-3-gallate and Amla (*Emblica officinalis*) extract for the treatment of diabetic-uremic patients. *Journal of medicinal food*. 2011;14(7-8):718-23.

96. Bhattacharya A, Kumar M, Ghosal S, Bhattacharya SK. Effect of bioactive tannoid principles of *Emblica officinalis* on iron-induced hepatic toxicity in rats. *Phytomedicine : international journal of phytotherapy and phytopharmacology*. 2000;7(2):173-5.

97. Asmawi MZ, Kankaanranta H, Moilanen E, Vapaatalo H. Anti-inflammatory activities of *Emblica officinalis* Gaertn leaf extracts. *The Journal of pharmacy and pharmacology*. 1993;45(6):581-4.
98. Bhattacharya A, Chatterjee A, Ghosal S, Bhattacharya SK. Antioxidant activity of active tannoid principles of *Emblica officinalis* (amla). *Indian journal of experimental biology*. 1999;37(7):676-80.
99. Zhang YJ, Abe T, Tanaka T, Yang CR, Kouno I. Phyllanemblinins A-F, new ellagitannins from *Phyllanthus emblica*. *Journal of natural products*. 2001;64(12):1527-32.
100. Zhang Y, Zhao L, Guo X, Li C, Li H, Lou H, et al. Chemical constituents from *Phyllanthus emblica* and the cytoprotective effects on H₂O₂-induced PC12 cell injuries. *Archives of Pharmacal Research*. 2016;39(9):1202-11.
101. Mjelle R, Hegre SA, Aas PA, Slupphaug G, Drabløs F, Sætrom P, et al. Cell cycle regulation of human DNA repair and chromatin remodeling genes. *DNA repair*. 2015;30(Supplement C):53-67.
102. Qi W-Y, Li Y, Hua L, Wang K, Gao K. Cytotoxicity and structure activity relationships of phytosterol from *Phyllanthus emblica*. *Fitoterapia*. 2013;84(Supplement C):252-6.
103. Kumar MS, Kirubanandan S, Sripriya R, Sehgal PK. Triphala promotes healing of infected full-thickness dermal wound. *The Journal of surgical research*. 2008;144(1):94-101.
104. Fujii T, Wakaizumi M, Ikami T, Saito M. Amla (*Emblica officinalis* Gaertn.) extract promotes procollagen production and inhibits matrix metalloproteinase-1 in human skin fibroblasts. *Journal of ethnopharmacology*. 2008;119(1):53-7.
105. Chanvorachote P, Pongrakhananon V, Luanpitpong S, Chanvorachote B, Wannachaiyasit S, Nimmannit U. Type I pro-collagen promoting and anti-collagenase activities of *Phyllanthus emblica* extract in mouse fibroblasts. *Journal of cosmetic science*. 2009;60(4):395-403.
106. Sharma A, Sharma MK, Kumar M. Modulatory role of *Emblica officinalis* fruit extract against arsenic induced oxidative stress in Swiss albino mice. *Chemico-biological*

interactions. 2009;180(1):20-30.

107. Ngamkitidechakul C, Jaijoy K, Hansakul P, Soonthornchareonnon N, Sireeratawong S. Antitumour effects of *Phyllanthus emblica* L.: induction of cancer cell apoptosis and inhibition of in vivo tumour promotion and in vitro invasion of human cancer cells. *Phytotherapy research : PTR*. 2010;24(9):1405-13.

108. Adil MD, Kaiser P, Satti NK, Zargar AM, Vishwakarma RA, Tasduq SA. Effect of *Emblica officinalis* (fruit) against UVB-induced photo-aging in human skin fibroblasts. *Journal of ethnopharmacology*. 2010;132(1):109-14.

109. Kumar N, Rungseevijitprapa W, Narkkhong NA, Suttajit M, Chaiyasut C. 5alpha-reductase inhibition and hair growth promotion of some Thai plants traditionally used for hair treatment. *Journal of ethnopharmacology*. 2012;139(3):765-71.

110. Ojha S, Golechha M, Kumari S, Arya DS. Protective effect of *Emblica officinalis* (amla) on isoproterenol-induced cardiotoxicity in rats. *Toxicology and industrial health*. 2012;28(5):399-411.

111. Kalekar SA, Munshi RP, Thatte UM. Do plants mediate their anti-diabetic effects through anti-oxidant and anti-apoptotic actions? an in vitro assay of 3 Indian medicinal plants. *BMC complementary and alternative medicine*. 2013;13:257.

112. Kalekar SA, Munshi RP, Bhalerao SS, Thatte UM. Insulin sensitizing effect of 3 Indian medicinal plants: An in vitro study. *Indian Journal of Pharmacology*. 2013;45(1):30-3.

113. Singh MK, Yadav SS, Gupta V, Khattri S. Immunomodulatory role of *Emblica officinalis* in arsenic induced oxidative damage and apoptosis in thymocytes of mice. *BMC complementary and alternative medicine*. 2013;13:193.

114. Sultana Z, Jami SI, Ali E, Begum M, Haque M. Investigation of antidiabetic effect of ethanolic extract of *Phyllanthus emblica* Linn. fruits in experimental animal models. *Pharmacology & Pharmacy*. 2014;5(1):8.

115. Thirunavukkarasu M, Selvaraju V, Tapias L, Sanchez JA, Palesty JA, Maulik N. Protective effects of *Phyllanthus emblica* against myocardial ischemia-reperfusion injury: the role of PI3-kinase/glycogen synthase kinase 3beta/beta-catenin pathway. *Journal of*

physiology and biochemistry. 2015;71(4):623-33.

116. Colucci R, Dragoni F, Conti R, Pisaneschi L, Lazzeri L, Moretti S. Evaluation of an oral supplement containing *Phyllanthus emblica* fruit extracts, vitamin E, and carotenoids in vitiligo treatment. *Dermatologic therapy*. 2015;28(1):17-21.

117. Pathak N, Kumar G, Chandra Chaurasia R. Evaluation of anti-diabetic activity of commercially available extracts of *Phyllanthus Emblica* in streptozocin induced diabetic rats 2016.

118. Srinivasan P, Subramaniyan V, Kothandaraman S, Palani M. Anti-diabetic activity of quercetin extracted from *Phyllanthus emblica* L. fruit: In silico and in vivo approaches. *Journal of Pharmaceutical Analysis*. 2017.

119. Fatima N, Hafizur RM, Hameed A, Ahmed S, Nisar M, Kabir N. Ellagic acid in *Emblica officinalis* exerts anti-diabetic activity through the action on beta-cells of pancreas. *European journal of nutrition*. 2017;56(2):591-601.

120. Kumar V, Aneesh KA, Kshemada K, Ajith KGS, Binil RSS, Deora N, et al. Amalaki rasayana, a traditional Indian drug enhances cardiac mitochondrial and contractile functions and improves cardiac function in rats with hypertrophy. *Scientific Reports*. 2017;7(1):8588.

121. Nain P, Saini V, Sharma S, Nain J. Antidiabetic and antioxidant potential of *Emblica officinalis* Gaertn. leaves extract in streptozotocin-induced type-2 diabetes mellitus (T2DM) rats. *Journal of ethnopharmacology*. 2012;142(1):65-71.

122. Sayed S, Ahsan N, Kato M, Ohgami N, Rashid A, Akhand AA. Protective effects of *phyllanthus emblica* leaf extract on sodium arsenite-mediated adverse effects in mice. *Nagoya journal of medical science*. 2015;77(1-2):145-53.

123. Mehta S, Singh RK, Jaiswal D, Rai PK, Watal G. Anti-diabetic activity of *Emblica officinalis* in animal models. *Pharmaceutical Biology*. 2009;47(11):1050-5.

124. Mandal S, Hazra B, Sarkar R, Biswas S, Mandal N. Assessment of the Antioxidant and Reactive Oxygen Species Scavenging Activity of Methanolic Extract of *Caesalpinia crista* Leaf. *Evid Based Complement Alternat Med*. 2011;2011:173768.

125. de Oliveira AC, Valentim IB, Silva CA, Bechara EJH, Barros MPd, Mano CM, et al.

Total phenolic content and free radical scavenging activities of methanolic extract powders of tropical fruit residues. *Food Chemistry*. 2009;115(2):469-75.

126. Paital B. A modified fluorimetric method for determination of hydrogen peroxide using homovanillic acid oxidation principle. *BioMed research international*. 2014;2014:342958-.

127. Nair R, Maseeh A. Vitamin D: The "sunshine" vitamin. *Journal of pharmacology & pharmacotherapeutics*. 2012;3(2):118-26.

128. Wölfle U, Seelinger G, Bauer G, Meinke MC, Lademann J, Schempp CM. Reactive molecule species and antioxidative mechanisms in normal skin and skin aging. *Skin Pharmacology and Physiology*. 2014;27(6):316-32.

129. Zhang J, Wang X, Vikash V, Ye Q, Wu D, Liu Y, et al. ROS and ROS-mediated cellular signaling. *Oxidative Medicine and Cellular Longevity*. 2016;2016:4350965.

130. Srirama R, Deepak HB, Senthilkumar U, Ravikanth G, Gurumurthy BR, Shivanna MB, et al. Hepatoprotective activity of Indian *Phyllanthus*. *Pharmaceutical Biology*. 2012;50(8):948-53.

131. Liu X, Cui C, Zhao M, Wang J, Luo W, Yang B, et al. Identification of phenolics in the fruit of emblica (*Phyllanthus emblica* L.) and their antioxidant activities. *Food Chemistry*. 2008;109(4):909-15.

132. He L, He T, Farrar S, Ji L, Liu T, Ma X. Antioxidants maintain cellular redox homeostasis by elimination of reactive oxygen species. *Cellular Physiology and Biochemistry*. 2017;44(2):532-53.

133. Paz ML, González Maglio DH, Weill FS, Bustamante J, Leoni J. Mitochondrial dysfunction and cellular stress progression after ultraviolet B irradiation in human keratinocytes. *Photodermatology, Photoimmunology & Photomedicine*. 2008;24(3):115-22.

134. Makino N, Mochizuki Y, Bannai S, Sugita Y. Kinetic studies on the removal of extracellular hydrogen peroxide by cultured fibroblasts. *Journal of Biological Chemistry*. 1994;269(2):1020-5.

135. Ricciotti E, FitzGerald GA. Prostaglandins and inflammation. *Arterioscler Thromb Vasc Biol*. 2011;31(5):986-1000.

136. Cooper SJ, Bowden GT. Ultraviolet B regulation of transcription factor families: roles of nuclear factor-kappa B (NF-kappaB) and activator protein-1 (AP-1) in UVB-induced skin carcinogenesis. *Curr Cancer Drug Targets*. 2007;7(4):325-34.
137. Abbas S, Alam S, Pal A, Kumar M, Singh D, Ansari K. UVB exposure enhanced benzanthrone-induced inflammatory responses in SKH-1 mouse skin by activating the expression of COX-2 and iNOS through MAP kinases/NF- κ B/AP-1 signalling pathways. *Food and chemical toxicology : an international journal published for the British Industrial Biological Research Association*. 2016;96:183-90.
138. Anwar A, Anwar H, Yamauchi T, Tseng R, Agarwal R, Horwitz LD, et al. Bucillamine Inhibits UVB-Induced MAPK Activation and Apoptosis in Human HaCaT Keratinocytes and SKH-1 Hairless Mouse Skin. *Photochemistry and photobiology*. 2020;96(4):870-6.
139. Zhang B, Zhao Z, Meng X, Chen H, Fu G, Xie K. Hydrogen ameliorates oxidative stress via PI3K-Akt signaling pathway in UVB-induced HaCaT cells. *Int J Mol Med*. 2018;41(6):3653-61.
140. Yue J, López JM. Understanding MAPK signaling pathways in apoptosis. *International Journal of Molecular Sciences*. 2020;21(7):2346.
141. Strozyk E, Kulms D. The role of AKT/mTOR pathway in stress response to UV-irradiation: implication in skin carcinogenesis by regulation of apoptosis, autophagy and senescence. *International Journal of Molecular Sciences*. 2013;14(8):15260-85.
142. Liu W, Huang S, Li Y, Li Y, Li D, Wu P, et al. Glycyrrhizic acid from licorice down-regulates inflammatory responses via blocking MAPK and PI3K/Akt-dependent NF- κ B signalling pathways in TPA-induced skin inflammation. *MedChemComm*. 2018;9(9):1502-10.

VITA

NAME Khwadow Kunchana
DATE OF BIRTH 25 Aug 1991
PLACE OF BIRTH Chiang Mai
INSTITUTIONS ATTENDED Srinakharinwirot University

